Chem Soc Rev

From Colloidal Particles to Photonic Crystals: Advances in Self-Assembly and Their Emerging Applications

Journal:	*Chemical Society Reviews*
Manuscript ID	CS-SYN-06-2020-000706.R2
Article Type:	Review Article
Date Submitted by the Author:	18-Feb-2021
Complete List of Authors:	Cai, Zhongyu; National University of Singapore, Chemical and Biomolecular Engineering; University of Pittsburgh, Department of Chemistry; Beihang University, Research Institute for Frontier Science, Beijing Advanced Innovation Center for Biomedical Engineering, School of Space and Environment Li, Zhiwei; University of California Riverside, Department of Chemistry Ravaine, Serge; Centre de Recherche Paul Pascal (UPR 8641, CNRS) He, Mingxin; New York University, Physics Song, Yanlin; Institute of Chemistry Chinese Academy of Sciences Yin, Yadong; University of California Riverside, Department of Chemistry Zheng, Hanbin; Centre de Recherche Paul Pascal Teng, Jinghua; Institute of Materials Research and Engineering Zhang, Ao; Beihang University, Research Institute for Frontier Science, Beijing Advanced Innovation Center for Biomedical Engineering, School of Space and Environment

From Colloidal Particles to Photonic Crystals: Advances in Self-Assembly and Their Emerging Applications

Zhongyu Cai,[abc] *Zhiwei Li,*[d] *Serge Ravaine,*[e] *Mingxin He,*[f] *Yanlin Song,*[g] *Yadong Yin,*[d] *Hanbin Zheng,*[e] *Jinghua Teng,*[*h] *Ao Zhang*[a]

[a] Research Institute for Frontier Science, Beijing Advanced Innovation Center for Biomedical Engineering, School of Space and Environment, Beihang University, Beijing 100191, China

[b] Department of Chemical and Biomolecular Engineering, National University of Singapore, 4 Engineering Drive 4, Singapore 117576

[c] Department of Chemistry, University of Pittsburgh, Pittsburgh, PA 15260, United States

[d] Department of Chemistry, University of California, Riverside CA 92521, United States

[e] CNRS, Univ. Bordeaux, CRPP, UMR 5031, F-33600 Pessac, France

[f] Department of Physics, Center for Soft Matter Research, New York University, New York, NY 10003, United States

[g] Beijing National Laboratory for Molecular Sciences (BNLMS), Key Laboratory of Green Printing, Institute of Chemistry, Chinese Academy of Sciences, Beijing 100190, P.R. China

[h] Institute of Materials Research and Engineering, Agency for Science, Technology, and Research (A*STAR), 2 Fusionopolis Way, Innovis, #08-03, Singapore 138634

* To whom correspondence should be addressed. E-mails: caizy@buaa.edu.cn (ZC), and jh-teng@imre.a-star.edu.sg (JHT).

Abstract

Over the last three decades, photonic crystals (PhCs) have attracted intense interests thanks to their broad potential applications in optics and photonics. Generally, these structures can be fabricated via either “top-down” lithographic or “bottom-up” self-assembly approaches. The self-assembly approaches have attracted particular attention due to their low cost, simple fabrication processes, relative convenience of scaling up, and the ease of creating complex structures with nanometer precision. The self-assembled colloidal crystals (CCs), which are good candidates for PhCs, have offered unprecedented opportunities for photonics, optics, optoelectronics, sensing, energy harvesting, environmental remediation, pigments, and many other applications. The creation of high-quality CCs and their mass fabrication over large areas are the critical limiting factors for real-world applications. This paper reviews the state-of-the-art techniques in the self-assembly of colloidal particles for the fabrication of large-area high-quality CCs and CCs with unique symmetries. The first part of this review summarizes the types of defects commonly encountered in the fabrication process and their effects on the optical properties of the resultant CCs. Next, the mechanisms of the formation of cracks/defects are discussed, and a range of versatile fabrication methods to create large-area crack/defect-free two-dimensional and three-dimensional CCs are described. Meanwhile, we also shed light on both the advantages and limitations of these advanced approaches developed to fabricate high-quality CCs. The self-assembly routes and achievements in the fabrication of CCs with the ability to open a complete photonic bandgap, such as cubic diamond and pyrochlore structure CCs are discussed as well. Then emerging applications of large-area high-quality CCs and unique photonic structures enabled by the advanced self-assembly methods are illustrated. At the end of this review, we outlook the future approaches in the fabrication of perfect CCs and highlight their novel real-world applications.

Keywords: Self-assembly; Photonic crystals; Colloidal crystals; Large-scale and High-quality; Complete photonic bandgap; Cubic diamond crystals; Metamaterials; Sensing; Biomedical applications.

1. Introduction

Photonic crystals (PhCs) are a class of novel optical materials,[1-3] in which the dielectric materials are spatially and artificially organized into a periodic structure. Initially, PhCs were first proposed independently by Yablonovitch[1] and John[2] in 1987 to control the spontaneous emission of light and to realize photon localization. One of the extraordinary properties of a PhC is that it features a photonic bandgap (PBG), in which electromagnetic waves having energy within this band gap are prohibited from propagating through the PhCs. The formation of the PBG is a result of the periodic arrangement of the dielectric materials. The most prominent feature of PhCs is that they can iridescences as a result of diffraction. Some natural examples are the multilayered structure of flashing wings of several insects (**Figure 1a and d**), peacock feather (**Figure 1b**), pearls and natural opals (**Figure 1c)**, and etc**.** A micrograph of a fractured iridescent green butterfly scale (*left bottom*) reveals the submicrometer-size face-centered cubic (*fcc*) periodic structure inside (**Figure 1a and d**). In the 1960s, when trying to characterize opals with scanning electron microscopy (SEM) and X-ray, researchers discovered that natural opals, in fact, are colloidal crystals (CCs).[4, 5] Opals, as shown in **Figure 1c**, consist of submicrometer-size silica (SiO_2) spheres arranged in an *fcc* (close-packed) structure. According to their structural periodicity, PhCs can be classified into one-dimensional (1D), two-dimensional (2D) and three-dimensional (3D) PhCs (**Figure 1e**).

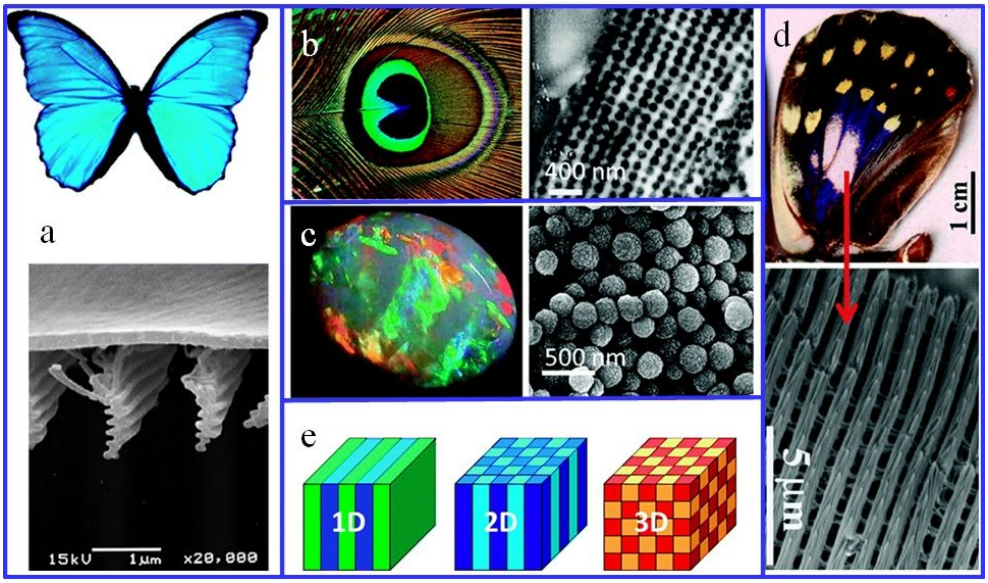

Figure 1. Photonic crystals occurred in nature: **(a)** the blue iridescence from the Morpho butterfly and SEM image of the 1D structure of the Morpho butterfly.[6] **(b)** A digital photograph (left) of multi-colored peacock feather (Image by Wikimedia Commons/CC BY-SA 3.0) and transmission electron microscopy (TEM) image (right) of the transverse cross-section of the 2D structure of the blue area of a wing.[7] **(c)** A digital photograph (left) of natural opal gemstone and SEM image (right) of the SiO_2 sphere structure inside the gemstone.[8] **(d)** A digital photograph of wing of the male *Sasakia Charonda* butterfly (top) and SEM image (bottom) of the 3D structure of the iridescent white area.[9] **(e)** Schematic representation of 1D, 2D, and 3D PhCs, with different colors indicating different dielectric constants.[3] Reprinted with permission from *Journal of Materials Chemistry C*,[10] copyright 2015 Royal Society of Chemistry.

In general, there are mainly four routes to fabricate 3D PhCs, namely "top-down" micromachining (**Figure 2a**),[11-17] holographic lithography (**Figure 2b**),[18-22] laser direct-writing technique (**Figure 2c**),[23-29] and "bottom-up" self-assembly (**Figure 2d-f**).[30-40] Although traditional "top-down" microfabrication techniques provide precise control over structured defects, they are very tedious, expensive and have trouble in making 3D PhC structures. The last "bottom-up" method, which is based on colloidal self-assembly, provides a straightforward and cheap approach to fabricating 3D PhCs. Because the size of colloidal particles is comparable to the wavelength of visible light, self-assembled CCs are good candidates for making PhCs. While conventional self-assembly of colloidal particles itself generally does not yield a PhC with a complete photonic band gap (cPBG), it produces a colloidal crystal (an artificial opal, **Figure 2e**), which can be utilized as a sacrificing template to prepare a 3D PhC (an inverse opal, **Figure 2f**).[33-36] Moreover, a myriad of computational studies indicated that self-assembly of special building blocks can lead to the formation of diamond or pyrochlore structure colloidal PhCs, which are sought-after for their ability to open a cPBG in visible region at a low refractive index contrast.[41-43] Recently, using DNA-coated tetrahedral colloidal particles, cubic diamond structure PhCs with a cPBG (**Figure 2d**)[38] and other novel structure PhCs were achieved via DNA-mediated self-assembly.[44-46]

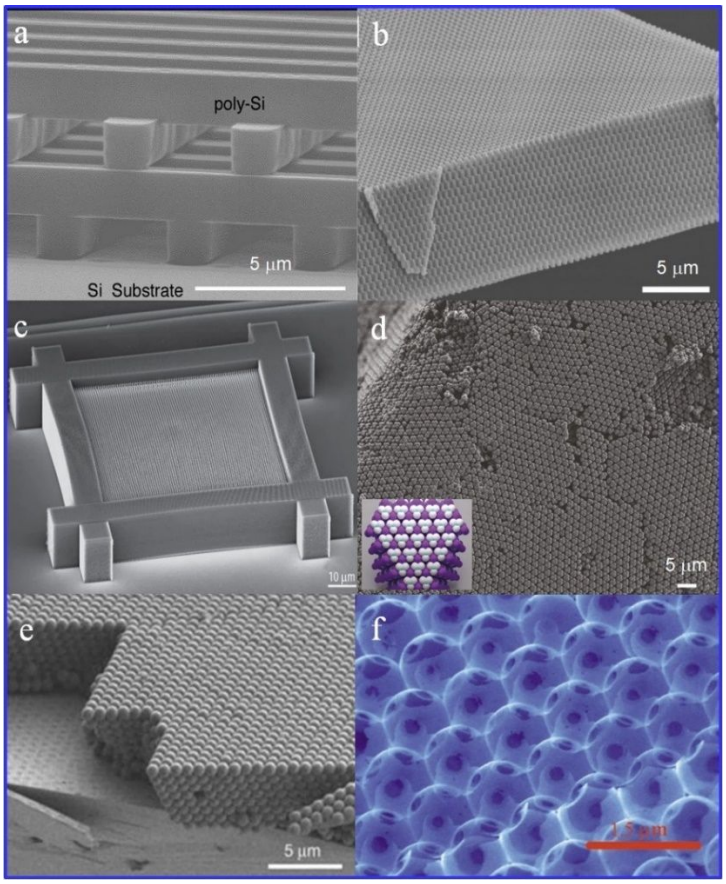

Figure 2. (a) SEM image of a cross-sectional view of 3D PhCs made of polycrystalline silicon (Si) via the photolithographic method. Reprinted from *Nature*,[12] copyright 1998 Springer Nature. **(b)** SEM image of polymeric PhCs generated using holographic lithography. Reprinted with permission from *Nature*,[19] copyright 2000 Springer Nature. **(c)** SEM image of 3D PhCs fabricated by direct laser writing. Reprinted from *Nature Materials,*[28] copyright 2004 Springer Nature. **(d)** SEM image of the (111) plane of diamond-like colloidal PhCs prepared via colloidal self-assembly of patchy compressed clusters. Reprinted from *Nature*,[38] copyright 2020 Springer Nature. **(e)** Cross-sectional SEM image of planar colloidal PhCs (synthetic silica opals) prepared via self-assembly. Reprinted from *Nature*,[34] copyright 2001 Springer Nature. **(f)** SEM image of internal (111) facet of Si PhCs fabricated with a colloidal crystal templating method. Reprinted from *Nature*,[33] copyright 2000 Springer Nature.

The colloidal self-assembly approach to 3D PhCs typically begins with the crystallization of CCs (opals). CCs are 2D or 3D periodic structures fabricated from sub-micron particles suspended in a colloidal suspension via self-assembly. CCs have various potential applications such as PhCs,[47, 48] refractive flat-panel displays,[49] optical filters,[50, 51] switches,[52-54] lasers,[55] optical sensors,[56-59] and non-bleachable color materials.[48, 60, 61] Self-assembly approaches have attracted intense interests as promising alternatives to conventional top-down methods for the scalable, low-cost synthesis of PhCs.[48, 61-64] The use of these self-assembly methods for large-area fabrication of colloidal crystal films, however, has typically led to the formation of cracks, vacancies, domain boundaries, dislocations and other types of defects.[65, 66]

The quality of the CCs is of paramount importance to the optical properties of the resultant PhCs. Researchers have extensively investigated the influences of various defects and disorders in PhCs on the optical properties in many different aspects.[67-69] The impact of those defects and disorders, including sphere vacancies, random position errors, and line dislocations,[70] planar stacking faults,[71] deviations of spheres sizes and positions,[72] controlled defects in PhCs,[73-75] and correlated and uncorrelated disorders in 1D structures[76] has been investigated. In general, a long-range disorder in PhCs, which refers to smooth distortion in lattice constant caused by size deviations of spheres or nonhomogeneity of the PhCs,[70, 72, 77] can broaden the bandgap, as well as slightly diminish the reflectance peak.[67, 70, 78-82] Furthermore, it is also found that, by introducing a particular type of long-range disorder into a PhC, the lower part of the Bragg diffraction peak of the PhCs is enlarged, and the Bragg reflection peak of the PhCs varies from inverted U-shape to inverted V-shape.[83] Short-range disorder, including grain boundaries, point defects, and unstructured colloids, widely exists in PhCs and it can remarkably decrease the Bragg reflection peaks. This mainly can be attributed to the diffuse scattering caused by these short-range disorders. The diffuse scattering results in much smaller reflectance intensity observed in experiments than that of being theoretically predicted from perfect PhCs.[79, 84] Moreover, the reflectance of PhCs containing specific short-range disorders have two distinct features, namely, a significant decrease of reflectance at the shortwave region, and slight alteration of the reflection peak

shape from an inverted "U" to a smooth inverted "V".[83] Li *et al*. demonstrated that the PBG of a self-assembled 3D PhC is extremely sensitive to the presence of geometric disorder in the CCs.[85] Particularly, a disordering strength of even less than 2% of the lattice constant will destroy the bandgap completely.[85] Albeit full of challenges, the fabrication of defect-free CCs is of both fundamental and practical importance. Therefore, various methods have been developed so far to self-assemble colloidal particles into CCs.

Among various defects and disorders, cracking in CCs after film formation is mainly ascribed to capillary stresses and further fracture upon post-treatment, such as drying and sintering. The formation of cracks restricts the application of the resulting colloidal PhC films in high-performance optical devices as the cracks significantly degrade the optical quality and mechanical strength of the colloidal PhCs.[86-89] In addition to cracks, the existence of a variety of other defects, such as point defects, dislocations, and stacking faults generated during the self-assembly process, drying stages, or infiltration steps also prevents the utilization of the resulting colloidal PhCs in many practical applications.[70] Therefore, the most significant challenge that remains to be conquered before CCs can be successfully engineered as PhC devices is their experimentally accomplishable degree of structural perfection and optical quality.

An interesting question may be raised here: how perfect of CCs is 'perfect'? For self-assembled CCs, a 'perfect' colloidal crystal sample should possess low crack density, low angular rotation between domains, large domain size, high mechanical strength, good chemical and thermal resistance, as well as spectrally distinct reflectance peaks.[65, 90-92] To date, considerable efforts have been devoted to growing CCs of high structural and optical quality, and significant progress has been achieved. In this review, we will provide a comprehensive overview of the recent progress achieved in the fabrication of defect-free CCs in large-area and self-assembly of CCs with the ability to open a cPBG, and present our outlook on the future development in this field. We start with the theoretical and experimental studies on the intrinsic defects, with a specific focus on key parameters determining the defect formation and colloidal crystal quality during and after the self-assembly process. Simulation studies on different self-assembly routes to fabricate CCs with the ability to open a cPBG are also discussed. In the following section, the general underneath strategies and individual methods to fabricate large-area high-quality CCs, including high-quality 3D CCs (opals, cubic diamond structure CCs, etc.), inverse opals, and 2D CCs, will be refined. In particular, a wide variety of novel methods on the minimization or elimination of cracks in these colloidal assemblies will be reviewed. Then, we summarize the emerging practical and fundamental applications of high-quality CCs obtained via these state-of-the-art colloidal self-assembly methods, and elucidate the working principles, practical strategies,

advantages, and limitations of CCs in developing advanced devices and functional materials. At the end of this review, a summary of current research activities on preparing high-quality CCs is presented. Perspective on potential approaches to high-quality, large-scale CCs is also provided to overcome several existing challenges in colloidal crystal production. Conventional self-assembly methods that are used to fabricate PhCs will not be included here. Readers can refer to several excellent reviews published elsewhere.[31, 48, 61, 93-99] The fabrication of large-area 1D PhCs is much more straightforward since it falls into the conventional way of making defect-free films.[100] For example, large-area and high-quality brush block copolymer 1D PhCs can be easily fabricated via self-assembly[101, 102] or direct-write 3D printing methods.[103] One recent review has summarized the fabrication and application of 1D PhCs.[104] Therefore, the fabrication of 1D PhCs will not be reviewed here either. Instead, this review is mainly focused on the assembly of spherical and related building blocks. The self-assembly of building blocks with other geometries will not be discussed much here.

2. Defect classification and description

A defect-free material is ideal and almost does not exist. In reality, any materials, no matter how perfect, possess some sort of defects. Generally, defects in CCs can be classified into two categories: spontaneous defects and designed defects. The spontaneous defects, also known as intrinsic defects, are undesirable in most cases. Therefore, it is necessary to eliminate or at least minimize them. The spontaneous defects include point defects, domains, stacking faults, dislocations, and cracks.[66]

A point defect in PhCs is often known in three types, (i) Schottky defect (missing of a sphere, **Figure 3a**), (ii) Frenkel defect (a sphere in size is remarkably smaller than its adjacent counterparts, **Figure 3b**) and (iii) the occurrence of a sphere that is notably larger than its neighboring spheres and alters the order of the lattice, thus giving rise to long-range distortions (**Figure 3c**). Dislocations are extended defects that are present in two forms, step dislocation, and screw dislocation. In a step dislocation of CCs, the lattice close to the edge of the extra half-plane is distorted by an extra half-plane of spheres. Screw dislocation in CCs involves the formation of a spiral ramp from sphere planes wound around the line of the dislocation (**Figure 3e**). Distortions attributed to a single defect can appear in the lattice that propagates much further than in atomic or molecular crystals. Domains generally can be treated as volume defects (3D defects), which can vary substantially in their dimensions. **Figure 3f** indicates a separated domain of a few tens of lattice constants. In addition, small volume defects consisting of local rearrangements and clusters of vacancies can also occur (**Figure 3c**). The empty volumes create internal stress that

results in disturbed areas in the lattice (**Figure 3d**). The formation of cracks (**Figure 3e**) occurs during the drying of wet ordered PhC structures upon shrinkage of the colloidal crystalline lattice. A recent review article provides detailed discussions on defects in colloidal PhCs.[66]

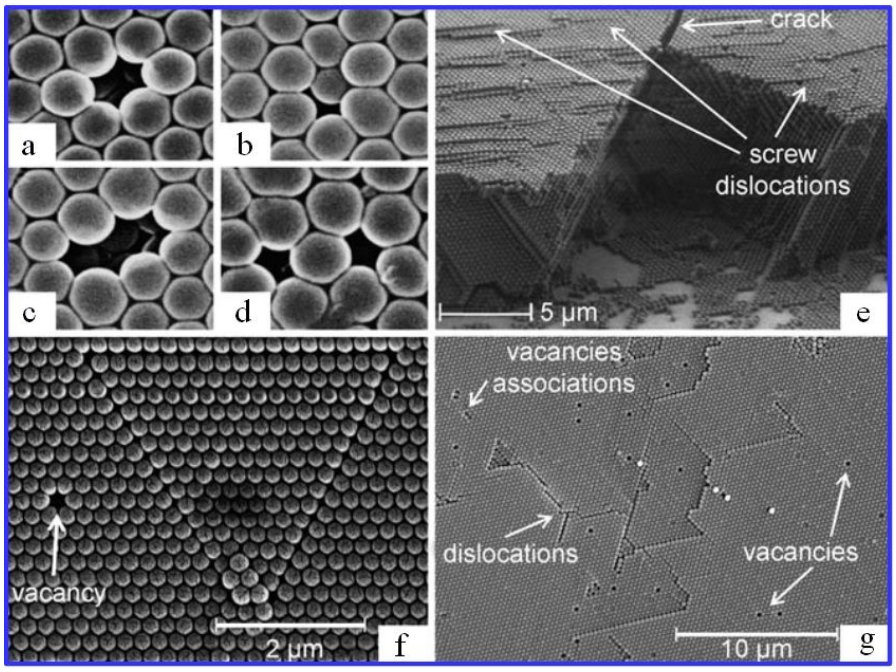

Figure 3. Examples of defects in self-assembled CCs. SEM images showing point defects: **(a)** vacancy, **(b)** Frenkel defect; **(c,d)** SEM images of vacancy associations; **(e)** a crack and screw dislocations; **(f)** SEM image showing screw dislocations running into the page and forming typical triangular features; **(g)** SEM image of a (111) plane displaying different defects (sedimented sample). The finite-length lines can be attributed to a section of the observation plane with ribbons penetrating this plane at a certain angle. Reprinted from *Angewandte Chemie International Edition*,[66] copyright 2009 Wiley-VCH Verlag GmbH & Co. KGaA.

The aforementioned defects are spontaneously formed during CCs self-assembly. As a matter of fact, defects can also be intentionally fabricated. In PhCs, it is believed that the imperfection of PhCs rather than their perfection provides them with interesting properties. The design of specific functional defects in 3D PhCs have developed into a hot research topic called "defect-engineering" in PhCs, which has been reviewed in previous literature.[105, 106] The reader is referred to these two excellent review papers for fundamental aspects as well as practical applications of defect-engineering in PhCs. In the following sections, we will introduce the theoretical and experimental studies on the intrinsic defects, which occur during and/or after the self-assembly process, and summarize the approaches developed to avoid or minimize these defects in self-assembled colloidal PhCs.

3. Fundamentals of self-assembly route to CCs

3.1. Mechanisms of defect formation and key factors affecting CCs quality

Spontaneous defects, which are inherent in all types of opaline CCs, are caused by a wealth of reasons. For example, localized lattice distortions or vacancies can result from the utilization of polydisperse building blocks in self-assembly. Besides, defects can generate during the self-assembly of colloidal particles for entropic reasons and inadequate times of lattice optimization (kinetic effect).[107]

Cracks have a considerable influence on scattered light with a wavelength smaller than the lattice constant of the CCs. The formation mechanism of cracks, however, has been argued for many years because of the complexity of the self-assembly process.[108] In preliminary studies, it was believed that cracks occurred as a result of the solvent evaporation during the assembly process.[109-111] Later, progressive studies confirmed that cracks mainly formed at the drying stage to release the tensile stresses.[112, 113] To date, researchers generally believe that, during the self-assembly and the drying stage of the fabrication of opaline CCs, the drying induced shrinkage of colloidal particles constrained by a rigid substrate gives rise to capillary stresses, which leads to the formation of cracks. The conditions for the fabrication of inverse opals are a little bit more complicated. The cracks can also form during the infiltration step and the calcination step in the fabrication of inverse opaline CCs.

Tremendous efforts have been devoted to understanding the mechanism on how drying films crack, and there is much disputation on the origins of cracks formation, with many competing mechanisms proposed.[111, 114] The fundamental question stems from what stress induces the colloidal film to crack. Dufresne and co-workers found that the evolution of the compaction front restricted the crack growth, which was regulated by an equilibrium of evaporation and fluid flow at the drying surface.[111] Moreover, the cracking film was wet, except at the position of cracks, indicating that the capillary forces were unambiguously accountable for the film failure. Lee and co-workers compared the experimental spacing between cracks with predicted values based on a model by assuming an equilibrium between the released elastic energy and the consumed surface energy.[110] They introduced a new scaling for the spacing between cracks in drying dispersions, which was related to the solvent flow distance for capillary stresses relief. It was found that the capillary pressures, generated by packed particle fronts horizontally traveling across films, resulted in the failure in dried films. In another study, Tirumkudulu *et al*. utilized colloidal particles of diverse radii to investigate conditions when capillary stresses normal to the film elastically deformed the particles and generated tensile stresses in the plane of the film.[115] In their experiments, the films cast from nanoparticle dispersions generated tensile stresses. The films eventually became transparent even when water is absent, implying that van der Waals forces can contort the colloidal particles. They further calculated the critical stress at cracking and the concomitant crack spacing, which was consistent with the observed values. Zhou *et al.* conducted a

computational study on the changing capillary in order to obtain a refined approach to controlling the growth of CCs.[116]

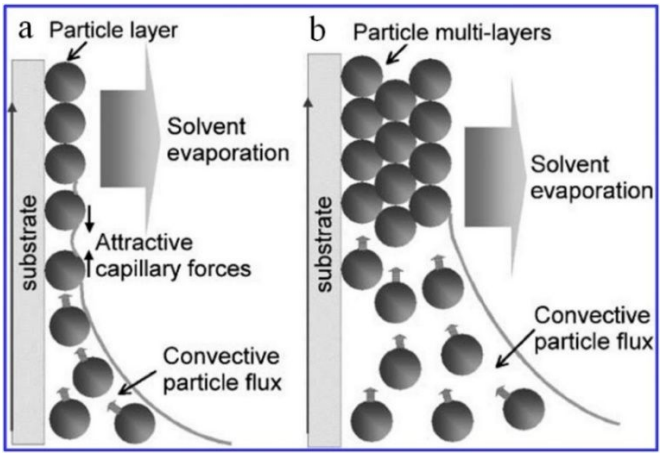

Figure 4. Schematic illustration showing the mechanism of self-assembly of colloidal particles in the vertical deposition method in the case of **(a)** single- and **(b)** multi-layer colloidal crystal arrays. Reprinted from *Soft Matter*,[117] copyright 2005 Royal Society of Chemistry.

Self-assembly approaches to PhC films possess their own unique features among various film formation processes. For example, convective self-assembly is the most commonly used approach to fabricating 2D and 3D CCs.[118, 119] For the fabrication of 2D CCs, the mechanism of colloidal crystallization, i.e., convective assembly, consists of two stages. In the first stage, attractive capillary immersion forces, mediated in the solvent meniscus between the colloidal particles at the drying front, induce colloidal aggregation and initiate colloidal crystallization (**Figure 4a**). In the second stage, solvent evaporation from the preformed ordered colloidal arrays generates a convective colloidal particle flux from the bulk of the colloidal suspension to the drying colloidal particle layer. The monotonic formation of 2D colloidal arrays is highly dependent on the intricate equilibrium between the capillary forces and the convective flux of colloidal particles in the course of solvent evaporation.[120] With respect to the self-assembly of 3D CCs, the process of convective transfer of colloidal particles from the bulk of the suspension to the thin wetting film is dominant (**Figure 4b**). The evaporative solvent loss drives the colloids towards the drying zone of the colloidal film. In the drying zone, colloidal particles are compressed towards the front of the crystal by the solvent influx, which percolates through the cavities of the colloidal crystal arrays.[118] Capillary bridges between particles are formed during the solvent evaporation from the colloidal drying film. These bridges impose strong attractive capillary forces that can generate cracks in the dried colloidal films.

In a typical self-assembly process, solvent evaporation from a thin film of colloidal suspension on a non-deformable substrate concentrates the sub-micron colloidal particles into a close-packed array. With further

evaporation, the liquid meniscus at the top layer of the particle network exerted a compressive capillary force on the colloidal particle network.[121] In general, the colloidal crystal thin film binds to the substrate and counteracts deformation in the transverse direction, generating transverse tensile stresses.[115] Soft colloidal particles are able to deform to close the pores, while for hard colloidal particles, the resulting film tends to crack in order to release the stresses. Even though many studies have investigated the cracking in a range of drying systems such as wet clays,[122-125] ceramic films,[126, 127] latex, and model colloidal dispersions,[128-130] the underlying cracking mechanism has only been explored recently.[110, 111, 115] For example, it has been observed that only above a critical film thickness, cracks nucleation occurs spontaneously, regardless of particle size and hardness. The reason lies in that the elastic energy recovered by cracking in thin films is not adequate to propagate a single crack.

The types of solvents and solvent evaporation are believed to be vital in the formation of CCs via a vapor induced self-assembly process. Routh and co-workers investigated the mechanism of the nonuniformity of latex films drying on a substrate.[109] A drying front separated fluid domains from solidified regions when it passed across the film. A total mass balance offered a solution for tremendous capillary pressure, and the positions of the fronts were determined by the maximum capillary pressure. Therefore, selective or non-uniform evaporation may result in irregular crystalline structures**.** The drying process was found to be a crucial factor in forming cracks in the study of Dufresne and co-workers. They investigated the dynamics of fracture in colloidal SiO_2 drying films.[131] During the drying process, a liquid-saturated elastic network of particles formed as water evaporated from the nanoparticle dispersions. In the meantime, cracks formation occurred to relieve drying-induced strain. The discrete motion of these cracks was caused by aging of the elastic network and the distortion of arrested crack tips. The evolution of a single crack is widespread, depicted by the viscous dissipation rate of the interstitial fluid and the balance of the driving elastic power with the total interfacial power. The Norris group investigated the underlying issues in the self-assembly of CCs. They revealed that the solvent flow could play a pivotal role in controlling the formation process.[132] Therefore, different preparation methods and solvents are expected to generate different types and amounts of defects. Marlow and co-workers determined the factors influencing the quality of CCs in a capillary deposition method by examining the solvent effects on the fabrication of CCs from polystyrene (PS) colloidal spheres suspensions.[133] They also optimized the solvent mixture for the fabrication of high-quality PhCs (opals) film. The influence of dispersive media was further proved by another independent study,[134] in which Míguez *et al*. employed volatile solvents to fabricate high-quality CCs via a spin-coating method.

Apart from solvent, there are many other factors that may affect the quality of CCs, such as humidity and temperature. In order to fabricate high-quality CCs, Meng *et al.* investigated the effects of different parameters on the quality of final CCs, including colloidal particle size, volume ratio, evaporation temperature, relative humidity, and the ultimate drying conditions using a cooperative assembly method.[65] Among these factors, the temperature was found to be the most important one. Moreover, the capability of controlling and maintaining the desired temperature is as significant as the chosen temperature. Temperature fluctuations can cause the formation of exceptionally low-quality samples. The quality of the thin films has been improved by raising the temperature to an optimum value of 50 °C at low values of a relative humidity of 30%.[65] In a similar study, using PS spheres of 300 nm in diameter, Kuai *et al*. optimized the self-assembly conditions to fabricate highly ordered CCs. It was found that a 0.1-0.2% volume fraction, an evaporation temperature of ~ 60 °C, a relative humidity of 80-90%, and a quasi-equilibrium drying process were suitable to obtain high-quality CCs.[113] However, this observation contradicts the previous understanding that high-quality CCs can only be obtained at low relative humidity even though the same method was applied. It should be noted that all the optimized conditions mentioned above are only valid for the given methods and solvents.

From the above studies, it seems that various factors may influence the density of cracks in a self-assembly process. Cracks generally are formed upon lattice shrinkage during the drying of wet CCs. However, Marlow and co-workers claimed that cracks seem to be notably independent of other parameters, such as temperature, the nature of the building blocks, or dispersive media.[66] Meng *et al.* found that no change in the cracking direction when varying growth temperature, although temperature, among all different preparation conditions, was identified as the most significant factor in the self-assembly of colloidal spheres.[65] It is noteworthy that their claims are only valid for a vertical deposition process, not applicable to other kinds of self-assembly methods.[135] For instance, in one recent study conducted by the Zhao group,[135] the composition of solvent was found to significantly affect the direction of cracks in a horizontal deposition method.[136] Marlow and co-workers also indicated that the composition of solvent could affect the cracks formation of self-assembled CCs by using a capillary deposition method.[133]

In summary, various factors were found to affect the quality of CCs prepared via self-assembly. It is possible to fabricate 'perfect' high-quality CCs in a relatively large domain once these factors are optimized. Defects of vacancies and faults can be removed easily through improving the monodispersity of colloidal particles, which in turn improves the crystallinity of CCs. However, the control of the crystallinity of CCs is more complicated since it involves complex self-assembly thermodynamics. Woodcock's calculation indicated that *fcc* and hexagonal

closed-packed (*hcp*) crystal structures might co-exist in the resulting CCs due to the negligible entropy difference.[107] The most serious and common defects, such as cracks, however, cannot be avoided entirely. The investigation of cracking formation may provide alternatives for the fabrication of high-quality CCs without defects. Nowadays, it has been identified that cracking mainly arises from capillary stress, which is developed from drying-induced shrinkage of colloidal particles and a rigid substrate imposed constraint on this shrinkage.[137] Hence, the avoidance of the crack formation in the resulting films can be achieved by either entirely eliminating the restrictions of the substrate imposed on the film or completely preventing latex shrinkage. Based on the cracking mechanism, a lot methods have been proposed to avoid cracking in the self-assembly processes of PhC films.

3.2. Self-assembly of CCs with cPBG *in silico*

The PBG properties of self-assembled CCs with *fcc* structures are sensitive to various defects. Therefore, high-quality perfect CCs are necessary for high-performance optical devices. Moreover, 3D PhCs with a cPBG are potentially useful for low-loss waveguides, optical microcircuits, thresholdless lasers, etc.[3] CCs with *fcc* structures obtained by self-assembly of colloidal spheres are not well-suited to generate PhCs with a cPBG due to degeneracy in the photonic band structure caused by the spherical symmetry of the lattice points. Under certain conditions, inverse *fcc* crystals (air spheres) exhibit a cPBG,[138] but the bandgap opens between 8th and 9th bands, making it difficult for optical applications. In addition, to open a cPBG in inverse *fcc*, it requires materials with higher refractive index contrast. The bandgap opens up when the refractive index of the materials is about 2.8 times of the background.[139] The narrow relative bandgap width[34] ($\delta = \frac{\Delta f}{f_c} = 0.05$, Δf is the bandgap width, f_c is the central frequency of the PBG) makes it vulnerable to disorder and crystal defects.

An alternative to constructing advanced optical devices is to produce CCs whose PBGs are wider and less sensitive to imperfections, such as cubic diamond structure CCs.[88, 138] Calculation showed that colloidal diamond crystals and pyrochlore crystals exhibit a complete and wide PBG and can be achieved at a refractive index contrast of 2 (**Figure. 5a**).[140] Moreover, inverse diamond crystals have an even wider PBG **(Figure. 5b**, $\delta = 0.20$). Although the bandgap width of pyrochlore can be optimized to some extent,[141] it is still narrower compare to colloidal diamond.[142] A lot of simulation work has been dedicated to model self-assembly routes to fabricate different types of CCs (mainly diamond and pyrochlore structures) with the ability to open cPBG at low refractive index contrast, which will be discussed below.

Diamond and pyrochlore share the same symmetry (Fd_3m) in space groups. A great deal of research has been devoted to self-assembly of colloidal diamond as the colloidal diamond network is one of the best candidates for PhCs with a cPBG. It is important to distinguish between cubic diamond and hexagonal diamond, which can be differentiated by the way each particle is linked to its four neighbors. In cubic diamond, all the four neighbors are connected in the staggered conformation. In hexagonal diamond, three of the four neighbors are connected in the staggered conformation, and the fourth is connected in the eclipsed conformation.[38] Colloidal cubic diamond has a cPBG, whereas colloidal hexagonal diamond does not. Therefore, to self-assemble colloidal cubic diamond, it is important to design particles with tetrahedral valence (just like sp^3 carbon atoms), which favor the staggered conformation.[143]

Nelson pioneered the concept of colloidal particles with tetrahedral valence .[144] In this particle design, the tetrahedral valence came from four topological defects on a nematic liquid crystal droplet. Later on, based on the experimental realization of colloidal tetrahedral clusters,[145] Zhang *et al.* provided another particle design and showed that these tetrahedral clusters could self-assemble into colloidal diamond,[146] but it required an interaction that prefers the staggered conformation. In 2012, Pine and co-workers[44] synthesized colloidal particles with valence, which were referred to as patchy particles. The experimental realization of patchy particles offers a versatile platform for computational studies toward the colloidal diamond. However, it was soon discovered that for self-assembling colloidal diamond by patchy particles, the size of patches should be significantly small.[147] Otherwise, random aggregates rather than diamond are thermodynamically stable.[148] That means, if tetrahedral patchy particles have big patches, the diamond region in the phase diagram disappears **(Figure 5c,d),** and they can never crystallize into the colloidal diamond. Although tetrahedral patchy particles with small patch sizes can be fabricated by colloidal fusion,[149] they were predicted to produce a mixture of cubic and hexagonal diamond as there is no selection between staggered and eclipsed conformation.[150] In the simulation, the selection of cubic diamond can be achieved via layer-by-layer assembly of tetrahedral patchy particles[151] or using particles with different sizes and different affinity of interaction.[152]

In addition to tetrahedral patchy particles, other types of colloidal particles can also self-assemble into CCs with diamond symmetry *in silico*. Romano *et al.* designed tri-block Janus particles with two triangle patches.[153] There are two different cases: two triangles are eclipsed (the projected triangles overlap) or staggered (the projected triangles form Star of David). It showed that when patches are large to bind with three other particles at the same

time, Janus particles with staggered triangle patches self-assemble into colloidal tetrastack (also known as pyrochlore). Similarly, Chakrabarti and co-workers designed tri-block Janus particles that have two circular patches but are different in size and have a hierarchy of interaction strengths.[42] They obtained cubic diamond and body-centered cubic crystals via distinct clusters of uniform size and shape. They further showed that a cascade of well-separated associations tetrahedral clusters and tetrastack crystals could further suppress the formation of five- and seven-membered rings that hinder the formation of crystals because only six-membered rings exist in crystals with diamond symmetry.[43] More recently, Chakrabarti and co-workers investigated the self-assembly of di-patch colloidal rods into colloidal diamond, which is robust to stacking faults.[154]

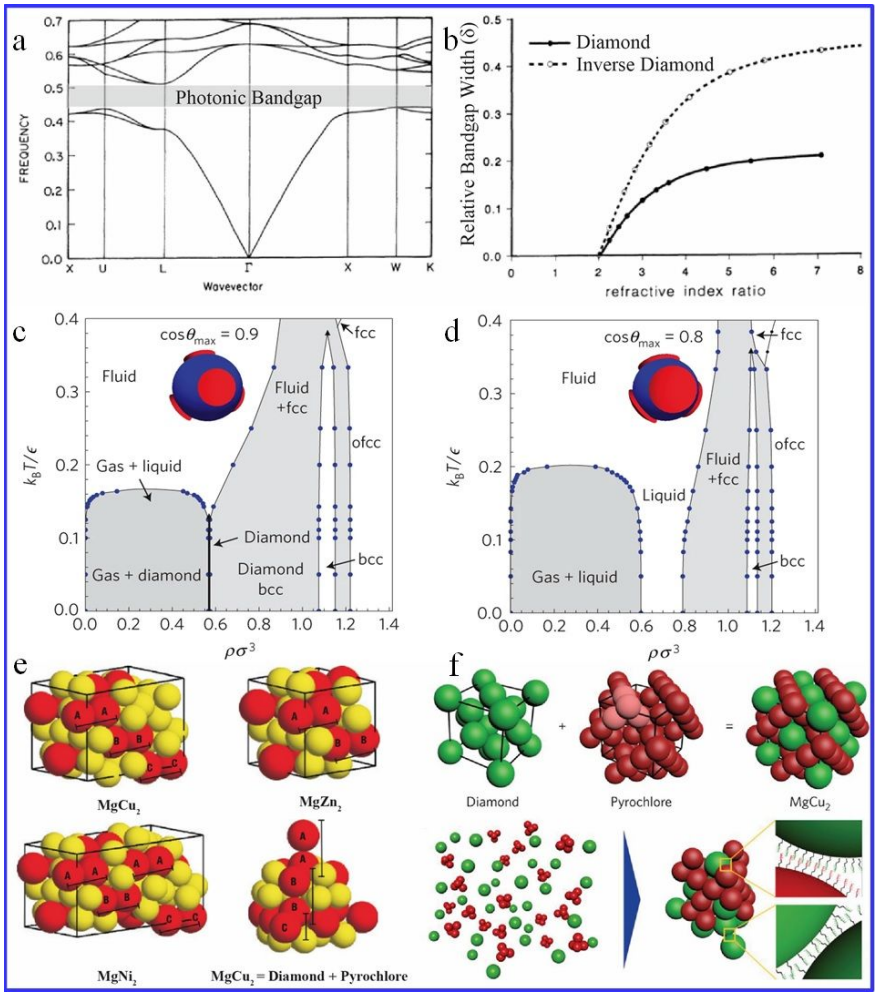

Figure 5. (a-b) Band diagrams of direct and inverse colloidal diamond. **(a)** Calculated photonic band structure for a diamond dielectric structure consisting of dielectric spheres of refractive index = 3.6 in an air background. The frequency is given in units of *c/a*, where *a* is the cubic lattice constant of the diamond lattice, *c* is the speed of light. **(b)** Relative bandgap width (δ) for both direct (solid line) and inverse (dashed line) colloidal diamond lattice. The relative bandgap width $\delta = \Delta f/f_c$, where f_c is the central wavelength of the PBG and Δf is the width of the PBG. Reprinted with permission from *Physical Review Letters* [140] copyright 1990 American Physical Society. **(c-d)** Phase diagram of patchy colloids with different patch sizes. Phase diagrams in the dimensionless density ($\rho\sigma^3$) - temperature (k_BT/ϵ) representation. Patch size is characterized by the opening angle 2θ. It shows that when patches are large, the diamond region in the phase diagram disappears.[147] Reprinted with permission from *Nature Physics*,[147] copyright 2013 Springer Nature.**(e-f)** Binary Laves crystal structures. **(e)**

A family of Laves phase can be produced by bi-dispersed colloidal particles with a certain size ratio. Large spheres are red and small spheres are yellow. $MgCu_2$ superlattice is the only structure that contains cubic diamond as a sublattice. Reprinted with permission from *Nature Materials*,[41] copyright 2007 Springer Nature. **(f)** Colloidal alloys with preassembled clusters and spheres. By grouping the spheres in the pyrochlore lattices into tetrahedral clusters, it only produces $MgCu_2$. Tetrahedral clusters (red) and spheres (green) interact via DNA-mediated interaction. Reprinted with permission from *Nature Materials*,[155] copyright 2017 Springer Nature.

An alternative route to colloidal cubic diamond is to make a Frank-Kasper phase in which cubic diamond is one of the sublattices. In particular, Hynninen *et al.*[41] pointed out an $MgCu_2$ superlattice (a class of Laves phase) has two sublattices: pyrochlore and cubic diamond, and they discovered that the $MgCu_2$ superlattice could be produced by bi-dispersed colloidal particles with a certain size ratio (**Figure 5e**). However, one of the disadvantages is that their system will form a whole family of Laves phase ($MgCu_2$, $MgZn_2$, and $MgNi_2$) where $MgCu_2$ is the only structure that has the desired cubic diamond sublattice. The selectivity of $MgCu_2$ can be achieved by grouping the spheres in the pyrochlore sublattice into preassembled tetrahedral clusters.[155] The new system contains tetrahedral clusters and single spheres with a certain size ratio. They interact via complementary DNA sticky ends and self-assemble into $MgCu_2$ superlattice only (**Figure 5f**). Calculation further showed that both diamond and pyrochlore sublattices possess a cPBG.[141, 142] Furthermore, using computer simulations, Dijkstra and co-workers[156-158] investigated the fabrication of colloidal Laves phase via sedimentation and mapped out the phase diagram. Because diamond crystals have a low volume fraction (34%), the strategy of making a Frank-Kasper phase solves the low-packing-density problem, but how to remove one of the sublattices has yet to be demonstrated.

In simulations, the self-assembly of colloidal diamond does not limit to colloidal spheres. Truncated tetrahedra can self-assemble into colloidal diamond,[159] but due to the high volume fraction of the resulting crystals, it is not clear whether this structure has a cPBG. Because of the crystallinity, the cPBGs are highly anisotropic, a possible drawback for many applications.[160] Since the PBG in a diamond crystal is robust to disorder and crystal defects, both ordered and random tetrahedral networks form by tetrahedral jacks can produce a cPBG.[161-163] The synthesis of tetrahedral jacks has been realized experimentally,[38, 149] but how to assemble them and extract them from a colloidal suspension remains a challenge. Hyperuniform materials can also have a cPBG, and the advantage is that it can offer an isotropic cPBG.[160]

Colloidal diamond has served as the holy grail of colloidal self-assembly. Very recently, He *et al.* demonstrated self-assembled colloidal diamond.[38] They designed a particle interlock mechanism so that particles intrinsically carry the rotational information that can select the staggered conformation, which is required for colloidal cubic

diamond. The calculation showed the inverse lattice exists a cPBG. The fabrication of CCs uses DNA-mediated interaction, which will be discussed in detail in **Section 4.1.7.**

4. Fabrication of high-quality CCs in large areas

In this section, we will summarize various methods developed to fabricate large-area, high-quality CCs, CCs with the symmetries to open a cPBG, and shed light on the working principle of these methods. In particular, the first part is mainly on the fabrication of opaline and cubic diamond structures, while the following part is focused on the fabrication of inverse opaline structures. Finally, typical approaches to the fabrication of high-quality 2D CCs in large-area will be reviewed in the last section. In addition, some other novel methods of fabricating unique PhC structures will be included in this section as well.

4.1. Fabrication of high-quality 3D PhCs in large areas

The fabrication of crack-free 3D PhCs in the large area usually takes similar strategies with those techniques to suppress cracking of drying colloidal films, which generally target the three prominent elements during the colloidal PhC film forming process. These elements are, (i) adjusting the colloidal suspension chemistry, (ii) manipulating the drying mechanism, and (iii) customizing the substrate properties.[100, 164, 165] The alteration in the suspension chemistry leading to an increase in the film strength, is usually achieved via the addition of surfactants,[166, 167] plasticizers,[168] polymeric binders,[168, 169] sol−gel precursors,[170-172] or by inducing the flocculation of particles[137, 167-169] within the suspension, or by complete restraint of the shrinkage of the latex particles to rule out the tensile stress generated during drying.[173] The control over the drying mechanism by supercritical[174] or humid[175] drying methods can decrease the stress placed on the colloidal particles network from the gas–solvent interfacial tension. The adjustment in the mechanical properties of the substrate through the utilization of deformable,[126] or specially surface-patterned substrates for favorable orientation in the low-density stacking crystal face via the template-assisted self-assembly,[176] or via the alternation of the film−substrate interface to actuate particle−substrate slip,[126, 177, 178] alleviates the stress induced by the air−solvent interface on the drying colloidal particles arrangement, or using a fluid substrate to maintain the free contraction of latex without limitation.[179] In addition to the above three prominent elements of the film−forming process, tailoring the chemical nature of the colloidal particles can also help to achieve high-quality PhC films.[91, 92, 180, 181] All of these approaches have been

reported to fabricate films with a thickness of several folds of the critical thickness with a given colloidal particle and solvent. However, it should be noted that some of these methods may make the film fabrication complicated and potentially lose their functionality.[182]

4.1.1. External forces method

External forces induced by, e.g., electric field, magnetic field, shear effect, and infrared heating, can be applied to improve the quality of CCs. While self-assembly of colloidal particles purely driven by capillary force is the most effective approach to CCs of different sizes, the ability to modulate the interparticle interactions during colloidal assembly provides an additional degree of freedom to prepare high-quality CCs.[183] Introducing external forces also enable efficient control over the positional and orientational orders of building blocks, which is expected to anneal out existing defects and leads to perfect CCs in a considerably large scale. Since the CCs are driven by external forces, maintaining a uniform force field is critical to prepare large-area crystals. One characteristic of this approach is that it needs additional setups to direct the colloidal assembly process. This may increase the cost of CCs in practical applications. Besides, the scale of as-prepared CCs is largely limited by the uniformity of the force fields. In the very early stage, researchers developed a number of approaches based on external forces to improve the quality of the CCs. These methods are generally based on the treatment of the building blocks prior or post self-assembly, including melting compression,[184] heat treatment,[173] shearing induces[185] and so forth.

Ruhl *et al*. reported a method to fabricate high-quality CCs without cracks, which is on the basis of shear flow in the melts of polymer core@shell latex spheres.[184] In brief, polystyrene-polymethylmethacrylate-polyethylacrylate (PS-PMMA-PEA) latex colloidal spheres with a hard crosslinked core and an elastomeric grafted-on shell were firstly synthesized. Then the latex spheres flowed at elevated temperatures under uniaxial compression, much like other polymer melts. The lattice was macroscopically oriented by the radial melt flow in order to make each radial sector of the opal disk form a monodomain crystalline. Using this method, opaline CCs were produced in wafer-scale (**Figures 6a-c**). The process is fast and can produce films with different thicknesses in large-area, where the latex spheres are crystallized in *fcc* structure.[184, 186] In addition, injection molding, extrusion, and other large-scale polymer processing techniques were also applied to produce opaline CCs.[187] One drawback of the melt flow method is that the CCs films contain a disordered center layer. The advantage, however, is that large-area CCs can be easily produced with a macroscopically oriented *fcc* lattice.

In an independent study, an air-pulse-driven technique was developed by Kanai and co-workers to fabricate

CCs on a large-scale.[188] In this study, pulse pressure generated from a compressed air can precisely control the flow strength, which can effectively preserve the excellent crystalline quality by the steady stop of the shear flow (**Figure 6d**). Consequently, a single domain crystal with angle-dependent structural colors was obtained upon the pulse pressure exceeded a critical value (**Figure 6e**). It was found that the colloidal crystal texture, which formed in the capillary, was a sensitive function of the air pressure. Beyond a critical pressure, the whole capillary exhibited an identical single-domain texture. In this method, the tensile generated during self-assembly was released by the complete constraint of the shrinkage of the latex particles. This method is readily applicable to industrial processes for mass production.

Moreover, a shear-induced organization of polymer opals was utilized to fabricate crack-free 3D CCs.[185] The polymer opals consisted of a coherently ordered "super-domain" characterized using a radial director vector and showed anisotropic photonic behavior, which depended on the relative vectorial orientation of strain and director.

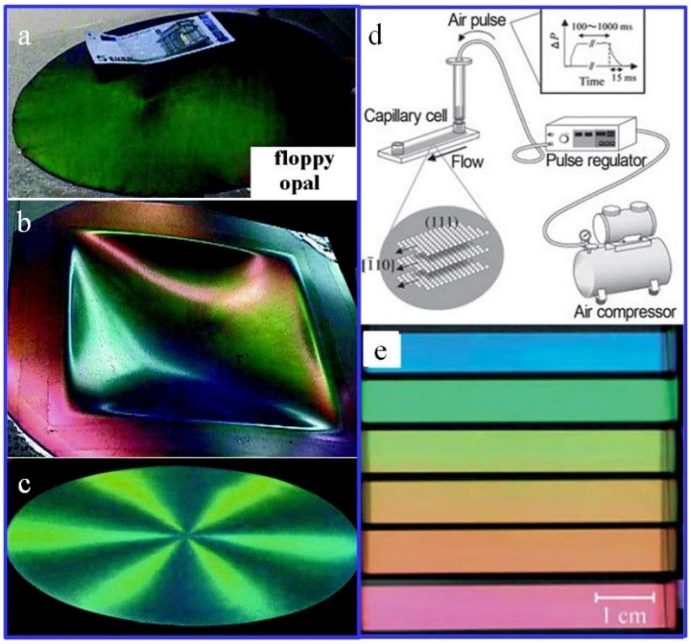

Figure 6. Colloidal crystal opal films fabricated with melt compression: **(a)** green (with a 5€ bill, to indicate the size of the film), **(b)** red on a polycarbonate relief foil and **(c)** an opal film from very large latex spheres, which reflects light only in six radial sectors due to the reflection from (220) planes. Reprinted from *Polymer*,[59] copyright 2003 Elsevier. **(d)** Scheme of air-pulse-driven flow for the fabrication of CCs. **(e)** Photograph of the CCs without cracks. Reprinted from *Advanced Functional Materials*,[188] copyright 2005 Wiley-VCH Verlag GmbH & Co. KGaA.

4.1.2. Template-directed method

The substrate mechanical properties can be tailored, by utilizing deformable or surface-patterned substrates, or by altering the interface of film−substrate to induce particle-substrate slip, which can relieve the stress on the

drying colloidal particles arrangement exerted by the solvent−air interface. The template-directed method and epitaxial method were developed based on these principles and proven to be effective and versatile in the fabrication of crack-free or monocrystalline structures. One dramatic benefit associated with the use of templates is the flexible choices of various templates with different patterns and features. These interesting templates can be readily fabricated in an extremely large scale by many well-established methods, such as photolithography and soft lithography.[189] The interaction between templates and colloidal particles is beneficial to the production of crack-free CCs, with cracks being normally observed in many free drying assembly processes. It also enables the design of exposed facets of the assembled CCs if templates of specific surface features are used to deposit colloidal particles. A noticeable example is the preparation of (100)-orientated CCs.[190, 191] Several influential factors, including the ratio of diameters of the colloidal particles to the size of the pattern, the depth of the pattern and so forth, were investigated systematically, which was summarized in a recent review article.[117] Here, we focus on the fabrication of high-quality defect-free CCs with the template-directed method.

van Blaaderen *et al*. pioneered the template−directed colloidal crystallization (**Figure 7a**).[192] They deposited colloidal particles onto a patterned substrate (or template) via slow sedimentation, which could direct the crystallization of bulk CCs, and also tailor the orientation, lattice structure, and size of the resulting crystals (colloidal epitaxy). It was suggested that colloidal epitaxy would open new avenues for the design and fabrication of materials based on CCs and also enable quantitative investigation of heterogeneous crystallization in real space.

By designing two specific patterns on a substrate, CCs with different orientations can be fabricated. In a separate study, using patterned silicon substrates, *fcc* (111)-orientated 2D and 3D crack-free SiO_2 CCs were fabricated through a modified vertical deposition method. In this study, Cai and his colleagues investigated the influences of surface properties of substrates and the colloidal suspension concentration on the self-assembly (**Figure 7b**).[193] SiO_2 colloidal particles self-assembled into 2D CCs on a hydrophobic substrate while 3D SiO_2 CCs formed on the hydrophilic substrate under identical conditions. The number of layers of CCs grown on the patterned substrate monotonically increases with the concentrations of the colloidal particle suspensions. This study indicates that the template-directed vertical deposition method can allow the formation of crack-free well-ordered 3D CCs in a large area. The reasons for the formation of crack-free CCs are two folds. On the one hand, the patterns can direct the growth of CCs along the substrate surface. On the other hand, the patterns can restrict the alignment of SiO_2 spheres and release the tensile stress generated during self-assembly.[194]

In addition to (111)-oriented CCs, 3D CCs with other crystalline orientations can be fabricated as well. Using

a template-assisted self-assembly method, Jin *et al.* fabricated cubic (100)-oriented 3D crack-free PhCs.[176] The key factor of this method is the design of a patterned substrate. The fabricated (100)-oriented 3D opaline PhCs thin film exhibited no cracks over areas without intrinsic size limit via a modified template-assisted colloidal self-assembly approach (**Figure 7c**). It is believed that this technology can potentially produce large-area single-crystalline PhCs, which can be used for optoelectronic devices.

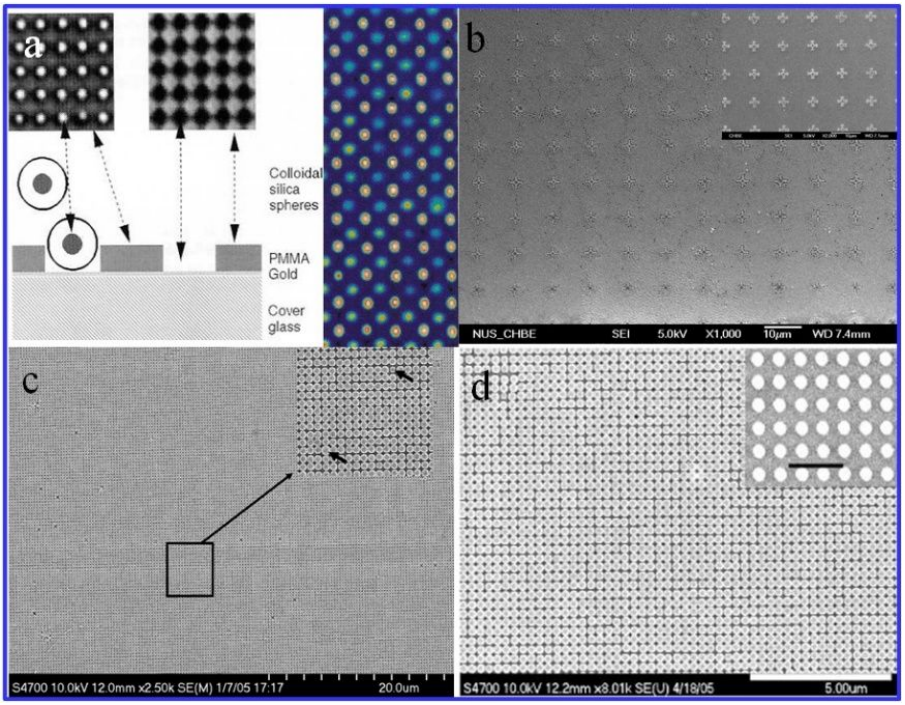

Figure 7. (a) Scheme of the colloidal epitaxy procedure (bottom) and two confocal micrographs (top) showing the fluorescently labeled polymer template (left), and local crystal plane symmetry of crystals grown on *fcc* (100) planes (right). Reprinted from *Nature,*[192] copyright 1997 Springer Nature. **(b)** SEM image displaying a (111)-oriented crystal grown on a patterned template. The inset SEM image showing the cross-like pillar patterned substrate. Reprinted from *The Journal of Physical Chemistry C*,[193] copyright 2011 American Chemical Society. **(c)** SEM images of a (100)-oriented crystal grown by the template-assisted colloidal self-assembly. A crack-free crystal on a large-scale can be observed. The magnified view with arrows (inset) displaying the abnormally large and small spheres. Reprinted from *Nano Letters*,[176] copyright 2005 American Chemical Society. **(d)** SEM image of the (001)-oriented PhC grown on the template. Inset: An enlarged SEM image of the pattern with a pillar spacing of 308 nm and the scale bar of the inset is 800 nm. Reprinted from *Journal of Applied Physics*,[195] copyright 2006 American Institute of Physics.

The template-directed self-assembly method is also versatile in the fabrication of PhCs with various orientations through varying the topology and periodicity of the template. Jin and co-workers reported the fabrication of a crack-free (001)-oriented 3D periodic PhCs using PS colloidal spheres as building blocks through a modified template-assisted self-assembly method.[195] The structure analysis revealed that this was a (001)-oriented face-centered tetragonal PhC, which showed different optical properties from those cubic structures. The spectroscopy study indicated a larger blue shift in the photonic stop band of the crack-free (001)-oriented PhCs

comparing with the same cubic structure oriented along the (001) direction (**Figure 7d**). Moreover, the template-directed self-assembly method is also versatile to fabricate complex and functional photonic structures. Yin and Xia *et al*. demonstrated the versatility of this template-assisted self-assembly method to prepare various complex and controllable photonic nanostructures.[196-198] They reported the capability and feasibility of the template-assisted self-assembly approach to organizing the PS or SiO_2 colloidal spheres into polygonal and polyhedral clusters, zigzag, linear and spiral chains, as well as circular rings.[198]

Song and co-workers presented an approach to the self-assembly of centimeter-scale CCs with narrow stop-bands on superhydrophobic substrates with low adhesion capacity (**Figure 8**).[199] The narrow stop-bands of CCs can be attributed to the synergetic effects as a result of the thick CCs, highly ordered crystalline structure, large-scale crack elimination, and a reduced void fraction. These excellent features can be ascribed to a special self-assembly process on the superhydrophobic substrate with low-adhesivity (**Figure 8a and b**). First of all, the latex colloidal suspension exhibited a diminishing three-phase contact line during evaporation on the substrate, which led to a release of tensile stress in time actuated by latex shrinkage. This resulted in complete inhibition of cracks as well as a more closely-packed structure in the CCs on the substrate (**Figure 8a**). Secondly, a highly ordered crystalline colloidal structure was formed as a result of the simultaneous crystallization of latex colloidal particles on the outermost layer of a spread liquid film (**Figure 8b and c**). Furthermore, the low-adhesive substrate allowed sufficient time for the solvent to evaporate and the latex to self-assemble, which promoted the formation of highly ordered structures during the rapid evaporation of the latex suspension. This simple approach to fabricating centimeter-scale CCs with narrow stopbands is significant for the fabrication of novel optical devices.[199] However, the complexity in designing a superhydrophobic substrate and the cost of developing such a superhydrophobic substrate may hinder its potentials for mass production of CCs.

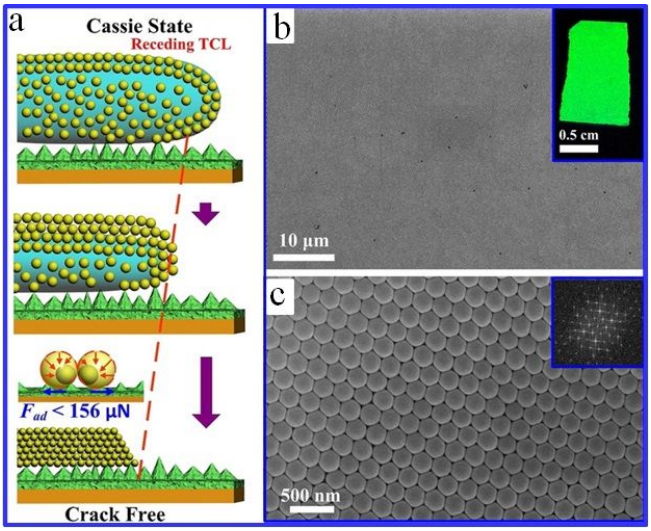

Figure 8. (a) Scheme of colloidal PhCs assembled on low Fad superhydrophobic substrate CCs with narrow photonic stopbands assembled from low-adhesive superhydrophobic substrates. **(b-c)** SEM images of the as-prepared colloidal PhCs with a diameter of 224 nm assembled on the low-adhesive superhydrophobic substrate. Inset in **(b)** is a photograph of the PhCs, with a scale bar of 0.5 cm. Inset in **(c)** is a Fourier format (FFT) image acquired from a large-area SEM image. The SEM images show perfectly ordered latex arrangement and assembled close-packed PhCs structures. Reprinted from *Journal of the American Chemical Society*,[199] copyright 2012 American Chemical Society.

Curvature surface of a glass vial can relieve shrinking stress during the drying of colloidal films. Recently, Jiang *et al.* presented the rapid fabrication of centimeter-scale 3D colloidal crystal belts through a vertical deposition method. This approach enabled the formation of centimeter-scale CCs by taking advantage of the curvature surface and negative pressure of a glass vial. In this method, the curvature accounted for the control of the dimension of the resulting colloidal crystal belts, while the well-tuned negative pressure was responsible for the rapid preparation of well-ordered colloidal crystal belts. The closed packing feature of colloidal crystal belts can be attributed to strong hydrogen bonding between carboxyl groups, which were functionalized on the surface of poly (acrylic acid-co-DVB80) colloidal particles.[200] Unfortunately, this method does not avoid the formation of cracks.

Kim *et al.* developed a method combining the merits of both an elastomeric substrate and a surface relief patterning structure to prepare crack-free 3D SiO_2 CCs.[201] In this study, a surface relief structure was firstly fabricated on an elastomeric polydimethylsiloxane (PDMS) stamp. The relief structures on the PDMS surfaces enabled the growth of colloidal crystal assemblies that cannot be accomplished on a flat PDMS substrate because of its hydrophobic surface. This approach not only provides one way for the fabrication of crack-free CCs on a soft hydrophobic substrate surface with the lift-up method but also enables the transfer of the crack-free CCs onto a curved surface.[201]

Cracking can also be eliminated by utilizing a fluid substrate, which retains the free shrinkage of latex particles.[179] The Zentel group achieved crack-free PhCs through crystallization on molten liquid gallium (Ga) substrate.[179] Using this method, Zentel and co-workers prepared crack-free 3D "monocrystals" with an extremely low defect density on a scale of millimeters. Besides Ga, mercury (Hg) surface was also used for the fabrication of PhCs. The Asher group demonstrated a facile method for the mass production of 2D PhCs by spreading PS colloidal aqueous/propanol suspension on mercury surface, which will be thoroughly discussed in **Section 4.3**.[202] Though a suitable liquid substrate can easily eliminate the lateral sticking of the substrate, it is still challenging to find a liquid substrate possessing both a moderate melting point and a low toxicity.

4.1.3. Spin and spray coating methods

As discussed above, a wide variety of methods have been developed to fabricate CCs with single- or polycrystalline domains ranging from millimeter to centimeter-size. However, these techniques take days to weeks to prepare CCs and are suitable for low volume, laboratory-scale production. It remains a challenge for scale-up to an industrial-scale mass production owing to their sophisticated fabrication processes and incompatibility to the wafer-scale batch microfabrication, which are widely used in the semiconductor industry. Furthermore, these methods result in either non-uniform CCs or uncontrollable thickness in CCs over large-area. Bearing such restrictions in mind, Jiang *et al.* developed a spin-coating method for mass-fabrication of CCs.[203, 204] The key to the mass production of crack-free CCs using this spin-coating method is to alter the suspension chemistry through the addition of a polymeric binder (triacrylate monomers), which increases the strength of the film.

There are three types of important materials that were fabricated rapidly by using this spin coating method, including macroporous polymer, CCs, and polymeric nanocomposite. Each of them was produced with high crystalline qualities and in wafer-scale sizes (**Figure 9a**).[204] In this method, the colloidal SiO_2 spheres were dispersed into triacrylate monomers. The mixture was then spin-coated onto many kinds of substrates. The shear-induced distinct order and successive photopolymerization may give rise to 3D ordered CCs, which were trapped inside a polymer matrix (**Figure 9b**). Afterward, selective removal of SiO_2 colloidal spheres and the polymer matrix resulted in the formation of three-dimensionally ordered macroporous (3DOM) polymers and large-area 3D CCs. Furthermore, the thickness of the CCs was very conformal and could be tuned simply by varying the spin time and speed.

They also extended this spin-coating method to fabricate periodic subwavelength structures, with a thickness ranging from a single layer to hundreds of layers by varying the spin-coating conditions.[205] The colloidal monolayers were further used as a template to pattern sub-100 nm pillar arrays directly on silicon substrates. This bottom-up method allows mass production of periodic nanostructures with high resolution over the optical diffraction limit, which endow them with potential for critical technological applications, including optoelectronics, high-density data storage, subwavelength optics, and biosensing.[203]

The crystalline orientations of the resulting CCs are controllable via altering the dispersion components. Mihi *et al*. developed a modified spin-coating method by dispersing the sulfonated PS and colloidal SiO_2 spheres in different mixtures of solvents, such as water, ethylene glycol, and ethanol.[134] By varying the composition of the solvent, CCs with different orientations can be obtained with this spin-coating technique.

The spin-coating method may pave a new avenue to the fundamental understanding of shear-induced melting,

crystallization, and relaxation. In addition, this spin-coating approach is compatible with standard semiconductor microfabrication and permits the mass production of microstructures for potential device applications. However, the re-dispersion procedure of highly viscous colloidal latex suspension and the use of special dispersant which can impair the resulting optical property may limit the broad applications of this technique. Moreover, the size of the resulting CCs films was confined to the top surface area of the spin-coating substrate or wafer. These restrictions force researchers to look for new solutions.

Ultrafast fabrication of CCs on a large-scale is highly desirable for real applications. Song *et al.* presented an ultrafast fabrication approach to large-scale colloidal PhCs using a spray coating method (**Figure 9c**).[206] Through this technique, CCs could be easily produced within seconds regardless of the shape or dimension of the substrate. In this method, the latex spheres were strategically designed with the hydrophobic core (PS) and hydrophilic shell (PMMA-PAA). As a result of abundant COOH groups on the surface of the latex particles, the latex particles have strong hydrogen bonding interactions, which enhanced the latex particles arrangement during the ultrafast spray procedure. This appropriate arrangement of the latex particles during the rapid spray process resulted in close-packed and well-ordered CCs. In addition, the adhesion force formed among the as-formed flexible and soft PMMA-PAA shell of latex particles facilitates the self-assembly of colloidal particles into a close-packed ordered structure. Consequently, close-packed well-ordered colloidal PhCs with bright color could be rapidly fabricated as large as 7 × 12 cm^2 within 1 min on a variety of substrates.

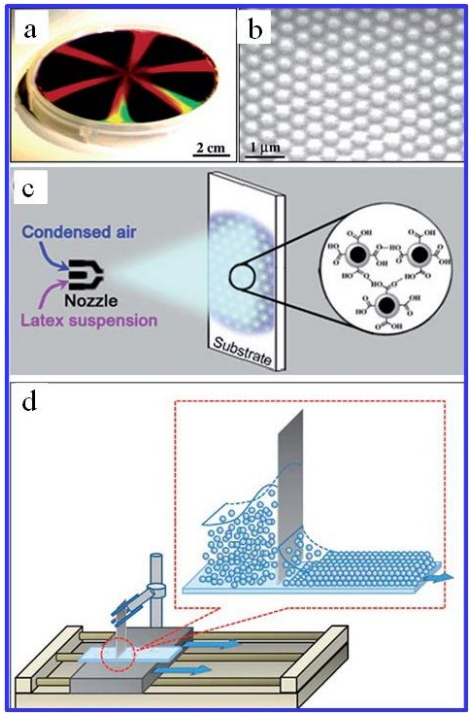

Figure 9. Representative approaches to large-scale fabrication of colloidal PhCs. **(a–b)** Spin coating. Reprinted from *Journal of the American*

Chemical Society,[204] copyright 2004 American Chemical Society. **(c)** Spray coating. Reprinted from *Macromolecular Rapid Communications*,[206] copyright 2009 Wiley-VCH Verlag GmbH & Co. KGaA, and **(d)** doctor blade coating. Reprinted from *Langmuir*,[207] copyright 2010 American Chemical Society.

A simple, roll-to-roll compatible coating technology has been introduced to produce 3D highly ordered colloidal PhCs with a doctor blade coating (**Figure 9d**).[207] In this method, a vertically beveled doctor blade is applied to align SiO_2 colloidal microsphere–monomer suspensions to create highly ordered nanocomposites in large-area within one step. In this process, capillary force is the primary driving force for colloidal crystallization. The shear-aligned crystal thickness depends on the coating speed and the colloidal suspension viscosity. The resulting 3D well-ordered structures showed even diffractive colors. This method can be further extended to the fabrication of large-area coatings for important technological applications, such as full-color displays, diffractive optics, and size exclusive filtration membranes.

4.1.4. Colloidal particles functionalization (hydrogels) assisted self-assembly

Thought Alfrey et al. first reported electronic photographs and optical properties of well-ordered PS CCs as early as 1954,[208] it was not until 1984 that Asher and co-workers reported the self-assembled 3D non-close packed (*ncp*) liquid CCs and filed the first CCs patent, which were fabricated by sandwiching monodisperse PS aqueous colloids between two quartz plates and named as "Crystalline Colloidal Arrays (CCAs)".[209-211] Later, the self-assembled CCAs were often polymerized within a responsive hydrogel to form polymerized crystalline colloidal arrays (PCCAs) for optical devices and sensing applications.[212-217] These are examples of *ncp* crack-free solid CCs that were fabricated using self-assembly with the assistance of hydrogel polymerization.

Core@shell colloidal particles with soft shells can be utilized as building blocks to minimize the cracks formation in CCs. The Hellmann group[187] and the Baumberg group[185] independently reported an identical and effective method using core@shell particles, where the soft shell collapses and fills the voids, prohibiting cracks formation over large areas. The avoidance of cracks is a structural improvement using this method comparing to other kinds of methods in opal film formation; however, all other types of defects still exist. In addition, the flexibility of this method allows defects to be combined with continuous lattice distortions. A new colloidal particle functionalization approach was reported to fabricate crack-free opal film.[218] A loosely packed colloidal crystal was immobilized in a hydrogel, which was uniformly shrunk and dried and transformed into a crack-free opal film. This sol-gel bounded method is very promising for the fabrication of CCs without cracks. Nevertheless, this method is

complicated, time- and chemical-consuming, and ineffective in fabricating inverse structures.

In recent years, hydrogel nanoparticles, for example, poly (*N*-isopropyl acrylamide) (PNIPAM) microgel particles, have been used as building blocks to fabricate CCs without cracks in long-range ordering. This method is compelling in the fabrication of crack-free CCs due to the unique property of hydrogel nanoparticles. Asher and co-workers pioneered the preparation of 3D *ncp* CCs as optical switches and limiters by self-assembling PNIPAM gel particles.[219] Hellweg *et al*. fabricated CCs using PNIPAM hydrogel particles and then investigated the particles with different cross-linker concentrations and their deswelling ratios.[220] Subsequently, Zhou *et al.* successfully fabricated CCs hydrogel films by self-crosslinking microgel (**Figure 10a and b**).[221] In their study, they firstly synthesized monodisperse microgel spheres consisted of a copolymer of PNIPAM and N-hydroxymethylacrylamide (NMA). Then, a dilute microgels dispersion was allowed to dry in air, giving rise to crystalline microgel structures at the air−dispersion interface. Taking advantage of the self-crosslinking property of NMA, the adjacent PNIPAM-NMA microgels reacted with each other to yield covalent bonds, which stabilized the crystalline structure after complete water evaporation from the particle dispersion at room temperature. When immersed in water, this film not only behaved like a conventional hydrogel that absorbed a huge amount of water but also displayed iridescent colors owing to the long-range ordering of the microgel arrays. The studies on microgels offer an effective way for the large-scale fabrication of PhCs without cracks.

As a matter of fact, gelation-driven crack inhibition is a viable and straightforward method to prepare uniform and crack-free coatings through the drying-mediated assembly of colloidal particles, which is thus also applicable for colloidal crystal films.[222] Iyer and Lyon exploited the utilization of soft colloidal particles to prepare crack-free CCs. They showed that the resulting CCs are tolerant with respect to disruptions of the crystalline structure that stems from the inclusion of a different sized colloidal particle.[223] The incorporation of such a particle normally results in packing defects since it does not generally fit into the grid. This work clearly indicates that these PNIPAM microgels are truly very “tolerant” with regard to defects, are not inclined to polydispersity, and thus can bear larger particle size deviations. Therefore, an alternative to obtaining crack-free PhCs is to fabricate microgel-based CCs.[224]

PNIPAM-based microgel PhCs were fabricated using a facile method called “high-temperature-induced hydrophobic assembly” as well.[224] A vessel containing a PNIPAM microgel suspension (10 mL) was put into an oven at a specific temperature (e.g., 80 °C). Then, water was evacuated from the PNIPAM colloids and evaporated at high temperatures, due to a hydrophilic to hydrophobic state transition, and the PNIPAM microgels self-assembled into a milk-like mass. A particular time later, e.g., 40 min, the container was brought out and horizontally

placed on a table. After reaching an equilibrium (about 2 to 20 min), the PNIPAM microgel PhCs displayed brilliant iridescent colors (**Figure 10c**). The assembly conditions changed the amount of water inside the crystals, thus determining their structural color. The resulting PhCs were solvents sensitive and showed reversible color changes, which can be observed with naked eyes.

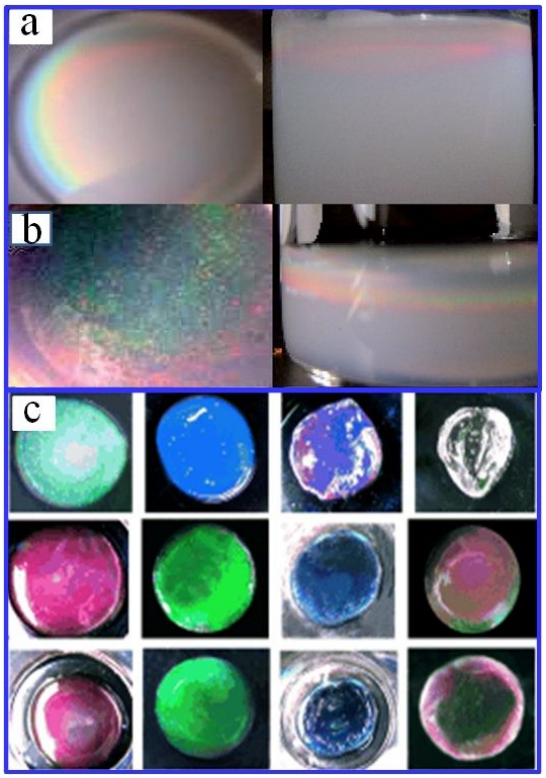

Figure 10. Photographs showing the air−water interface of the PNIPAM-co-NMA particle dispersion with a polymer concentration of 0.8 wt%. The dispersion was exposed to air at room temperature for: **(a)** 1 day and **(b)** 4 days. The left and right images are the top view and the side view, respectively. The diameter of the beaker is 4.5 cm. Reprinted from *Soft Matter*,[221] copyright 2005 Royal Society of Chemistry. **(c)** CCs of PNIPAM-co-AA and PNIPAM microgels self-assembled at different conditions (temperatures and sedimentation times). The perceived color results from Bragg diffraction in the visible region. Reprinted from *ChemPhysChem*,[224] copyright 2009 Wiley-VCH Verlag GmbH & Co. KGaA.

The incorporation of a hydrogel network into a drying film can lead to the formation of crack-free colloidal crystal films. First of all, the hydrogel network is able to hold the colloidal particles over a distance, which reduces the capillary pressure that causes crack formation.[225] Second, the polymer network can relieve structural stress by providing a soft medium that can deform without crack formation.[218]

The combination of a hydrogel network with a flexible substrate can result in high-quality CCs in a large area as well. Recently, Song and co-workers explored an approach to fabricating crack-free PhCs using polymerization-assisted assembly on aluminum foil (**Figure 11a and b**). During the self-assembly process, the monomer (NIPAm)

polymerized and formed an elastic polymer hydrogel in the voids among the colloidal particles. The elastic collapse of the as-formed polymer counteracted the volume change resulting from latex spheres contraction and alleviated the tensile stress. In the meantime, the substrate deformation released the residual stress (**Figure 11c-f**).[226]

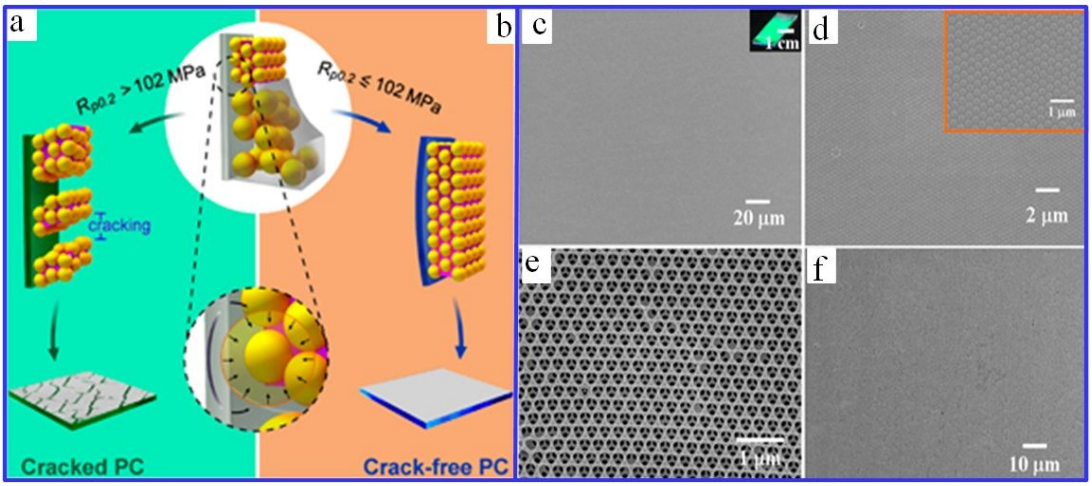

Figure 11. (a-b) Scheme of the crack-avoiding mechanism. Proper PNIPAM infiltration can minimize the tensile stress to 102 MPa during the self-assembly process. **(a)** Substrates with $Rp_{0.2}$ >102 MPa could not release the tensile stress in time, resulting in the stress accumulation and crack formation in the PhCs. **(b)** The tensile stress generated from shrinkage of colloidal particles is released by the combined effects of substrate deformation and polymer infiltration (with $Rp_{0.2}$ ≤102 MPa), which results in the crack-free PhCs. SEM images of the crack-free PNIPAm/colloid composite opal (**c**–**d**) and PNIPAM inverse opals (**e**–**f**) assembled on Al foils. The inset in (**c**) is a photograph of the crack-free PhCs, and the scale bar is 1 cm. The inset in (**d**) is the magnified SEM image. These SEM images indicate that cracks were completely eliminated from the PhCs. Reprinted from *NPG Asia Materials*,[226] copyright 2012 Springer Nature.

By tailoring the nature of the building blocks of self-assembly, hybrid structures comprising of soft and hard materials, as well as solvent-swollen microgels have been extensively used to fabricate defect-free CCs. During the self-assembly process, the building blocks interact with each other with much softer interaction potentials. These materials can dissipate defect energy over long distances through the lattice and thus give rise to intrinsic defect tolerance.[227] In contrast to hybrid materials and microgels, polymer colloidal spheres with tunable interaction without undermining interstitial space were synthesized to prepare large volume PhCs with excellent chemomechanical stability.[91] Monodispersed PS colloidal spheres were firstly synthesized and then were followed by swelling synthesis to obtain highly monodispersed microspheres with functional surface reactive side-chain monomers, soft polymers, acids for anhydride formation, or physical crosslinkers by H-bonds and/or polarity. These motifs can create noncovalent and covalent homodimers or hetero-bridges after convective self-assembly. The cross-linking at these special microspheres interfaces led to the least crack formation and a 10-fold enhancement in chemomechanical stability against exposure to water and isopropanol.[91]

4.1.5. Modified vertical deposition method

Vertical deposition method, also known as convective self-assembly method, is an efficient method to fabricate CCs, which was firstly developed by the Nagayama group to fabricate 2D CCs and then was extended to fabricate 3D CCs by Jiang *et al*.[118, 119] Typically, a substrate is dipped into the colloidal suspension containing spherical building blocks, and the capillary force-induced meniscus at the interface of substrate and dispersion will drive the crystallization of spheres into PhCs with a controllable thickness. During the drying process, the meniscus will sweep continuously across the substrate, and consequently, opal photonic film will form on the surface.[34] Since this process is accompanied by the sedimentation process of colloidal nanoparticles, it is commonly accepted that this method is effectively limited to nanospheres smaller than 400 nm in diameter. For nanospheres out of this criterion, sedimentation will dominate during the drying process and ruins the feasibility of uniform deposition. On the other hand, the 3D CCs fabricated using this method may demonstrate cracks and thickness variations. Researchers made a range of modifications and advances on this method to fabricate high-quality CCs or extend this approach to larger colloidal nanospheres (larger than 500 nm) by controlling the assembly kinetics or *in situ* fixation.

3D PhCs for the application in the field of telecommunication needs to meet an exceptionally high standard in their degree of structural perfection and optical quality. To this end, the Ozin group developed a strategy for the fabrication of SiO_2 colloidal crystal films with a substantially high degree of structural perfection and optical property.[228] **Figure 12a** shows the scheme of the isothermal bath setup for isothermal heating evaporation-induced self-assembly (IHEISA) of colloidal crystal films. Three key synergistic factors in the film-forming process should be satisfied in order to obtain high-quality PhCs. The first one is to synthesize high-quality SiO_2 spheres with a polydispersity index significantly better than 2%. Secondly, the population of spheres must be devoid of even the smallest fraction of considerably smaller or larger spheres or spheres doublets. The third one is related to the film-forming method itself, which necessitated the development of a novel process founded upon IHEISA of spheres on a planar substrate. Using this IHEISA method, as shown in **Figure 12b-e**, highly ordered 3D PhCs with different colloidal particle sizes were achieved. This new method is robust to deposit very high-quality SiO_2 colloidal crystal film rapidly over large areas, with a controlled thickness and without any restrictions on sphere sizes.

Apart from the above contribution, Ozin and his colleagues also proposed another approach to minimize crack formation in this study, where small amounts of tetraethylorthosilicate (TEOS) or tetramethylorthosilicate (TMOS) were added to the SiO_2 colloidal sphere dispersion in ethanol during IHEISA deposition to react with water physisorbed on the surface and to form an additional SiO_2 layer, thus preventing SiO_2 spheres from shrinkage.[228]

Nevertheless, no further experimental studies were reported on this proposed approach from the Ozin group.

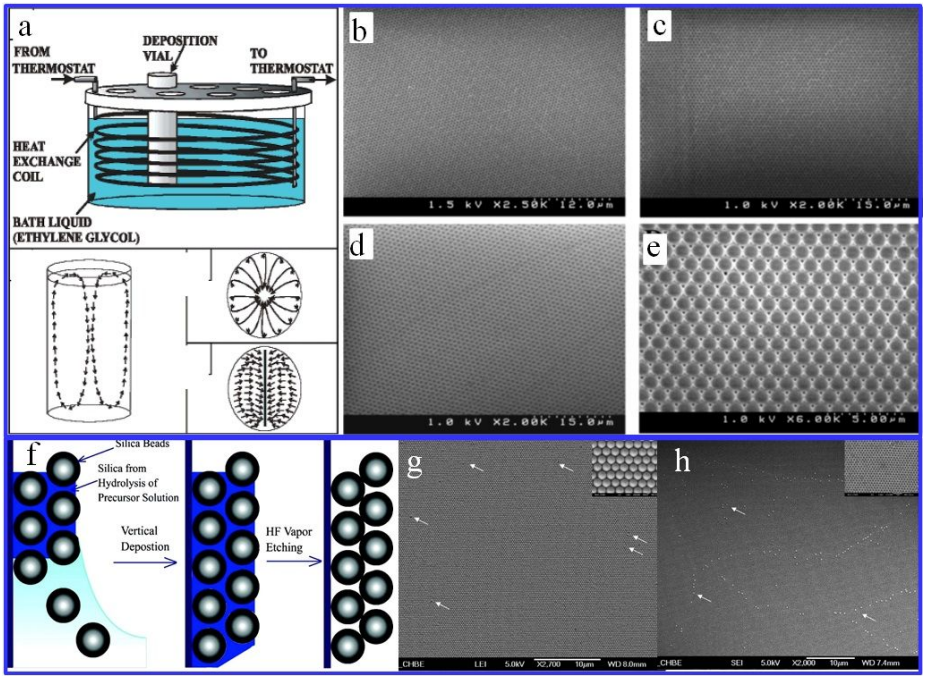

Figure 12. (a) Scheme of the isothermal bath setup used for the fabrication of colloidal crystal films via IHEISA deposition.[228] SEM images of a top view of the highly ordered colloidal crystals using SiO_2 colloidal particles of **(b)** 480 nm, **(c)** 635 nm, **(d)** 850 nm, and **(e)** 1.0 μm in diameter as building blocks. Reprinted from *Journal of the American Chemical Society*,[228] copyright 2004 American Chemical Society. **(f)** Schematic illustration of the steps of fabricating crack-free colloidal crystal films. **(g)** Top view of the sample after HF etching with an inset image of higher magnification (the inset image of the scale bar is 100 nm). **(h)** SEM image showing an exposed nanobowl array of the sample (the inset image is a magnified view, and the scale bar of the inset is 1 μm). Reprinted from *Journal of the Physical Chemistry C*,[170] copyright 2007 American Chemical Society.

The Zhao group first experimentally demonstrated the use of TEOS to minimize cracking formation. They presented a modified method based on vertical deposition to fabricate crack-free non-close packed (ncp) CCs.[170] In this method, a SiO_2 colloidal suspension containing a SiO_2 precursor (an acidic TEOS solution) was used during the vertical deposition process. Hydrolysis of the precursor of SiO_2 resulted in silicate species, which filled into the interstices among the self-assembled SiO_2 spheres to avoid cracking upon drying of the colloidal crystal film. The silicate species in the interstices of the SiO_2 spheres can be selectively removed using hydrofluoric acid (HF) vapor, leaving behind a highly crystalline and crack-free colloidal crystal film (**Figure 12f-h**). In their seminal work, Zhao and co-workers proposed that the silicate species played the role of "glue" to adhere the SiO_2 beads together to avoid cracks. The Zhao group further extended this method using PS colloidal beads instead of colloidal SiO_2 beads as building blocks to fabricate crack-free PS/SiO_2 hybrid CCs.[135, 229, 230] The PS spheres can be selectively removed via calcination or dissolution in benzene, resulting in 3DOM structures.[170, 229] The distinctive structure of the resulting CCs lies in that the CCs on the same plane are *ncp* while the neighboring PS colloidal spheres on different

planes are still close-packed as revealed after HF etching.[230, 231] The sol-gel matrix generated as a result of TEOS hydrolysis during colloids self-assembly can glue the assembled colloidal spheres and release the capillary force during self-assembly.[135, 229] The SiO_2 inverse opal heterostructures can be fabricated in the relatively large domain without cracks. In addition, such kind of structure has a large surface/volume ratio and broad stop bands, which may find broad applications in a wide variety of fields, such as solar cells and gradient drug release.

Cai *et al.* have further extended this method to self-assembly of 2D CCs. They developed a co-self-assembly method to fabricate high-quality 2D CCs in large monodomain.[232] The addition of TEOS sol into the colloids helps prevent the formation of cracks during the co-assembly process. 2D plasmonic PhCs were also fabricated by depositing Au onto the surface of the crack-free 2D CCs.[232] The mechanism of self-organization into crack-free CCs, as yet completely understood, might provide insight into similar phenomena in colloids science. In this method, the addition of sol−gel precursors within the suspension, which is similar to the addition of polymeric binders, surfactant or plasticizers (e.g., Polyvinylpyrrolidone, PVP), consequently leads to an increase in the film strength and relaxation of tensile within the interconnected Si-O-Si networks. In a separate study, Kang and co-workers modified the surface of SiO_2 colloidal spheres with vinyltriethoxysilane (VTES) and then photo-cross-linked the surface-modified SiO_2 colloids *in situ* during self-assembly. The resulting CCs showed no cracks in a large area.[233] These studies indicate that silane is a good candidate for the fabrication of high-quality CCs without cracks.

$SiCl_4$(l), as one of the precursors of SiO_2, can also be employed to fabricate high-quality CCs and to enhance the mechanical property of CCs. The Ozin group exploited a method to enhance the mechanical stability of CCs through layer-by-layer (LbL) growth of continuous SiO_2 using a chemical vapor deposition (CVD) method.[90] They first fabricated SiO_2 CCs via the conventional vertical deposition method,[119] then deposited SiO_2 onto the CCs using a CVD process at atmospheric pressure and room temperature. $SiCl_4$(l) was placed in a bubbler through which an N_2 (gas) stream was flown. This method not only greatly improves the mechanical stability of the lattice without distorting its long-range ordering but also can control the pore size and microsphere connectivity of colloidal crystal lattices. A detailed discussion on the CVD approach will be given in **Section 4.2.2**.

So far, the techniques discussed above are effective for nanospheres smaller than 500 nm in diameter generally. In terms of applications, however, PhCs with bandgap in the near-infrared (NIR) range are highly desirable and technologically important. One way to overcome the size-limitation induced by competitive sedimentation is by creating controllable convective flow during drying deposition. More specifically, this was achieved by a temperature gradient (from 80 ^oC at the bottom to 65 ^oC on the top) in the colloidal suspension. Such a vertical

convective flow can minimize the sedimentation process and bring large nanospheres to the meniscus, making those processes applicable to sub-micrometer building blocks (~ 800 nm). The assembled planar opal PhCs showed uniform periodicity with negligible defect density (~ 1% stacking fault and ~ 10^{-3} point defect) compared to the sedimented opals (~ 20% stacking fault and ~ 10^{-2} point defect [71]). In this way, multi-layer opals can be deposited on the Si substrate on the scale of centimeters. The perfect periodic structures in large-scale were also evidenced by the uniform blue color across the whole assembled films as well as a clear characteristic 6-spot diffraction pattern with weak Kossel ring features.

4.1.6. Inkjet printing method

The aforementioned methods are effective for the fabrication of large-scale colloidal PhCs. However, they are infeasible for the fabrication of PhCs with special patterns or structures, which are especially desirable in photonic device fabrication and application. For meeting the needs, a variety of printing methods have been proposed to fabricate patterned CCs through combining self-assembly with direct writing.[25, 26, 234] Moon *et al.* first reported the use of single-orifice inkjet printing to fabricate patterned colloidal crystal arrays with two different sized latex spheres.[235-238]

Recently, this inkjet printing method was further refined by Song and co-workers to fabricate large-scale patterned PhCs.[239] In their study, a typical inkjet printing technique was applied, and the resulting colloidal crystal films showed a well-ordered structure and excellent optical properties (**Figure 13a and b**). Highly monodispersed latex colloidal particles and an appropriate amount of solvent with a high boiling point (ethylene glycol) were used as an 'ink.' The addition of ethylene glycol facilitates the latex particles assembly on the substrate (**Figure 13a**). In addition, to promote the effective spreading of the colloidal latex suspension, optimization of the printing substrate was also performed. It was found that, during the fabrication process, the wettability of the substrate was accountable for the size and shape of the ink droplets, while the latex assembly occurred before the solvent front started to dry. Therefore, the resultant PhCs quality was directly affected by the printing substrate wettability, the evaporation conditions, and the ink content. For instance, the low-adhesive substrate was found to have a beneficial impact on the well-ordered latex assembly. The inkjet printing technique for the fabrication of patterned PhCs has many advantages over other methods. This method is capable of designing various images, flexible adjustment of the ink composition, precise positioning of ink droplets, and a variety of deposition patterns by changing the

substrate. PhCs with customizable patterns fabricated via this facile inkjet printing method are promising for a good variety of applications, such as optical circuits, photonic devices and so forth. For example, Chen *et al.* developed various patterned CCs and a white-lighting LED backlight device by combining a "colloids skin"-regulated assembly with a bar coating method.[240]

Kim and Yin *et al.* explored a high-resolution patterning of CCs with multiple structural colors for practical applications.[241] The fast fabrication of CCs were achieved within seconds through successively regulating and fixing the color with a single material accompanying a maskless lithography system (**Figure 13c and d**). In this study, a unique 'Magnetic-Ink' is used, which is a three-phase material system consisted of superparamagnetic colloidal nanocrystal clusters (CNCs), a photocurable resin, and solvation liquid.[242, 243] The CNCs were self-assembled to produce chain-like structures when an external magnetic field was applied. Therefore, the structural color of the films can be easily adjusted by altering the interparticle spacing using an external magnetic field. Deprived of the external magnetic field, the CNCs were randomly dispersed and showed a natural brown color of the magnetite.

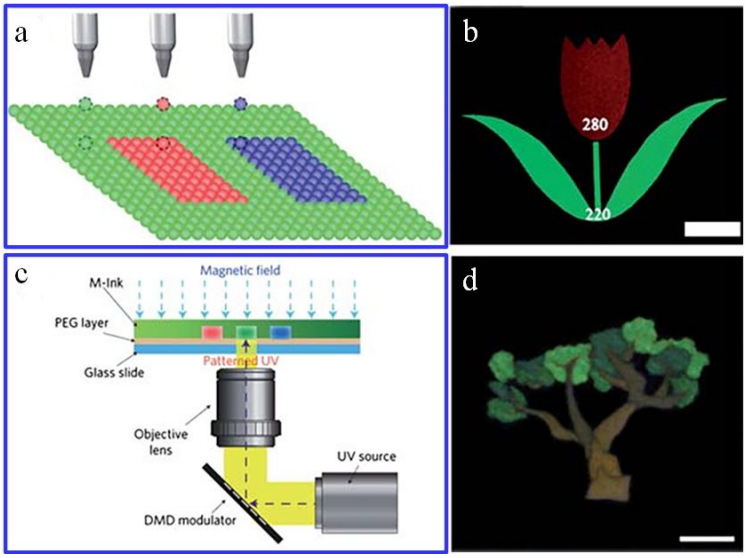

Figure 13. Scheme of the protocol on the fabrication of patterned PhCs via printing techniques. **(a)** Fabrication of PhCs from inkjet printing and **(b)** the corresponding patterned PhCs. The scale bar is 1 cm. Reprinted from *Journal of Materials Chemistry,* [239] copyright 2009 Royal Society of Chemistry. **(c)** Setup of maskless lithography for color fixing. Instantaneous exposure using patterned UV light reflected from a digital micromirror array (DMD) modulator allows the fast production of structural color and **(d)** the corresponding patterned PhCs. The scale bar is 250 mm. Reprinted from *Nature Photonics*,[241] copyright 2009 Springer Nature.

In addition to the above efforts on the fabrication of crack-free CCs, intense attention has also been paid to the fabrication of high-quality 3DOM photonic structures, namely, inverse opals. The 3DOM materials intrigue great interests owing to their novel structural properties and various applications.

4.1.7. DNA-mediated assembly of CCs with cPBG

The self-assembly of colloidal particles becomes a well-developed scientific area, and a variety of attractive interactions between colloidal particles have been explored extensively, including DNA-mediated interaction,[44, 45, 155, 244-259] electrostatic interaction,[260, 261] depletion interaction,[262-266] hydrophobic interactions,[267-269] critical Casimir forces,[270-274] light-mediated interaction,[275-277] capillary forces,[278-281] molecular recognition,[282, 283] and interactions induced by electric [284-286] or magnetic fields,[287, 288] or by topological defects in nematic liquid crystals.[289-292] Using these interactions, different crystal structures were self-assembled from two-dimensional structures to *fcc*,[246, 248, 250, 251, 293, 294] Frank-Kasper phases,[41, 155] colloidal clathrate hydrates[45] and colloidal diamond.[38] Among these types of CCs, colloidal diamond is one of the best candidates for producing a cPBG but it is very difficult to fabricate. Therefore, colloidal diamond has been viewed as the holy grail of the colloidal self-assembly community.[295] In this section, we will briefly summarize the efforts toward the self-assembly of colloidal diamond.

Carbon atoms in a diamond structure are tetrahedrally coordinated (sp^3 hybridization), and thus the self-assembly of colloidal diamond requires colloidal particles have tetrahedral valence. These kinds of particles are also referred to as tetrahedral patchy particles. Manoharan *et al.* reported the synthesis of colloidal clusters with tetrahedral configuration, which paved the way for patchy particles for colloidal diamond.[145] In their experiments, they made a toluene-in-water emulsion where crosslinked PS spheres were immersed in the toluene phase. After the slow evaporation of toluene, PS spheres within the same oil droplet bound to each other and formed colloidal clusters with a certain configuration. Complete removal of the oil from the droplets led to the dense packing of colloidal particles that minimized the second moment of mass distribution. If there were four particles in one oil droplet, they formed tetrahedral clusters (**Figure14a**). Later on, Wang *et al.* demonstrated the synthesis of tetrahedral patchy particles by encapsulating tetrahedral clusters with a different type of material **(Figure14b)**.[44] Because of the difference in surface groups, they can selectively functionalize patches with DNA and let these particles bind through the patches. However, as mentioned in **section 3.2**, the crystallization of tetrahedral patchy particles requires sufficiently small patches,[147] otherwise random aggregates are thermodynamically stable than crystals.[296] Tetrahedral patchy particles with small patches can be synthesized by colloidal fusion,[149] in which binary colloidal particles first coordinate into tetrahedral clusters, and the introduction of a plasticizer deforms the tetrahedral clusters and produces tetrahedral patchy particles **(Figure14c)**. However, the simulation showed that

these particles would crystallize into a mixture of cubic diamond, hexagonal diamond and clathrate hydrates.[150]

In addition to tetrahedral patchy particles, there are several different approaches to colloidal diamond.[41] Ducrot *et al.* fabricated colloidal $MgCu_2$ superstructures, in which cubic diamond and pyrochlore are two sublattices.[155] Either cubic diamond or pyrochlore structure can be obtained by selectively removing one of the sublattices. Both diamond and pyrochlore structures can exhibit a cPBG,[141, 142] but how to extract the diamond sublattice from the superlattice remains unknown. Wang *et al*. made colloidal double diamond using bi-dispersed colloidal building blocks.[255] The crystallization requires strong interactions between two species and weak interactions between large particles and no interactions between small particles, but the double diamond crystals do not have a cPBG. By taking advantage of DNA origami, cubic diamond structures were realized in the nanoscale.[258] However, the particle size is too small to open a cPBG, and the crystals cannot be dried out, which makes further applications difficult.

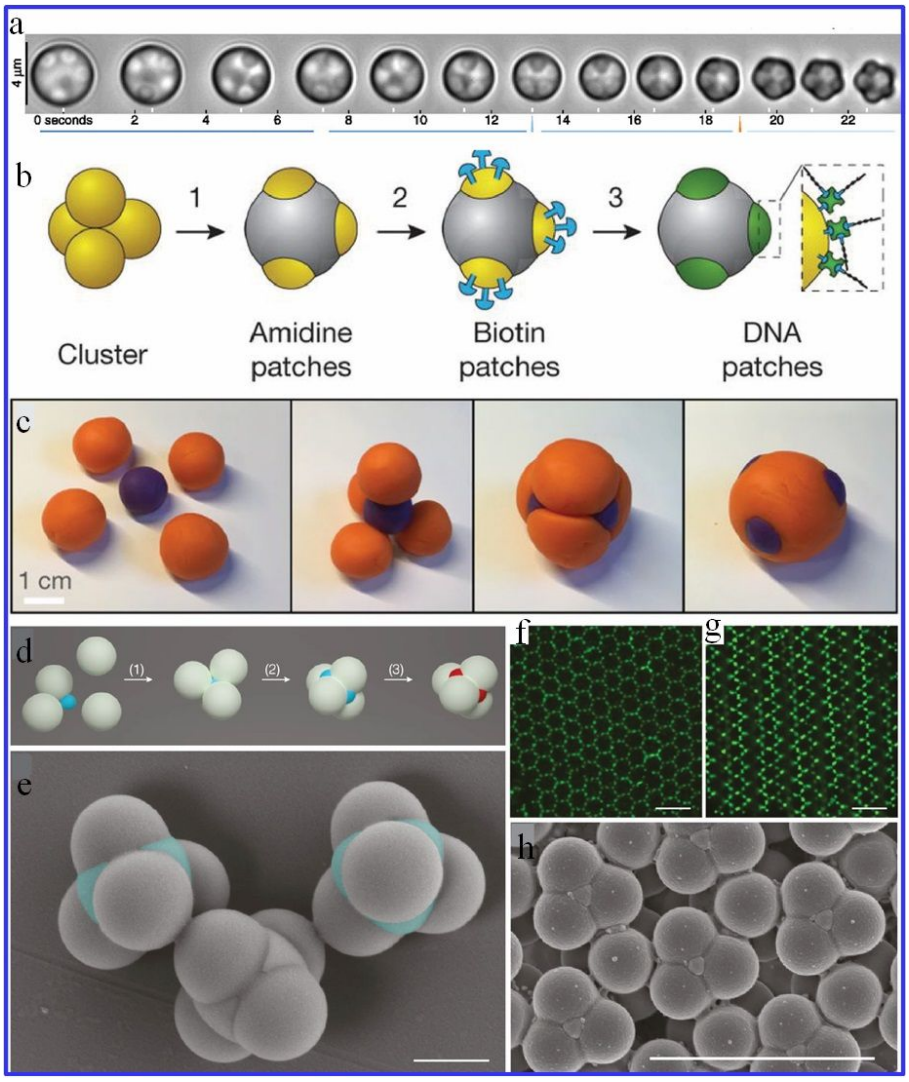

Figure 14. Self-assembly of colloidal diamond from colloidal patchy particles. **(a)** Synthesis of colloidal clusters. Reprinted with permission

from *Science,*[145] copyright 2003 American Association for the Advancement of Science. **(b)** Synthesis of tetrahedral patchy particles and DNA functionalization of patches. Reprinted with permission from *Nature*,[44] copyright 2012 Springer Nature. **(c)** Synthesis of tetrahedral patchy particles by colloidal fusion. Reprinted with permission from *Nature*,[149] copyright 2017 Springer Nature. **(d-h)** Self-assembly of colloidal diamond from compressed clusters. **(d)** Synthesis of tetrahedral compressed clusters. **(e)**, SEM micrograph of partially compressed clusters. Scale bar, 1 μm. (f,g) Confocal micrographs showing the 111 **(f)** and 110 **(g)** planes of the self-assembled colloidal diamond. Patches are fluorescently labeled, and spheres are not visible because they are not dyed. **(h)** SEM micrograph of the self-assembled colloidal diamond by partially compressed clusters. Reprinted with permission from *Nature*,[38] copyright 2020 Springer Nature. Scale bar, 5 μm.

Very recently, colloidal diamond was realized in the Pine group.[38] They prepared partially compressed tetrahedral colloidal particles which intrinsically carry the rotational information required for the self-assembly of colloidal diamond **(Figure14d-h)**. The synthesis of these particles is based on colloidal fusion, and they can selectively functionalize the retracted patches with DNA. Because of the geometry of these particles, they can only bind to each other in the staggered conformation, which makes cubic diamond with 100% selectivity **(Figure14d)**.

The colloidal cubic diamond made by the Pine group is mechanically stable, which can be dried out and serve as a template for making inverse cubic diamond structure. From Maxwell's stability criterion, colloidal diamond structures are, intrinsically, mechanically unstable. This does not mean colloidal diamond cannot be self-assembled (thermodynamic stability), but it means that these crystals may collapse upon drying. To be mechanically stable, the number of constraints for each particle should be at least 2 times the degree of freedom (for spheres, 3). Because particles are tetrahedrally coordinated in colloidal diamond, they have two less constraints than the six required for mechanical stability and can be collapsed upon drying. In contrast, with the same coordination number, carbon diamond is one of the hardest materials in the world. Carbon diamond is mechanically stable because atoms are connected by electron clouds (σ bonds). Although rotation of a single bond generates different conformations, these σ bonds cannot be bent which offers three extra orientational constraints in each of the four bonds. Similarly, in the particle design by He *et al.* (degree of freedom, 5), the particle interlock mechanism offers extra orientational constraints. Upon binding, a pair of tetrahedral clusters has 28 points of contacts which helps to guarantee orientational order and make the crystal structure stable. Therefore, it is possible to dry the suspension, retain the structure and use these crystals as templates for making inverse diamond crystals **(Figure14e-h)**. The calculation showed that the inverse diamond crystals have a complete and wide PBG.

4.1.8. Microfluidics-assisted assembly method

Spherical colloidal crystal beads (SCCBs) are one kind of unique PhCs due to their excellent angular independence optical property.[297-299] The unique optical performance is because of their spherical symmetry, which broadens their applications, especially in optical devices and sensors.[300] Velev and co-workers pioneered the

fabrication of SCCBs.[297] In their seminal work, both SCCBs and porous structures were fabricated via evaporative assembly at the interface of organic solvent and air. From then on, the Yang research group,[299, 301-303] the Gu research group[304, 305] and several other research groups have achieved significant progress in the fabrication of spherical PhCs using the microfluidics-assisted assembly method.

Both evaporation-induced colloids crystallization and polymerization of ordered colloids crystallization arrays can give rise to SCCBs. However, both methods rely on the droplet template to produce SCCBs. Microfluidic devices can produce uniform droplet templates, which facilitate the rapid and mass fabrication of various SCCBs because they can continuously generate uniform droplet templates. Therefore, the introduction of microfluidic device into the fabrication of SCCBs, which acts as one kind of powerful tools to assist the self-assembly of spherical CCs, further boosted the development of this emerging field. To this end, this method is also known as microfluidics-assisted assembly method.

The microfluidics-assisted assembly method is so far the most widely used method to produce SCCBs.[306] In a typical process, a microfluidic device is firstly used to generate monodisperse droplet template.[307] Then SCCBs are formed on a large-scale by slowly evaporating the solvent of the droplets, which are composed of different polymeric or inorganic colloidal particles as building blocks. In general, there are four types of SCCBs fabricated in recent years, including spherical opal structured colloidal crystal beads,[297, 301, 308-310] spherical inverse opal structured colloidal crystal beads,[300, 302, 311-314] Janus or multicomponent colloidal crystal beads[315-318] and core@shell structured colloidal crystal beads.[299, 319-324] In addition, we will also discuss the direct self-assembly in different microdevices.

Several different microfluidics-assisted assembly strategies were used to fabricate these different types of SCCBs.[304] Among various methods, evaporation induced colloidal self-assembly is the most widely used method.[297, 308, 310, 325] Similar to the fabrication of colloidal crystal film, capillary forces play a crucial role in the preparation of SCCBs, which can compress the colloidal particles symmetrically and ultimately arrange them into close-packed spherical beads with *fcc* structure (**Figure 15a**). It should be pointed out that the intrinsic defects or grain boundaries cannot be avoided in the resulting SCCBs due to the curvature effect.

NCP SCCBs can be achieved from oil or water droplet templates that consist of highly charged colloidal particles (**Figure 15b**).[326] During self-assembly, the strong electrostatic repulsion leads the colloidal particles to form a thermodynamically stable non-close-packed *fcc* or *bcc* PhC structure within the droplets. The droplet templates show distinct PBG properties but the PhC structure can become disordered upon distribution or exposure

to ionic impurities. The way to solve this issue is to solidify such non-close-packed structure with polymers or hydrogels. For example, nonionic monomers such as NIPAm and PEG-DA can be polymerized into a hydrogel network, which surrounds the non-close-packed PhC, to obtain stabilized non-close-packed SCCBs.[327] In addition, non-close-packed SCCBs can also be obtained from colloidal particle self-assembly within nonpolar oil phases. Yang and co-workers recently developed an optofluidic-assisted assembly method to develop non-close-packed SCCBs with negligible cracks.[303] They first dispersed monodispersed SiO_2 colloidal particles into viscous ethoxylated trimethylolpropane triacrylate (ETPTA) resin. When the suspension was broken into silica-in-ETPTA (oil-in-water) droplets at the tip of the microfluidic device, the colloidal particles started to form concentric hexagonal-array spherical shells from the outer layer to the inner layer. This approach thus reduced the repulsive energy. Then, the non-close-packed SiO_2 PhCs within ETPTA were consolidated with photopolymerizable ETPTA with the UV exposure equipped with the microfluidic devices. Finally, non-close-packed SiO_2-in-ETPTA SCCBs were successfully obtained. However, the PhCs in the inner layer of the SCCBs are less ordered due to the high concentration of SiO_2 colloidal particles. At low concertation, the SiO_2 colloidal particles can form a more ordered structure as a result of a relatively larger repulsive potential comparing to the reduced van der Waals attraction.[303]

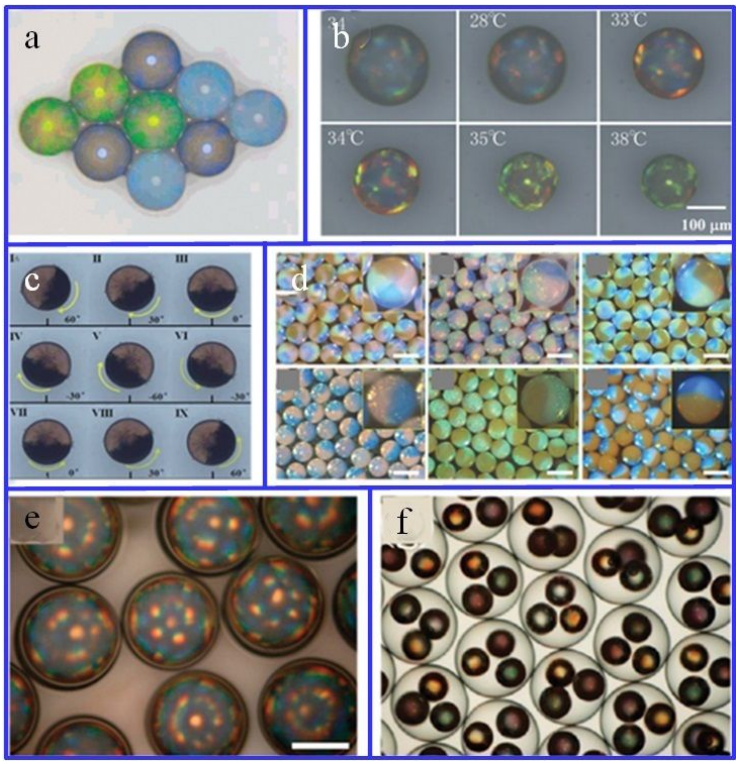

Figure 15. Photographs of **(a)** close-packed spherical CCs.[328] **(b)** Non-close-packed spherical CCs. The scale bar is 100 μm.[326] Spherical CCs with **(c)** Janus [317] or **(d)** multicomponent structure. The scale bars are 100 μm in (d).[329] **(e, f)** Spherical CCs with core@shell structure.[299] [330] Reprinted with permission from *Small*,[331] copyright 2020 Wiley-VCH Verlag GmbH & Co. KGaA.

Spherical inverse opal beads, similar to inverse opal films, can be obtained through either replica of SCCBs template or colloidal co-assembly. Many materials, including ultrafine nanoparticles, hydrogel monomer solution, prepolymers, precursors, etc., can be infiltrated into the interstices of the prepared opaline SCCBs for the fabrication of spherical inverse opal beads.[302, 311-313, 332] In a typical process, the SCCBs need to be completely immersed in the infiltration materials to achieve a full filling of the interstices. Subsequently, after removing the colloidal particles via heat treatment or etching, a relatively robust spherical inverse opal bead structure can be obtained.[333]

The spherical inverse opal beads can also be prepared via the colloidal co-assembly approach, in which the formation of SCCBs and infiltration of the desired framework materials occur simultaneously. [302, 314, 332, 334] Gu and co-workers reported the fabrication of a spherical inverse-opaline beads using the co-assembly of PS colloids as the template and colloidal silica particles as the matrix.[332] Droplet templates were firstly prepared from an aqueous suspension of PS and SiO_2 colloidal particles. The oil flows broke the suspension into droplets using a microfluidic device, and then the droplets were collected in a container. The co-assembly process involves the evaporation of the solvent within the droplets. During the evaporation process, the PS colloidal spheres self-assembled into highly ordered CCs while the small SiO_2 particles just filled the interstices of the CCs. Then the silicon oil on the SCCBs was cleaned with hexane after solidification. In the end, the PS colloidal spheres were selectively removed to obtain spherical inverse opal beads via calcination, which in turn enhanced their mechanical strength. They further functionalized the spherical inverse opal beads for colorimetric tumor marker detection. It should be noted that, a PS to SiO_2 volume ratio of 9 was optimized for the co-assembly process to achieve the best performance.

"Janus" or multicomponent SCCBs, in general, can be fabricated from monodisperse droplet templates where phase separation occurs among the colloidal particles.[315-317] Gu and co-workers reported the fabrication of a Janus SCCBs using droplet templates that contain both ultrafine magnetic particles and monodispersed SiO_2 colloidal particles. Phase separation occurred upon applying a magnetic field. SiO_2 colloidal particles within the droplet self-assemble into close-packed SCCBs when heated in an oven, while the magnetic particles infiltrated into the interstices of the SiO_2 particles at the bottom of the microsphere (**Figure 15c**).[317] Apart from the magnetic properties, the fabricated Janus SCCBs possess an anisotropic band structure.

The Janus SCCBs can also be obtained from the self-assembly of more than monophasic single droplets, which are composed of two or more individual domains.[303, 318] Typically, a capillary microfluidic device with multibarreled capillaries is used to prepare the emulsion droplet templates, where distinct fluids are introduced in parallel with the angular distribution. Gu and colleagues developed a four-channel microfluidic device that can

inject four dispersed phases at one time. This novel microfluidic device can generate Janus emulsions on-demand.[329] They used SiO_2-in-ethoxylated trimethylolpropane triacrylate (SiO_2-in-ETPTA) solutions as dispersed oil phase. The fluids are miscible, which can form multiple parallel flows within the channels of the capillary microfluidic device. Consequently, the flows were emulsified to generate multiphasic droplet templates at a junction, where a drag force was placed on the parallel streams by a continuous phase. The compartments of the resulting droplet templates can be preserved for a certain distance within the symmetric microfluidic channels. The Janus SCCBs were obtained via polymerization of the droplet templates with the respective multiphasic geometry (**Figure 15d**).

Core@shell structured SCCBs can be produced by using double emulsion droplet templates generated with a microfluidic device .[299, 319, 320, 335] Yang and co-workers first developed a microfluidic device that can produce double emulsion droplet templates in stepwise. After self-assembly, the non-close-packed CCs were encapsulated within the ETPTA resin, which can preserve the droplet by forming a hard shell upon photopolymerization (**Figure 15e**).[299] The resulting core@shell structured SCCBs can maintain the ordering of CCs inside since the ionic species cannot penetrate into the hard shell. Using the same method, Weitz and co-workers demonstrated the fabrication of core@shell structured SCCBs with CCs immobilized in the shell.[320] In this case, a microfluidic device was strategically designed to integrate both co-flow and flow-focusing structure, which enabled the generation of monodispersed oil-in-water-in-oil (O/W/O) double emulsions with CC shells. The shell of the SCCBs was subsequently photopolymerized to immobilize CCs within the hydrogel network (**Figure 15e**). Core@shell structured SCCBs can also be fabricated through template replication of SiO_2 SCCBs similar to the methods used to fabricate SCCB inverse opals. Partial etching was carefully conducted from the outer to the inner of the SiO_2 SCCBs, where hydrogel formed via photopolymerization of the filled pre-gel solution of AA and PEGDA in the interstices. The precise control over the etching process resulted in SCCBs with a core of opal SiO_2 PhCs and a shell of inverse opal PhC hydrogels. The unique core@shell SCCBs gave rise to two distinctive PBGs, which are very useful for immerse applications.[323]

Chen and Weitz recently reported the fabrication of self-healable SCCBs with a modified microfluidics-assisted assembly strategy.[336] They first synthesized monodisperse core@shell colloidal particles (polystyrene@poly(2-hydroxypropyl acrylate-*co*-*N*-vinylimidazole) (PS@poly(HPA-*co*-VI)). Later, the microfluidics-assisted assembly method was used to produce emulsion-droplet dispersions with the colloidal particles, which subsequently formed SCCBs. Then they injected a supermolecular system (β-cyclodextrin (host) and *N*-vinylimidazole (guest)) into methacrylated gelatin (GelMA) to prepare a hydrogel precursor. After

photopolymerization, a covalently crosslinked hydrogel network was formed to solidify the SCCBs. Using this method, a broad range of photonic structures, include spiral, planar and linear assemblies with defined micro-/nanostructures, were achieved for different applications.

Though significant progress has been made in the microfluidic-assisted assembly, high-throughput fabrication of high-quality CCs remains a challenge for two major reasons. First, the mass fabrication of SCCBs is still very challenging though SCCBs can be produced continuously with the assist of microfluidic devices. In the future, the development of emulsification technology could be a good alternative. Second, it remains a challenge to fabricate defect-free SCCBs using the microfluidics-assisted assembly method. This is because the precise localization of colloidal particles is very difficult using the microfluidics-assisted assembly.

Due to the possibility of mass fabrication of a broad range of SCCBs, this method may find potential applications in selective separations, drug release, fuels, catalyst supports, as well as solar cells, which we will discuss in detail in **Section 5**.

4.2. Fabrication of high-quality inverse opals

It is well known that the *fcc* structure of 3D CCs does not open a cPBG due to the low refractive index of the commonly used building blocks. It was demonstrated that the minimum required refractive index contrast to open a complete PBG is ~2 for a diamond D structure.[337] In order to realize high-refractive-index CCs from inorganic materials, the inverse opals (also note as 3DOM) and many other functional photonic structures were proposed, and many strategies have been developed in the past decade.[94, 99, 338]

Colloidal crystal templating (CCT) technique has attracted intense interest since the seminal work of Velev *et al*.[339] and the pioneering study of the Stein group.[340] Up to date, the most frequently used method for the fabrication of 3DOM materials is based on CCT technique (**Figure 16a**). The CCT method generally involves three steps: (i) the self-assembly of CCs with monodispersed latexes or SiO_2 colloidal spheres; (ii) the infiltration of matrix materials into the interstitial spaces of the template via a dry process or wet chemical methods; (iii) selective removal of the template through dissolution or calcination or etching.[338] However, most of the fabricated inverse opals displayed various defects and cracks initially resulting from the template, infiltration process, or thermal shrinkage due to sintering.

In addition to the CCT method, there are two crucial alternate assembly methods. One is to co-assemble small nanoparticles with larger colloidal particles, producing analogous structures to those depicted above when

nanoparticles infill the interstices formed among the templating colloidal spheres during self-assembly (**Figure 16b**).[341] This method can be very useful if nanoparticles of the desired composition are more readily prepared prior to templating. The other alternate route involves the synthesis of core@shell colloidal particles followed by self-assembly of the core@shell particles into a colloidal crystal (**Figure 16c**).[342, 343] This method offers excellent control over the shell thickness. Moreover, thicker shells maintain a relatively closed structure even after removing the cores, resulting in the lower interconnectedness of macropores than that acquired by infiltration approaches.

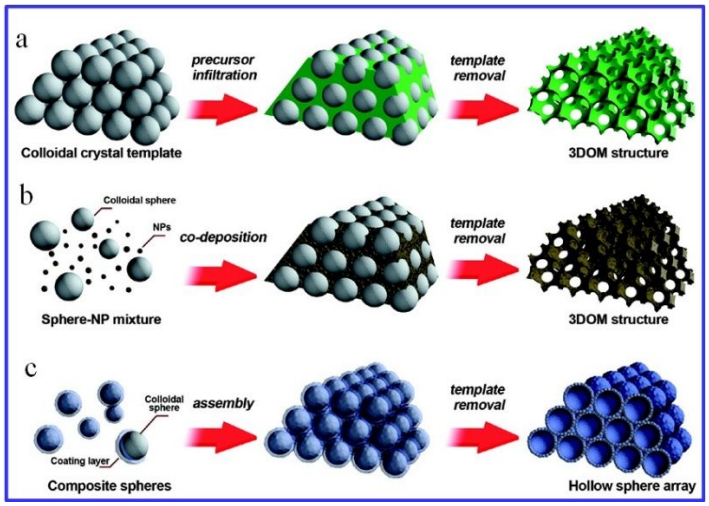

Figure 16. Schematic illustration of three typical routes to periodic macroporous structures via colloidal crystal templating methods. **(a)** A preformed colloidal crystal is infiltrated with precursor material, which is processed to form the 3DOM structure after selectively removing the template. **(b)** Highly uniform colloidal spheres and nanoparticles (NPs) are co-assembled to form a 3DOM structure after selective removal of the template. **(c)** Core@shell structures are assembled into periodic arrays, and removing the cores leads to the formation of close-packed hollow shells. Reprinted from *Chemistry of Materials*,[344] copyright 2008 American Chemical Society.

4.2.1. Wet chemical process

In a typical wet chemical process, there are two steps to prepare inverse opals. In the first step, 3D CCs are assembled normally on a substrate as an opal template. The second step involves the infiltration of reactive precursors into the interstices of the 3D CCs template, polymerization or hydrolyzation of the precursors in a wet chemical reaction, and removal of the initial templates using chemical etching or calcination.[345] In the formation of large-scale inverse opals, the initial quality of CCs is important because any defects in the initial template will ruin the structures of the complementary inverse opals. In addition, the chemical reaction after precursor infiltration is also likely to induce defects in the wet chemical environments, such as insufficient filtration of precursors or uneven chemical reactions in the interstices. To this end, chemists have established a few advanced methods to prepare inverse opals using the wet chemical process.[345-347]

Despite its wide applications, the inverse opals without cracks can only be fabricated on a very small scale by using a conventional self-assembly approach, usually smaller than 10 μm in one dimension. Zeng *et al*. described a facile method to fabricate highly ordered inverse opals derived from the long-range ordering of the 3D CCs, which were obtained by the self-assembly of highly charged PS spheres.[112] They firstly fabricated highly ordered 3D CCs by increasing the electrostatic screening length with the addition of a given amount of electrolytes into the colloidal suspension and then infiltrated the SiO_2 precursor sol-gel solution into the interstices of the 3D CCs template. After selective removal of the PS microspheres through calcination, the defect-free area of the resultant inverse opal structured SiO_2 CCs extended to over 10 μm, which covered with thousands of voids. It is noteworthy that the defect-free area of the SiO_2 inverse opal structure derived from the high-quality 3D CCs and the high-quality area of inverse opal structure is less than $100 \times 100\ \mu m^2$.

The formation of cracks in an inverse opal structure in the CCT method usually transfers from the host opal template or generates during the infiltration and pyrolysis steps. One way to avoid the formation of cracks in CCs in the CCT method is to infiltrate "self-healing" precursors. Song and Xu *et al.* reported the fabrication of crack-free polysilazane-based inverse opal PhCs in large-area. They applied a poly (styrene-methyl methacrylate-acrylic acid) [poly(St-MMA-AA)] opal film as a template and a thermosetting polysilazane (PSZ) as the infiltrating polymer to fabricate PSZ-based inverse opal PhCs.[348] **Figure 17a-f** shows the scheme of the fabrication process to obtain a crack-free inverse opal hybrid PhC in large-area. A vertical deposition method was firstly utilized to fabricate poly(St-MMA-AA) opal film. Then liquid PSZ was infiltrated into the voids of the poly (St-MMA-AA) opal to obtain a PSZ–opal composite template. Then the composite template was cured at 170 °C. The template from the composite was removed via full pyrolysis of the composite at 500 °C. Meanwhile, the PSZ was concomitantly transformed into an organic-inorganic hybrid (HPSZ). PSZ was reported to generate a thermally stable and mechanically robust organic-inorganic hybrid material with a Si-N backbone and organic side groups over 400 °C via solidification and pyrolysis.[349] Therefore, the hybrid structure rendered the resulting material to be thermally stable and crack resistant.[350] Consequently, a large-area and crack-free hybrid PhC (I-HPSZ) inverse opal was obtained. **Figures 17g** and **h** show crack-free I-HPSZ PhCs in large-area replicated from templates with a colloidal sphere of 240 nm and 300 nm in diameter, respectively. In addition, this approach also eliminated the cracks from the opal template. The ''self-healing'' effect can be attributed to the unique character of PSZ.

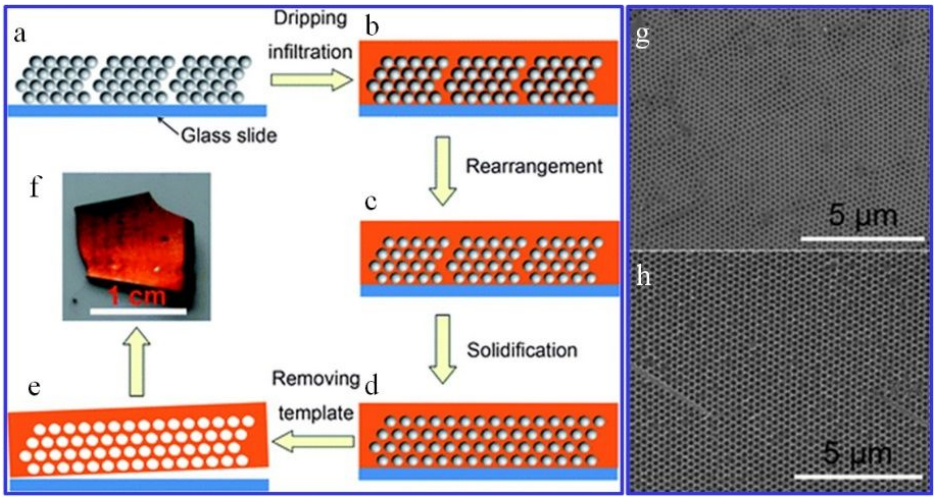

Figure 17. Scheme of procedures for the preparation of HPSZ photonic crystals using poly (St-MMAAA) template. An opal template **(a)** is dripping infiltrated with PSZ solution. When heated, the filled structure **(b)** undergoes a rearranging process to obtain a PSZ–opal composite template with decreased cracks **(c)**. After curing at 170 °C for 2 h, the viscous PSZ changes into a hard solid **(d)**. Meantime, the spatial arrangement of CCs is fixed. This hard-solid composite is transformed into the ultimate inverse opal structure **(e)** by calcination at 500 °C under Ar to remove the opal template. (g) I-HPSZ 1 replicated from an opal template with 240-nm colloidal spheres. (h) I-HPSZ 2 replicated from an opal template with 300-nm colloidal spheres. Reprinted from *Journal of Materials Chemistry,*[348] copyright 2012 Royal Society of Chemistry.

They further revealed the underlying mechanism for the preparation of crack-free I-HPSZs. Polysilazanes (PSZs) are precursors of SiCN ceramics in the polymer-derived ceramics route, which can remain in liquid form below 200 °C.[351-356] In this study, the PSZ can easily form a crosslinked solid through radical polymerization with the addition of dicumyl peroxide at a temperature above 150 °C.[352] The slow flow of the viscous PSZ through the interstices among CCs is sufficient to obtain uniform infiltration during both the infiltration step and drying step. The PSZ does not evaporate or react at the drying stage. During the removal of the solvent, the PSZ retains its viscous state at room temperature, thus preventing the formation of "glassy" cracks and general cracks caused by capillary forces. The cracks can be effectively eliminated using this method since the viscous PSZ precursors serve as ''glue'' to release the stress and to heal the cracks.

Among various defects in inverted CCs, the existence of overlayers on top of the films limits some of their applications in photonics and light-energy conversion.[89, 357, 358] This is because that the interconnected open pores are critical for the transportation of mass and propagation of light.[89, 358, 359] Bartl and co-workers have attempted to fabricate titanium dioxide (TiO_2) without overlayers. It was proposed to use a modified TiO_2 precursor to facilitate the infiltration of the interstices.[360] This method is effective in improving the infiltration of the TiO_2 precursor into hydrophobic PS CCs. However, the overlayer of TiO_2 cannot be removed entirely. In the Zhao group, Cai *et al*. developed a novel sandwich technique to completely remove the formation of the overlayers on top of the 3DOM films.[361] Briefly, a sandwich-vacuum method was used to fabricate binary TiO_2 inverse opals. Colloidal crystal

templates were firstly self-assembled via a convective deposition method[119] or horizontal deposition method[136, 362] on a substrate. The resultant colloidal crystal template was covered with another cover slide. Therefore, the sandwich-like configuration was used to infiltrate the TiO_2 precursor into the interstices of the CCs and dried in the air. The cover slide was then removed after drying. Finally, the sample was calcined to remove the colloidal crystal template to obtain 3DOM TiO_2 without overlayers (**Figure 18a-f**). **Figure 18g and h** compares the TiO_2 inverse opals prepared through a conventional CCT method and the sandwich-vacuum infiltration technique, respectively. It is evident that the overlayers can be eliminated via this sandwich-vacuum infiltration technique. This approach can avoid excess TiO_2 precursor atop the colloidal crystal template and prevent the formation of overlayers. Moreover, it is simple and universal for the fabrication of many other metal oxides inverse opals without overlayers. Cai, Liu and co-workers recently developed an electrically tunable photonic crystal device by using this sandwich-vacuum infiltration method.[54] They fabricated high-quality TiO_2 inverse opals on FTO glass slide and then infiltrated the open macropores with electric-responsive liquid crystals (E7). The Bragg diffraction peaks of the active photonic device can be switched by an electric bias voltage because the electric-responsive liquid crystal molecules within the macropores of the TiO_2 inverse opals can be reoriented by the external electric field.

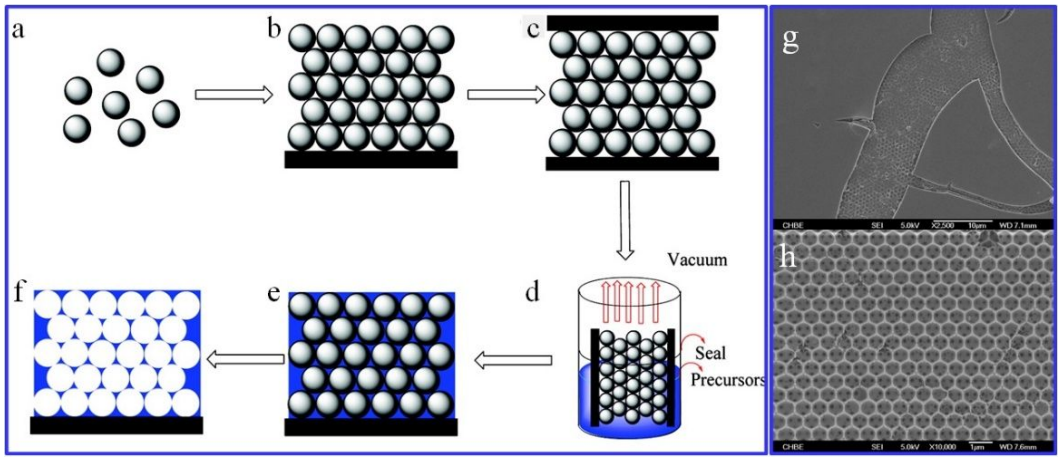

Figure 18. (a-f) Scheme of the fabrication of TiO_2 inverse opals without overlayers using the sandwich-vacuum infiltration technique. **(g)** TiO_2 inverse opals prepared using a conventional colloidal crystal templating method; **(h)** TiO_2 inverse opals fabricated with the sandwich-vacuum infiltration technique. Reprinted from *Langmuir,*[361] copyright 2011 American Chemical Society.

4.2.2. Chemical vapor deposition (CVD)

Apart from the wet chemical process, the dry process is often used to fabricate inverse opals with high refractive index contrast as well. Compared with wet chemical methods, the dry process, such as chemical vapor deposition (CVD) and atomic layer deposition (ALD), offers more precisely controlled and conformal coatings on

a template surface.

A CVD method can be applied to prevent the formation of cracks during the fabrication of inverse opals. Initially, a double templating method is often employed using a sequential SiO_2/Si CVD.[27, 90] Ramanan and co-workers described a single conversion technique to convert holographic lithography (HL) patterned SU-8 3D structures to silicon-air structures by depositing a 30-nm conformal layer of alumina (Al_2O_3) at 90 °C via ALD, followed by low-pressure CVD of disilane at 325 °C for 15 h.[363] The Al_2O_3 thin layer was used as a sacrificial layer, which was later removed by HF, thus exposing the polymer network to air (**Figure 19a-d**). This strategy was found to be useful in restricting crack formation when calcinating the SU-8 template at 410 °C for 4 h. The Al_2O_3 layer demonstrated excellent mechanical and thermal stability, therefore enhancing the stability of the SiO_2 layer and avoiding crack formation during subsequent processing steps.[45] Braun and co-workers recently applied self-assembled CCs to replicate the growth of a refractory material deposited by CVD to generate hafnium diboride (HfB2) PhCs, which can act as the selective thermal-emitting component of a solar thermophotovoltaic device.[364] The resulting photonic materials showed comparable thermal and optical properties to those tungsten PhCs at high temperatures.[365, 366] This is a general and scalable approach to producing high-temperature stable 3D PhCs.

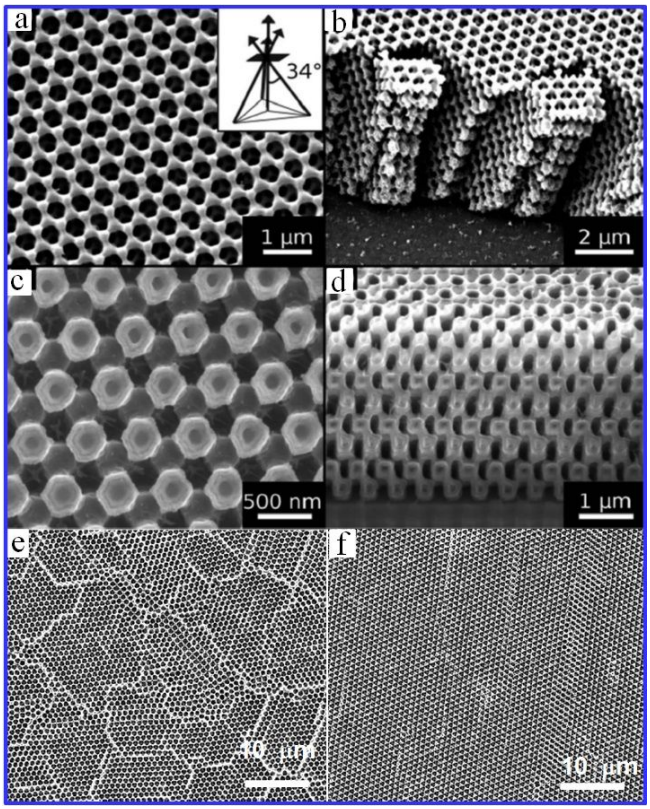

Figure 19. SEM images of the **(a)** top view and **(b)** cross-section view of polymer-air PhCs prepared by holographic lithography with an umbrella beam geometry. SEM images of **(c)** top view and **(d)** cross-section view of air-silicon PhCs from polymeric templates. Reprinted from *Applied Physics Letters,*[363] copyright 2010 American Chemical Society. **(e)** SEM image showing a heavily cracked Si inverse opal. The opal template for the crystal was assembled of 850 nm-SiO_2 spheres; the cracks appeared due to shrinkage of the spheres during Si low-

pressure CVD; **(f)** SEM image showing a "crack-free" Si inverse opal. The spheres were sintered as a dry powder at 600 °C for 4 h before the assembly of the opal; after the heat treatment, the diameter of the spheres was reduced to 792 nm. Reprinted from *Applied Physics Letters,*[173] copyright 2004 American Institute of Physics.

Although homogeneous filtration has been reported as a reliable method to fill opal structures, it does not offer efficient control over vapor deposition to fill thin planar opal films. Instead, a low-temperature CVD technique was developed as a surface-reaction-limited process to a conformal filling gap within the opal structures. At lower temperature (550 ^{o}C), the reduced sticking coefficient of the precursor could facilitate the homogeneous penetration as well as the smooth deposition process, which are critical for the formation of uniform amorphous Si. Subsequent high-temperature annealing (600 ^{o}C) could transfer the amorphous Si to polycrystalline without losing the internal interface smoothness. After deposition, the SiO_2 template was selectively removed via etching. The component homogeneity with Si wafer rendered incorporation between them and enhanced the mechanical properties of inverse opal. The uniformity of inverse opal structures was evidenced by the SEM images in **Figure 20a-c**, which showed the cross-section view of opal structures with different thicknesses. No apparent defects, such as cracks or point defects, were observed. In combination with reactive ion etching (RIE), different planar crystal surfaces were clearly observed in **Figure 20 d, e, and f**. Based on the parameters derived from **Figure 20e**, a PBG located at ~ 1.3 μm was predicted between the eighth and ninth bands.[34]

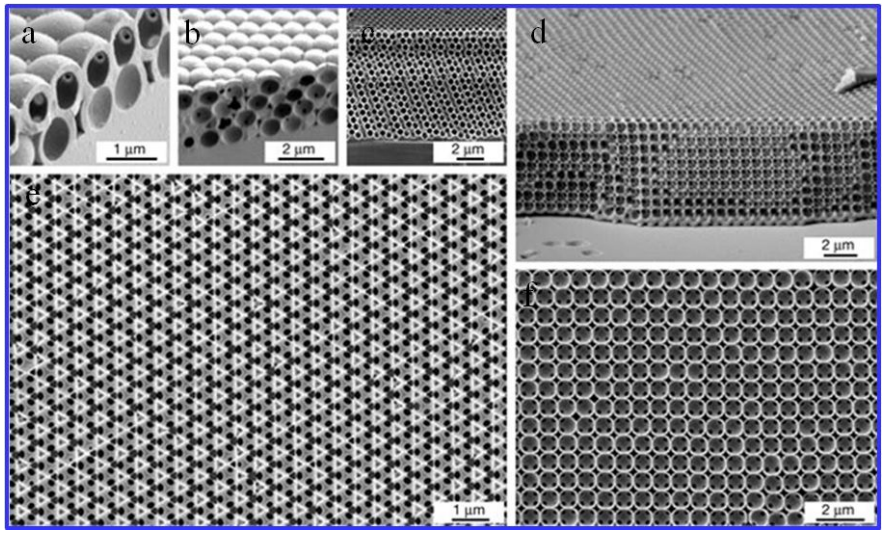

Figure 20. Cross-section SEM images of inverse opal structures with layers of 2 **(a)**, 4 **(b)** and 16 **(c)** layers. **(d)** SEM image of the sample edge showing the (100) surface. **(e)** SEM image showing the planar (111) crystal surface exposed by reactive ion etching (RIE). **(f)** SEM image showing the (100) crystal surface exposed by RIE. The microsphere diameter is 670 nm (c and e), 855 nm (d and f) and 1 μm (a and d), respectively. Reprinted from *Nature*,[34] copyright 2001 Springer Nature.

4.2.3. Atomic layer deposition (ALD)

Atomic layer deposition (ALD) is another flexible and practical method for the fabrication of high-performance PhCs and optical microcavities. One prominent characteristic of ALD over CVD is the self-limiting film growth, which enables accurate control over the film thickness, large-area uniformity, and good conformity and reproducibility.[98]

In a typical ALD process, a binary reaction is divided into two half-reactions. In ALD, the growth of inorganic materials is obtained layer-by-layer via consecutive exposure to one of two complementary chemical species, where individual precursors are fed into the reactor one at a time, coupled with optimization of the substrate temperature. King *et al*.[22, 367] infiltrated ZnS: Mn and TiO_2 into SiO_2-based opal templates with high filling fractions. Highly conformal and uniform coatings were obtained, which contributed significantly to the PBG properties. A wealth of materials, including WN, TiO_2,[22, 368, 369] ZnS:Mn,[367] W,[364] TaN_5, Al_2O_3, and GaAs,[370] have been successfully deposited onto a sacrificial template to create high refractive-index PhCs. **Figures 21a and b** show typical SEM images of the TiO_2 inverse opals fabricated using an ALD method. The ALD can yield continuous and uniform coatings and avoid the formation of cracks associated with liquid infiltration or drying. However, this approach is relatively costly, time-consuming, and necessary to grow upon a defect-free colloidal template in order to obtain a crack-free photonic crystal.

In an independent study, a spin coating method followed by an ALD approach was used to fabricate wafer-scale 2D hole-arrays (**Figure 21c and d**).[371] The hole size and pitch can be controlled by heat treatment and using PS colloidal spheres with different diameters, respectively. This ALD-assisted PS colloidal lithography would be easily incorporated into the mass fabrication of optoelectronic devices, such as light-emitting diodes (LEDs).

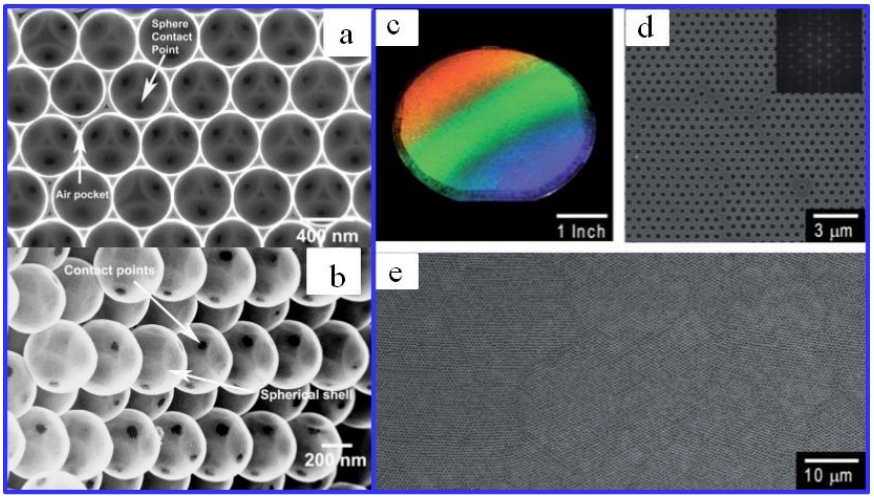

Figure 21. SEM images of 433-nm TiO_2 inverse opal: **(a)** ion-milled (111) surface, and **(b)** fractured surface. Reprinted from *Advanced Materials*,[368] copyright 2005 Wiley-VCH Verlag GmbH & Co. KGaA. **(c)** A photograph of a 4-inch wafer with a SiNx hole array pattern under white light illumination. **(d)** SEM image and its corresponding fast Fourier transform (FFT) image (inset) of a hole-array. **(e)** SEM

image of the hole-array pattern over a large area (~90 μm × 45 μm). Reprinted from *Journal of Materials Chemistry*,[371] copyright 2010 Royal Society of Chemistry.

4.2.4. Co-self-assembly method

Whereas layer-by-layer vapor phase processes, such as ALD, may yield continuous and uniform coatings and inhibit cracking associated with liquid infiltration or drying, these approaches are relatively time-consuming and expensive and need to use a defect-free colloidal template to deposit upon. In addition, the templates need to be thermally and mechanically stable at a high backfilling temperature and may not be filled completely. Up to date, only a few low-cost, reliable, scalable methods have been developed for preparing crack-free, robust inverse opal films composed of single-crystal domains over large lateral dimensions. Among them, the co-self-assembly method seems very promising. Compared with templating methods that involve multiple chemical and physical processes, the co-self-assembly method produces inverse opals with reduced steps. In a typical preparation, the host opal building blocks will be assembled, and the interstitial guest materials will be infiltrated between the CCs simultaneously. The interstitial guest materials can be small colloidal particles or reactive precursors. This advanced technique avoids possible defect formation during the assembly of CCs templates and the precursor infiltration in the templating methods.[172, 372]

Cooperative-self-assembly (CSA) of multiple colloidal components of varying dimensions is one way to fabricate ordered inverse opal structures.[65, 373] However, this method has suffered from low crystalline qualities of the obtained PhC structure, long growth time, and limited size and materials of multiple colloids. More seriously, a jamming effect occurs in CSA at a fairly large growth rate, which makes it very difficult to achieve optimized conditions for fast CSA of multiscale colloids in high quality. Meng and co-workers recently developed an infrared-assisted CSA (IACSA) method to prepare highly ordered multiscale porous materials.[374] In this approach, a unique infrared technique, which can speed local evaporation on the growth interface without varying the growth environment, combined with a concise three-parameter (pressure, temperature, and IR intensity) CSA method to efficiently conquer the jamming effect.[374] Both mono-scale and multiscale PhC inverse opals in a broad range of lattice scales can be fabricated within 15-30 min, which makes this approach favorable for mass fabrication. The several millimeters sized single-crystal domains can be achieved when the optimal growth conditions are obtained. In addition, this method endows optimal conditions for CSA without restrictions on the sizes and materials of multiple colloids. More importantly, this strategy makes a significant breakthrough in the applicability and

universality of both CCs and ordered porous materials. However, the growth temperature should be carefully controlled to prevent property distortion of the building blocks.

Based on their previous work, one significant progress has been further achieved in fabricating crack-free inverse opal films in the same group. Cai and co-workers firstly prepared PS opaline structure by adding a certain amount of TEOS sol during the self-assembly process. Binary CCs and their inverse opal structures were fabricated by this method as well.[229] This method is derived from the fabrication of crack-free SiO_2 CCs via co-self-assembly of SiO_2 colloidal spheres and TEOS sol.[170] Instead of SiO_2 colloidal spheres, PS colloidal spheres were used as the sacrificing template in order to fabricate an inverse opal structure. After co-self-assembly, the resulting binary CCs were calcined to remove PS colloidal spheres and strengthen the inverse opal structure (**Figure 22a**). They further extended this method to the fabrication of the inverse opal structure of SiO_2 and TiO_2 hybrid CCs. The heterostructure of SiO_2 or TiO_2 CCs were fabricated by the sequential deposition of PS colloidal spheres with SiO_2/TiO_2 precursors followed by calcination. The resulting inverse opaline SiO_2/TiO_2 heterostructure showed long-range ordering with multiple photonic stop bands (**Figure 22b**).[231] Moreover, by replacing the hydrochloride with chloroauric acid, they fabricated high-quality Au-loaded SiO_2 and TiO_2 inverse opal structures for sensing and photocatalytic applications.[375, 376] Crack-free gold-loaded SiO_2 or TiO_2 inverse opals can be fabricated at a comparable size scale with pure SiO_2 or inverse opals.[229, 377] And the size-tunable Au nanoparticles can be relatively uniformly distributed on the SiO_2 or TiO_2 inverse opal (i-Au-SiO_2-o or i-Au-TiO_2-o) films, which further improve their property and enhance their potential applications (**Figure 22c-f**). It is worth noting that this method can be extended to *in situ* load Au or other noble metal nanoparticles into the 3DOM structures to obtain various novel photonic/plasmonic structures, which makes this method versatile for photonic and plasmonic applications.

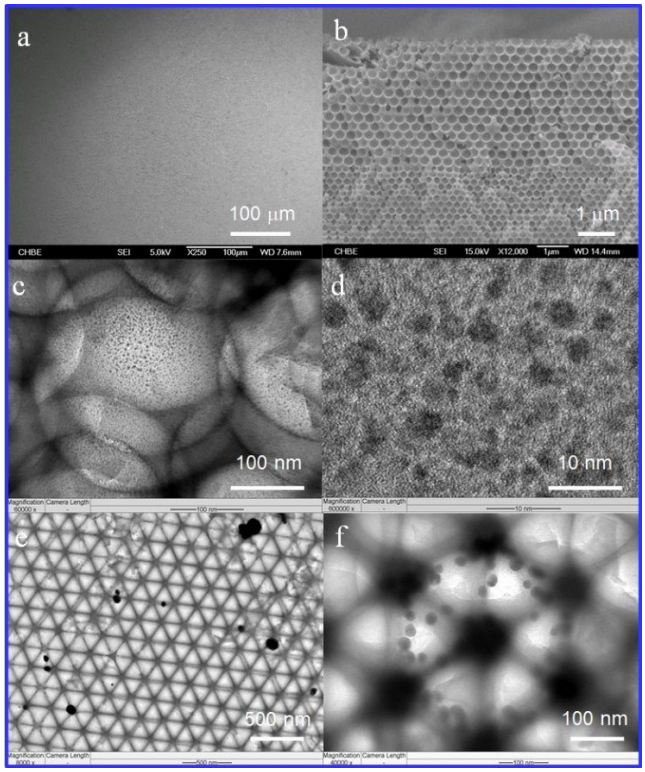

Figure 22. Photonic structures fabricated by a co-self-assembly method. **(a)** Binary CCs in a relatively large area; Reprinted from *Journal of Colloid and Interface Science*,[229] copyright 2012 Elsevier **(b)** SiO_2/TiO_2 photonic heterostructures; Reprinted from *ACS applied materials and interfaces,*[231] copyright 2012 American Chemical Society. **(c)** TEM image of i-Au-SiO_2-o in a relatively large area; **(d)** Au nanoparticles are uniformly distributed in the i-Au-SiO_2-o film; Reprinted from The *Journal of Physical Chemistry* C,[375] copyright 2013 American Chemical Society. **(e)** TEM image of i-Au-TiO_2-o in a relatively large area; **(f)** Au nanoparticles are uniformly distributed in the i-Au-TiO_2-o film. Reprinted from *Journal of Materials Chemistry* A,[376] copyright 2014 Royal Society of Chemistry.

Zhao and his colleagues pioneered the fabrication of crack-free opaline and inverse opaline CCs using their improved vertical deposition (co-self-assembly) method.[170] Hatton *et al.* further extended Zhao's work by co-self-assembling PMMA/TEOS suspension to fabricate PMMA/SiO_2 composite CCs. Instead of SiO_2 and PS colloidal spheres, PMMA colloidal spheres were utilized as building blocks to fabricate the sacrificing template.[172] After removal of the PMMA spheres via calcination, the high-quality, crack-free SiO_2 inverse opals were obtained (**Figure 23**). They also demonstrated that these robust SiO_2 inverse opals could be converted into a variety of materials via a "magnesiothermic" reaction,[378] such as TiO_2 and Si, which keeps the morphology and order of the original films as demonstrated by the reactive conversion. The colloidal co-assembly depicts a facile, scalable method for creating high-quality, chemically tailorable inverse opals for various applications.[379] They proposed a possible underlying mechanism of this co-assembly method to fabricate crack-free inverse opal film. The interconnected silicate network generated during self-assembly of the composite films was believed to prevent the formation/propagation of cracks. Later, the Aizenberg group incorporated gold nanoparticles into a porous 3D SiO_2

inverse opals using a three-phase co-assembly method, which is similar to the above co-assembly method.[379, 380] In addition to TEOS sol, Chen *et al.* demonstrated the fabrication of crack-free films using polyurethane, in which the isocyanate moieties can interact with carboxy moieties on colloidal spheres to form hydrogen bonds to relieve the tensile generated during self-assembly and drying process, resulting in crack-free CCs.[381]

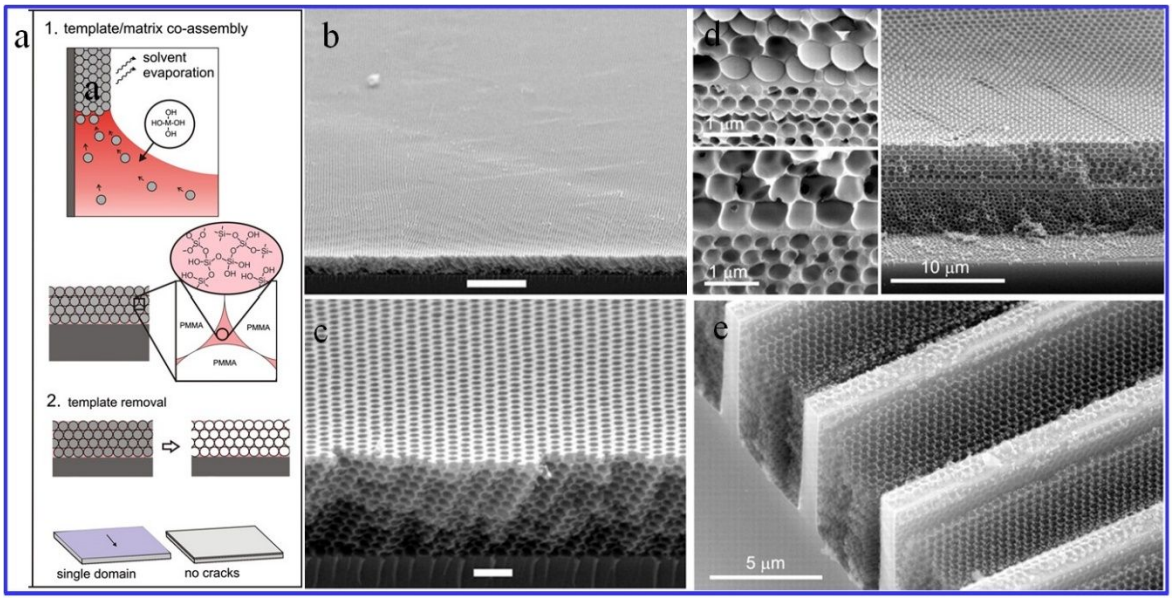

Figure 23. (a) Scheme of the fabrication process of the CCs without cracks by the co-assembly method. **(b)-(c)** SEM images of the CCs without cracks in a large area. **(d)** SEM images showing the cross-section of a bilayer SiO_2 structure prepared by utilizing 300-nm and 720-nm PMMA colloidal spheres. **(e)** SEM image showing the fractured cross-section of inverse opals grown in 4-µm wide, 5-µm deep channels on a Si substrate. Reprinted from *Proceedings of the National Academy of Sciences of the United States of America*,[172] copyright 2010 *National Academy of Sciences USA*.

4.3. Fabrication of large-area high-quality 2D CCs

The aforementioned methods mainly focus on the fabrication of 3D PhCs or PhC films with multi-layer of CCs and their inverse structures. 2D CCs have attracted tremendous interest in recent years. 2D PhCs have found broad applications in photonics and others, including optical switches,[219] all-optical chips,[382] LEDs,[383] and tunable superhydrophobic surface.[384] Moreover, 2D CCs may expand applications of colloidal crystal in angle-resolved nanosphere lithography (NSL) and in the fabrication of high-quality quasi-three-dimensional plasmonic crystals. The fabrication of 2D PhCs, however, is dramatically different from their 3D counterparts. In 2D CCs systems, a meniscus is formed towards the missing dimension. The formation of a meniscus gives rise to strong capillary forces between the colloidal particles that greatly affect the crystalline structure formation. 3D CCs consist of multilayers instead of a single monolayer. In moving from a monolayer in 2D CCs to multilayers in 3D CCs, the effect of the capillary forces does not have the same influence on the overall structure as 2D CCs as a result of the

complete wetting in the inner part of a thicker layer stack during crystal formation. This complete wetting in the inner of multilayers excludes the meniscus effect and hence the influence of capillary forces.[66]

4.3.1. Self-assembly of high-quality 2D CCs at interfaces

Tremendous efforts have been devoted to developing advanced approaches for the fabrication of crack-free 2D single-domain CCs. These approaches include dip coating,[385] spin coating,[204] and electrophoretic deposition[386] of colloidal particles on planar substrates to prepare 2D colloidal crystal arrays. In addition, colloidal particle assembly at air-liquid interface can be used to fabricated 2D CC monolayers, too.[387-390] For example, 2D colloidal arrays have previously been self-assembled on water surfaces.[391-395] During self-assembly, the water surface functions as a substrate on which colloidal spheres can move and organize into an ordered structure more freely than on solid substrates. Self-assembly of colloidal particles at the water-air interface has been evolved into a promising method for the high-throughput fabrication of large-area 2D CCs. More importantly, cracking can be avoided since the used substrate is fluid, which retains the free shrinkage of latex without limitation. Korley and colleagues first developed a colloidal crystal self-organization method at the water-air interface.[396] It should be noted that there are a myriad of factors that may affect the self-assembly of CCs at the water-air interface.[397] Yan and co-workers first used this method to fabricate CCs in a layer-by-layer way.[398] Later, they extended this method to fabricate 2D binary CCs at the water-air interface by adding surfactants.[395] By adding ethanol into the colloidal solution, Cai and co-workers also fabricated the same 2D binary CCs at water/air interface in a large area (larger than 10 cm^2) as a result of convection flow of solvent caused by the rapid evaporation of ethanol.[399] This method avoids the needs of special equipment or surfactants.

Similar to previous studies for the fabrication of 3D CCs on the liquid surface, the Asher group developed a method to the mass production of 2D CCs by spreading PS colloidal aqueous/propanol suspension on mercury surface (**Figure 24a**).[202] This method derives from a previous study, in which PS colloidal aqueous suspension was spread on mercury surface to fabricate 2D CCs.[389] On Hg surface, liquids with moderate surface tension promptly spread as thin films. As a consequence, solvent evaporation during the rapid spreading of the colloidal particle suspension leads to the self-assembly of monolayers. **Figure 24b** shows the bright diffraction of yellow light from a PS colloidal crystal array on a surface of Hg. **Figure 24c** further indicates the ordering of the 2D CCs. This method is affordable for large-area 2D CCs fabrication. However, the mercury is acutely toxic to human health.

Later, the Asher group further improved this method and developed a needle tip flow method to self-assemble

PS on H_2O surface, which avoids the use of toxic mercury.[400] They fabricated large-area (hundreds of square centimeters) 2D CCs within several minutes at the air/water interface by spreading a mixture of alcohol and colloidal spheres on the air-water interface (**Figure 24d**). Meng *et al.* fabricated a 2D CC heterostructure with PMMA colloidal spheres using an identical method.[400, 401] Typically, the air/water interface self-assembly utilizes Marangoni effect to spread the colloidal suspension, where a liquid surface is pushed away from the regions of low surface tension as a result of a surface tension gradient. In this approach, the addition of an alcohol-containing colloidal suspension onto the water surface causes the Marangoni flow. The colloidal suspension rapidly spreads outwards due to the Marangoni flow, which overspreads the water surface with colloidal particles.[402] This is a facile and novel method where the resulting 2D CCs can be transferred onto a number of substrates and functionalized for chemical or biological sensing applications. Using an essentially identical method, Ye and co-workers fabricated 2D CCs as extraordinarily large as 1 m^2 on a glass substrate.[403] Unfortunately, both studies show that the resultant 2D CCs are in multi-domains and lack long-range ordering, which can be confirmed via Debye ring diffraction.[400] Moreover, the cracks cannot be avoided. Most recently, the Asher group developed a novel sensing technique based on the 2D PhCs,[59] in which the 2D PhC is incorporated into a hydrogel, forming crack-free 2D hydrogel PhCs. They firstly prepared the 2D PhCs at the air-water interface and then transferred onto a hydrophilic glass slide, and then cross-linked the monomer solution to form hydrogels on top of the 2D PhCs.[404, 405] Later, Asher *et al.* reported the fabrication of 2D *ncp* PhCs with controllable particle spacing through the swelling or shrinkage of the hydrogel.[406] It should be pointed out that the ordering of the 2D PhCs within the hydrogel mainly depends on the ordering of the original 2D PhCs on the glass slide. Transferring 2D PhCs from a glass slide to a hydrogel does not change the ordering of 2D PhCs. In their methods, as mentioned earlier, the 2D PhCs are often in the form of multi-domains.[202, 400] Fortunately, the sensing technology developed in the Asher group is tolerant to the presence of these multi-domains.[59, 407-410] This method is also affordable for the fabrication of free-standing CC films. By replacing alcohol with toluene, Meng and co-workers fabricated free-standing 2D CCs with PMMA colloids using a similar self-assembly approach.[411]

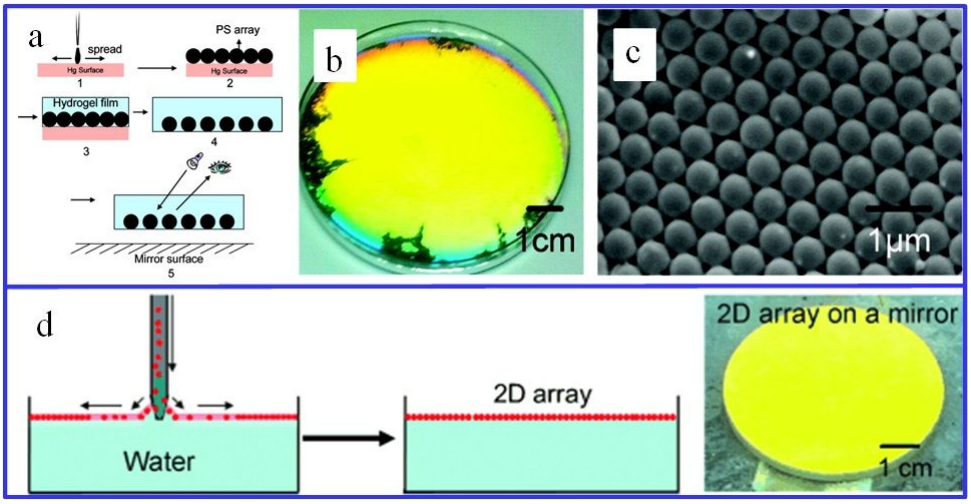

Figure 24. (a) Scheme of fabrication of a 2D PhC on a Hg surface for sensing applications. **(b)** Photograph showing bright diffraction of yellow light from a PS crystalline colloidal array on a Hg surface. **(c)** SEM images of a 2D CCs transferred onto a plastic sheet after sputtering with Au. Reprinted from *Journal of the American Chemical Society*,[202] copyright 2011 American Chemical Society. **(d)** Fabrication of a 2D PhC array using the needle tip flow method. The transfer of the 2D arrays onto a substrate is shown by draining out the water or by lifting the array on a substrate. Photograph of 2D CCs on the water surface in a glass dish 19 cm in diameter using 580-nm PS colloidal particles as building blocks. Reprinted from *Angewandte Chemie International Edition,*[400] copyright 2012 Wiley-VCH Verlag GmbH & Co. KGaA.

Furthermore, Vogel *et al.* independently developed an identical method to fabricate close-packed PhC monolayers, in which a glass slide was used to add colloidal suspensions to the air-water interface. They diluted colloidal aqueous suspensions (typically ≈5 wt.-%) with ethanol to yield a mixture of dispersion and ethanol (50 vol.-%). Then, close-packed monolayer patches crystallized upon spreading of an ethanolic PS colloidal dispersion. When further add colloids, the patches ultimately assembled into a monolayer covering the whole water surface.[412]

In a distinct study, Oh and colleagues developed a method combining the self-assembly of PS colloidal spheres at the air-water interface and the layer-by-layer scooping transfer technique (**Figure 25**).[413] They fabricated wafer-scale 2D CCs in a 1D stack with a combination of these two simple steps. This approach can routinely produce multilayers of PhCs over 4-inch wafers with controlled layer numbers and vertically crack-free over the wafer-scale area (**Figure 25b and c**). In addition to the unary structure, they also investigated the fabrication of mixed binary CCs. Later, Singh *et al.* fabricated multicomponent CCs over large areas using the layer-by-layer method as well.[414] However, this method is laborious and expensive for practical applications. Moreover, the crystallinity of the resultant CCs is poor since the crystalline structure of the next layer is determined by its bottom layer.

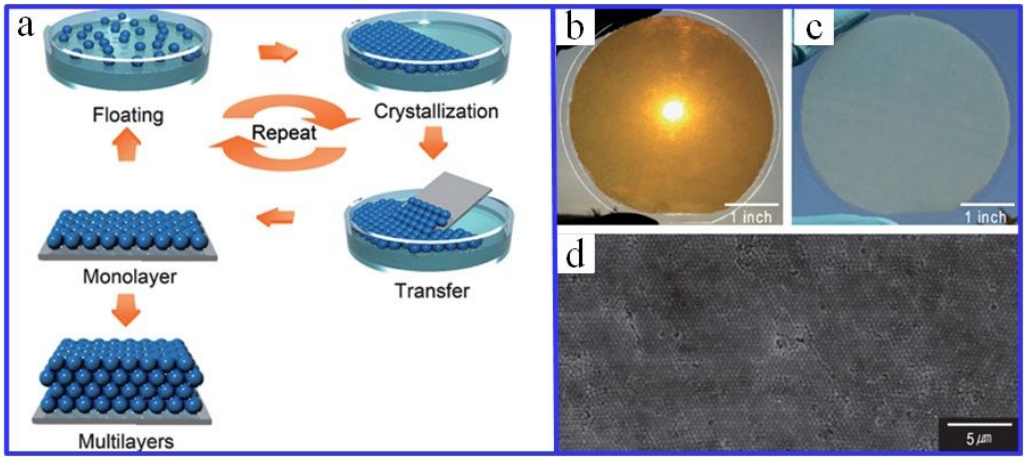

Figure 25. (a) Scheme of the fabrication process: dispersed PS microspheres floating on the water surface, the formation of a monolayer of PS spheres at the air-water interface via self-assembly, scooping transfer to the glass surface, repetition of the scooping transfer of the PS monolayer from the air-water interface to PS microsphere coated glass. A photograph of a transmission **(b)** and reflection **(c)** images under sunlight on a 4-inch glass substrate in diameter with fifteen layers of the multilayer CCs film (d=350 nm). **(d)** FESEM images of the top view in the low magnification. Reprinted from *Journal of Materials Chemistry*,[413] copyright 2011 Royal Society of Chemistry.

4.3.2. Magnetic assembly

The nanoscale magnetic assembly uses external magnetic fields to direct the assembly of colloidal particles.[415] Under a carefully prepared conditions, it is possible to produce 2D CCs on a large scale. This assembly process is fully reversible, remote, and fast to produce 2D CCs on a centimeter scale. It provides CCs with not only good positional orders but also active control over the crystal orientation by simply changing the field directions. Therefore, it offers an additional degree of freedom to modulate the assembled structures, which is not attainable in other assembly methods. In addition, the easy control over both the crystal periodicity and orientation represents an open platform to prepare stimuli-responsive PhCs.[242, 416] On the other hand, however, this method is only appliable to magnetic particles and its scalability is limited by the uniformity of the applied magnetic field. For superparamagnetic particles dispersed in solution, they will be magnetized upon an external magnetic field.[417, 418] The induced magnetic dipole within individual nanoparticle couples with one another if nanoparticles are close enough, forming dipole-dipole interactions. On the other hand, the induced dipole will couple with the external magnetic field as well, known as the packing force under the gradient of the external magnetic field.[419, 420] The dipole-dipole interaction between two neighboring nanospheres can be expressed as

$$\boldsymbol{F} = \frac{3(1-3cos^2\alpha)m^2}{d^4}\boldsymbol{r}$$

where α, (between 0° and 90°), is the phase angle between the magnetic field direction and the line connecting the

centers of two nanoparticles, m is the magnitude of induced magnetic dipole moment, d is the distance between the two nanoparticles, and **r** denotes the unit vector parallel to the line pointing from one nanoparticle to another.[415] Based on this equation, the interaction between nanoparticles in an external magnetic field is highly dependent on the relative configuration of the two nanoparticles. Basically, the dipole-dipole interaction is repulsive if the angle is between 54.74° and 90° and attractive otherwise. Therefore, magnetic nanoparticles tend to assembly into chain-like structures once the dipole-dipole interaction is strong enough to overcome the thermal fluctuations. Such dipole-dipole attraction also couples to long-range inter-particle repulsion, like the electrostatic force between nanoparticles carrying a large number of charges on the surface, hence establishing an equilibrium state with tunable separations.[242, 421, 422]

This scenario could be best fulfilled by superparamagnetic Fe_3O_4 colloidal nanocrystal clusters (CNCs) with controllable diameters (between 100 and 200 nm).[57, 242, 423] Once exposed to an external magnetic field, they will assemble into 1D chainlike structures dynamically regulated by the dipole-dipole attraction and surface electrostatic repulsion under low concentrations.[417] Since the two forces dominating the assembly process are distance-dependent, the separation, as well as the optical properties, can be immediately and reversibly tuned by the strength of the applied magnetic field.[57, 242, 424-426] As shown in **Figure 26a and b**, the structural color was continuously tuned from red to blue once the distance between the permanent magnet and colloidal suspension decreased (increased field strength simultaneously). In terms of spectra, the reflection peak blue-shifted meanwhile. **Figure 26c and d** illustrated dynamic equilibrium between the magnetic attraction-electrostatic repulsion force pairs during the tuning process. Under the scenario of a weak strength, the interparticle separation (d) tends to increase until new equilibrium is established between the two forces. As field strength increases, d will decrease accordingly, resulting in blue-shift of reflected wavelength (λ) originating from their linear correlation in Bragg's Law.[288]

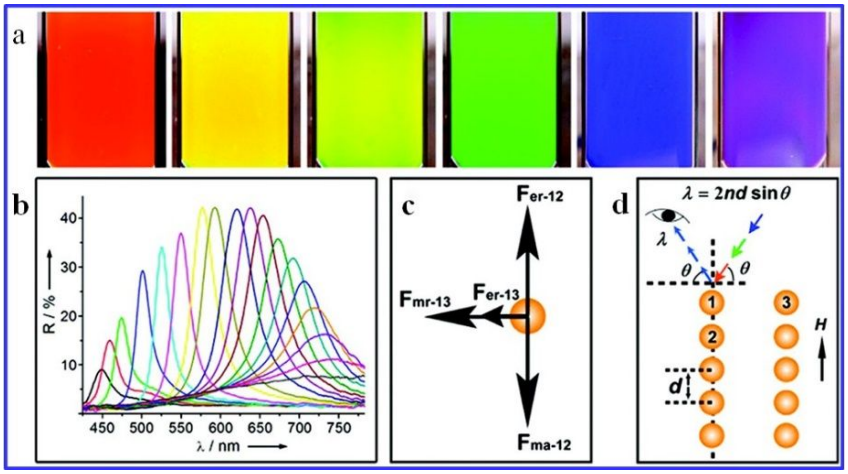

Figure 26. **(a)** Structural colors in a colloidal dispersion of CNCs under different distance from a permanent magnet. From left to right, the

distance increased gradually. **(b)** Reflectance spectra measured by varying the distance between the sample and a magnet. **(c)** Schematic illustration of inter-particle forces during magnetic assembly. **(d)** Schematic illustration of Bragg diffraction from the assembled chains. Reprinted from *Accounts of Chemical Research*,[415] copyright 2012 American Chemical Society.

As the concentration of CNCs increases, the inter-chain interactions become effective under a strong magnetic field. The system is thermodynamically unstable due to the strong repulsive force between chains so that they tend to aggregate and form a zigzag 2D sheet to minimize the repulsive potential. By a sol-gel process, the assembled structures can be fixed and stabilized without modifying their order uniformity. As shown in **Figure 27**, the assembled 2D sheet was uniformly made of monolayered CNCs, and the height was around ~20 μm. Notably, in an external magnetic field, the height direction of the assembled 2D sheet was parallel to the direction of the field.[427-429] The inner arrangement of CNCs was observed in the TEM image as shown in **Figure 27d** and three neighboring nanoparticles formed an equilateral triangle roughly with a phase angle (α) of 60°. By simply varying the diameter of building blocks, different structural colors were observed from the top of 2D sheets (**Figure 27**). Since there was hard contact between nanoparticles, the diffraction was mainly determined by the size of the building blocks. 2D nanosheets diffracted light with a longer wavelength once larger CNCs was used during assembly.[430] Further increase in the concentration induced phase change of assembled entity from 2D nanosheets to high crystalline 3D structures. This crystallization was initiated by the local concentrating of nanoparticles under the gradient of the external magnetic field, and 3D lattices with different phases were achieved by changing the field strength.[431, 432]

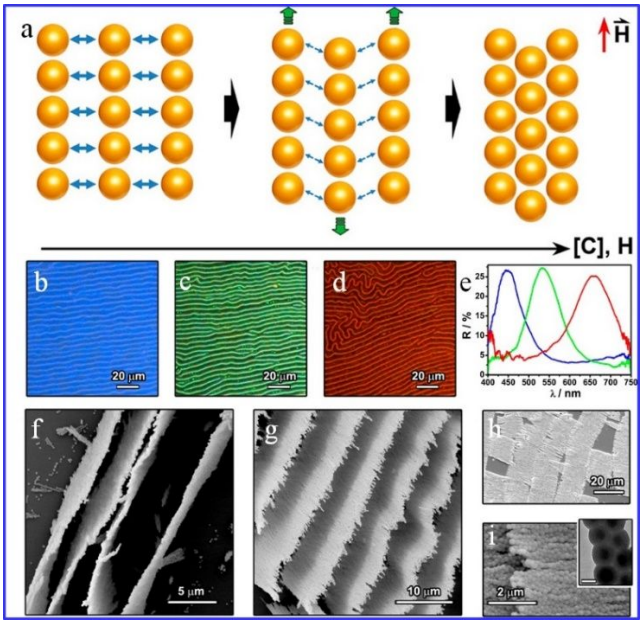

Figure 27. **(a)** Schematics illustrating the formation of 2D nanosheet. Dark field optical microscopy images of fixed 2D photonic structures assembled by CNCs with diameters of **(b)** 120 nm, **(c)** 150 nm and **(d)** 190 nm. **(e)** The corresponding reflectance spectra. **(f-i)** SEM images

of 2D photonic structures. Insert in (i) was the TEM image showing the zigzag arrangement of CNCs. Reprinted from *Nano Letters*,[430] copyright 2010 American Chemical Society.

4.3.3. Langmuir-Blodgett method

Langmuir-Blodgett (LB) method is a method that is affordable for the growth of PhCs in a large area. The LB technique involves the controlled contraction of molecular monolayers that are produced through spreading amphiphilic compounds at the air-water interfaces. Although a monolayer can be fabricated with well-ordered structure, it is hard to fabricate well-ordered 3D PhC structure using this LB technique.[433, 434] For the detailed description of features and applications of this interesting technology, one can refer to a progress report on LB technique.[413]

Vogel *et al*. reported the preparation of large-area binary colloidal monolayers in large areas with the conventional LB technique.[435] In this method, the interstitial sites were tailorable, and the stoichiometry of binary CCs could be controlled over a broad range of size ratios using a Langmuir trough. The films were transferred to solid substrates by utilizing a surface lowering technique. A number of substrates with arbitrary topographies can thus be decorated with colloidal monolayers in large areas. However, this method is not effective to fabricate high-quality 2D CCs as one can observe the uneven structural color of the 2D CCs. The obtained 2D binary CCs via this LB technique still contained many defects, such as grain boundaries, vacancy defects, and line defects, resulting in a polycrystalline structure. To obtain high-quality 2D CCs with LB technique, ultrasonic annealing at 1.2-1.5 MHz and barrier-sway process were applied, and remarkably increases of the ordered area were achieved.[436]

In an independent study, Pan and colleagues invented a facile approach to promptly fabricating large-scale monolayer colloidal crystal arrays on substrates.[391] A close-packed colloidal crystal monolayer was first assembled on a vortical water surface using latex particles; then the monolayer was transferred onto substrates by a withdrawer.[391] Conceptually, this approach is very similar to the LB method for film deposition but without the need for an LB trough.[437] The resulting samples show a large-scale periodic feature according to both SEM observations and optical microscopy, and diffract the laser beam. This novel technique is time-saving, widely accessible, and applicable to large colloidal particles (up to 2 μm). It is thus very promising for nanofabrication.[391]

It should be noted that the application of the LB technique has been restricted by the size of the substrate for depositing PhC structures. Most recently, Parchine and colleagues further improved the LB method and developed a roll-to-roll LB method to fabricate 2D colloidal PhCs on flexible poly(ethylene terephthalate) (PET) film in an

area as large as 340 cm^2 to meet the demand of high volume manufacturing.[438] A NIMA LB trough (model 1222D2) was applied for the LB deposition process of SiO_2 spheres on the PET film. The difference between this roll-to-roll LB method and the conventional LB method lies in that a special roll-to-roll unit replaces the standard alternate dipper mechanism in the NIMA trough (**Figure 28a and b**). **Figure 28c** shows a large-area monolayer of SiO_2 spheres fabricated with a roll-to-roll slot-die coater. **Figure 28d** displays the SEM image of SiO_2 monolayer fabricated with this roll-to-roll LB method on the PET film, indicating the high quality of the 2D close-packed silica spheres hexagonal structure. The roll-to-roll LB method enables large-area applications of colloidal PhCs, such as flexible polymer solar cells, thin-film photovoltaic panels, colloidal lithography, flexible OLEDs, and others.[438]

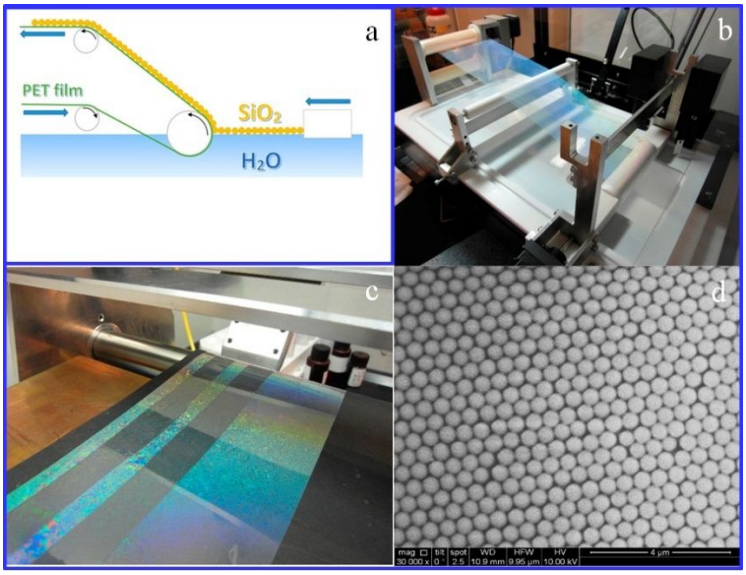

Figure 28. (a) Schematic illustration of the roll-to-roll LB method. **(b)** Photograph of the NIMA trough, the roll-to-roll unit, and the PET substrate deposited with an LB monolayer of SiO_2 spheres. **(c)** Photograph of the roll-to-roll slot-die coating with strips of optical adhesive NOA164 on the PET substrate with the LB monolayer of 550-nm SiO_2 spheres. **(d)** SEM images of the monolayer of 550-nm SiO_2 spheres assembled on the PET film using the roll-to-roll LB method. Reprinted from *Langmuir*,[438] copyright 2016 American Chemical Society.

4.3.4. Spin-coating method

The spin-coating method is versatile for the fabrication of a wealth of 2D nanostructures as well. Jiang *et al.* first fabricated wafer-scale 3D PhCs and 3DOM polymeric structure by using a spin-coating method.[204] Later, they fabricated 2D *ncp* CCs in wafer-scale using the same spin-coating method.[439] The key to fabricate 2D CCs via the spin-coating method lies in the control of the spin-coating speed. In contrast to the abrupt acceleration (~2000 rpm/s) as demonstrated in their previous spin-coating approach, the moderate increase of the spin speed (~200 rpm/s) was found to be essential for the fabrication of high-quality monolayer CCs. After selective removal of the polymer

matrix using oxygen plasma etching, 2D *ncp* SiO_2 CCs were obtained (**Figure 29a-b**). These 2D *ncp* CCs can also be used as a template to fabricate wafer-scale periodic nanohole arrays from a variety of functional materials, ranging from metals, semiconductors, to dielectrics.[440]

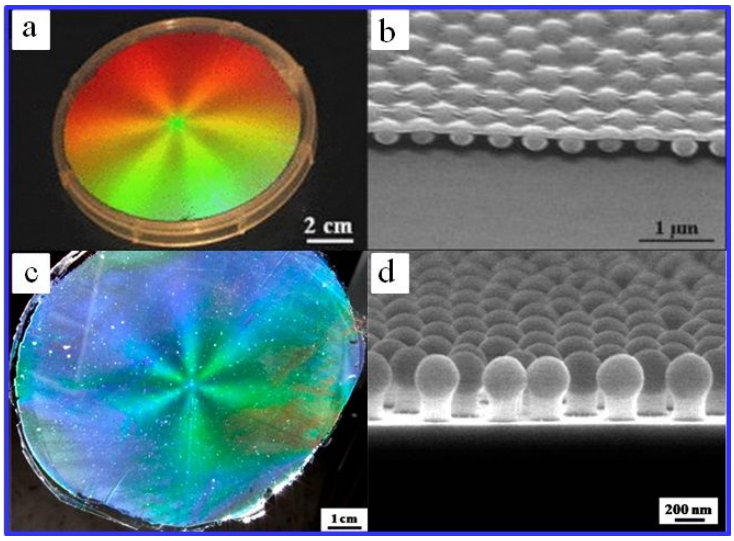

Figure 29. (a) Photograph of a 4-inch wafer-sized sample illuminated with white light. **(b)** A typical cross-sectional SEM image of a monolayer colloidal crystal-polymer nanocomposite prepared by spin coating. Reprinted from *Applied Physics Letters*,[439] copyright 2006 American Institute of Physics. **(c)** Photograph of a 4-inch wafer-scale PVA composite film with 330-nm SiO_2 colloidal spheres inside illuminated with white light. **(d)** Cross-sectional SEM images of a periodic array of "mushrooms" composing of spherical SiO_2 caps and ethoxylated trimethylolpropane triacrylate polymer stems made via combining spin-coating and oxygen plasma etching. Reprinted with permission from *Langmuir*,[441] copyright 2013 American Chemical Society.

Later, Jiang and colleagues further developed a colloidal transfer technique that allows scalable fabrication of 2D *ncp* SiO_2 CCs on a number of substrates via the spin-coating method. Using a spin-coating approach, 2D CCs with an unusual *ncp* structure were deposited on silicon wafers. Next, a polyvinyl alcohol (PVA) film was cast upon the spin-coated CCs to transfer the *ncp* particle arrays onto a variety of substrates (**Figure 29c**). Thermal treatment of the composite film was used to easily tune the lattice spacing of the monolayer CCs by varying the treatment duration.[441] After spin-coating and oxygen plasma etching, "mushrooms" like 2D *ncp* SiO_2 CCs were fabricated (**Figure 29d**).

4.3.5. Microgel self-assembly

It has long been well demonstrated in the fabrication of 3D PhCs in long-range ordering with the aid of gelation. Similarly, large-area 2D PhCs can be fabricated as well by using, e.g., PNIAM microgels. However, there are few reports on the utilization of PNIPAM colloidal particles to fabricate crack-free and self-healing 2D PhCs

in a large area.[442-445] Recently, Quint and co-workers fabricated 2D *ncp* PhCs with exceptional long-range ordering by using PNIPAM microgels.[442] In this work, PNIPAM microgel colloidal suspension was firstly deposited on a cleaned glass slide. Then a drop of ethanol was added to the PNIPAM suspension to give rise to a gradient in surface tension. The gradient in surface tension spontaneously divided the large droplet into several smaller droplets and coalesced within several seconds. During this process, the PNIPAM microgel particles self-assembled into the ordered 2D CCs at the air/liquid interface. The low solubility of PNIPAM microspheres in alcohol/water mixtures caused the formation of highly ordered 2D CCs at the air/liquid interfaces. These small crystalline domains were merged into monocrystalline by using mechanical force. In prior to spin coating, grain boundaries were eliminated by treating the 2D PNIPAM CCs at the air/liquid interface with an oscillatory air stream. The applied shear force merged small crystalline domains to a large monocrystalline area. Finally, spin coating was utilized to inhibit density stripes formation in the crystal. The extraordinary long-range ordering 2D PNIPAM PhCs can be as large as square millimeters using this method.

It has been well illustrated that 3D microgel CCs can intrinsically tolerate defects. As a matter of fact, one can also derive 2D PhCs from highly ordered 3D PhCs. Most recently, Zhang and co-workers fabricated large-area 2D CCs starting from 3D CCs. They first assembled large-area and high-quality 3D CCs using SH-modified PNIPAM microgel spheres.[443] The first layer of the 3D CCs close to the substrate was then *in situ* fixed onto the substrate via the UV-induced interfacial thiol-ene click reaction. Subsequently, the reaction cell was opened, and the substrate was thoroughly rinsed in water followed by air drying. The resulting 2D CCs inherit the highly ordered crystalline structure from the 3D CCs in an area as large as 7.7×3.5 cm^2. A similar method was also utilized by the same research group to fabricate high-quality 3D microgel CCs via alkyne-azide click reaction.[445]

4.3.6. Confined convective assembly

Convective self-assembly, which was first devised by Dimitrov *et al.*, has been successfully used to fabricate 2D CCs on a centimeter scale.[118] Convective self-assembly is driven by the solvent evaporation, and convective flow of solvent, during which a three-phase contact line forms at the meniscus of the colloidal suspension film and a laterally capillary force will bring the colloidal particles to the contact line upon the solvent thickness is comparable to the size of the colloidal particles.

Despite its success in fabricating 2D CCs, this method still requires a long time and a large volume of colloidal dispersions. For overcoming these obstacles, convective self-assembly confined between two planar substrates has

been developed to fabricate 2D CCs due to its simplicity and robustness.[118, 446-448] Using a confined convective assembly method, Kim *et al.* explored a method for the rapid fabrication of well-ordered 2D and 3D colloidal crystal films over a large surface area.[447] In this study, the lift-up rate of the substrate were used to modulate the meniscus thinning rate in order to assemble the colloidal particles into 2D or 3D structures. In addition, the method was also used to fabricate binary CCs by consecutively depositing colloidal particles with two different sizes.

Though the confined self-assembly method can be employed to fabricate 2D CCs, the uniformity and crystallinity of the resulting 2D CCs are still poor. The presence of a polycrystalline structure generated using this method inhibits their broad applications. Template-directed self-assembly can be employed to address these drawbacks.[193, 198, 449-452] However, it is difficult to transfer the resulting 2D CCs from the patterned substrate to a flat substrate. Single-domain 2D CCs with centimeter size were successfully fabricated by capillary forces under a straight drying front generated in a wedge-shaped cell.[453] Three types of cells, including a rectangle-shaped cell with one open side, a rectangle-shaped cell with three open sides, and a wedge-shaped cell with three open sides, were applied to examine the impact of the shape of the drying front line on colloidal crystal growth (**Figure 30a-c**). The formation of polycrystalline CCs was inhibited to the greatest extent when a wedge-shaped cell was applied to confine the assembly process. While altering the cell shape can curve the contact line of the drying front, which consequently leads to the formation of colloidal crystal structures containing high-density crystal domains. **Figure 30d** shows a typical optical microscopy image of the 2D CCs self-assembled in a wedge-shaped cell.

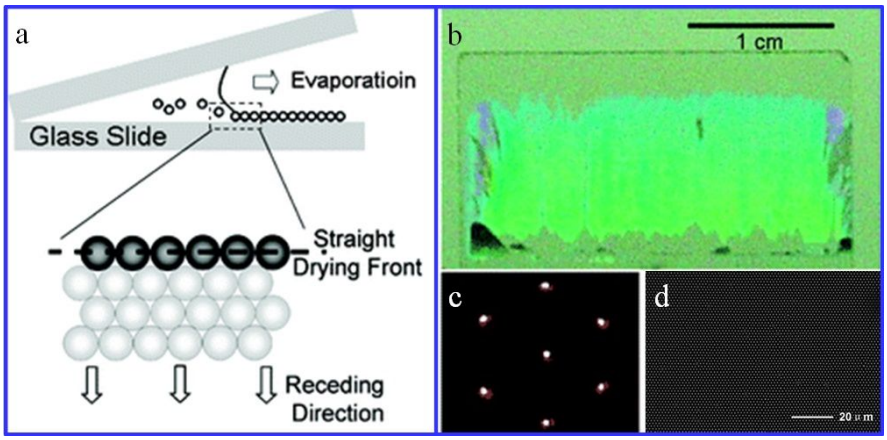

Figure 30. (a) Scheme of a wedge-shaped cell with three open sides. **(b)** Optical photograph of the colloidal PhCs self-assembled in a wedge-shaped cell. **(c)** A representative laser diffraction pattern when illustrating the laser beam on the sample surface. **(d)** An optical microscopy image showing a typical area of the 2D CCs deposited in the wedge-shaped cell. Reprinted from *Langmuir*,[453] copyright 2010 American Chemical Society.

4.3.7. Dynamic hard-template method

Apart from the 2D opaline structure, 2D inverse opaline structure based on CCTs has also been investigated for their distinctive properties and potential applications in photocatalysis, solar cells, sensors, and electrochromic devices.[454, 455]

Most recently, Djaoued and colleagues exploited a 'dynamic-hard-template' infiltration approach to prepare crack-free 2D inverse opal films (WO_3 and anatase TiO_2) in large-area on both ITO coated rigid glass substrates and flexible substrates (**Figure 31a**).[456-459] Since cracking mainly occurs during the infiltration and calcination steps, it is important to develop a method to prevent crack formation during the two steps. For example, in the fabrication of 2D TiO_2 inverse opal structure, Djaoued et al. applied a solution containing preformed anatase TiO_2 crystalline nanoparticles to backfill the opal structure, and tetrahydrofuran (THF) was used to remove the PS CCT. In a typical process, a dynamic 2D PS opal film was firstly self-assembled on the water surface containing surfactant sodium dodecyl sulfate (SDS). Then, the preformed anatase TiO_2 nanoparticle sol was infiltrated into the PS colloidal crystal interstices as a guest material from the bottom, which eliminates the high-temperature calcination step. The resultant floating PS/TiO_2 colloidal crystal composite film was picked up and deposited on ITO substrates. Optimized mild heat treatment was adopted to reinforce the structure and THF was used to remove the PS template, which consequently yielded 2D inverse TiO_2 opal films. The fabrication of 2D WO_3 inverse opal structures involves identical steps except for the use of WO_3 powder or sol to replace crystalline anatase TiO_2 nanoparticles.[456, 458] **Figures 31b-d** show the structural color of 2D PhCs fabricated in large-scale on soft substrates with good ordering.

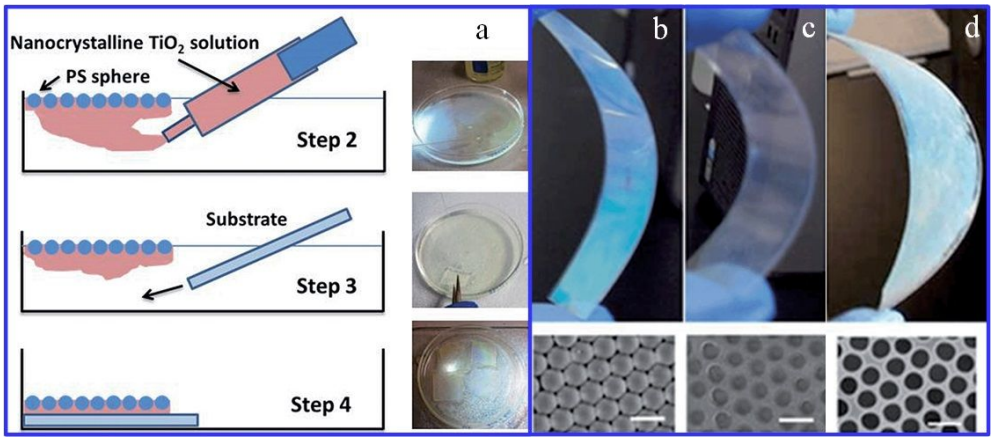

Figure 31. (a) Steps of the dynamic hard template strategy. The first step (not shown in the scheme) is to prepare 2D opal film floating at the air-solution interface with the aid of surfactant of SDS. Photographs and SEM images for **(b)** 2D PS opals; **(c)** PS/TiO_2 opal composite and **(d)** anatase 2D-TiO_2 inverse opal films on soft ITO/PET substrates templated from 410-nm PS CCs. Scale bars in the SEM images: 500 nm. Reprinted from *Journal of Materials Chemistry C*,[457] copyright 2014 Royal Society of Chemistry.

4.3.8. Other methods

Apart from the above methods, there are still many other methods that can be used to fabricate high-quality 2D CCs in large-area. For instance, mechanical annealing was explored to diminish grain boundaries in the CCs. Wei *et al*. investigated the structures and dynamics of grain boundaries by embedding 2D colloids into a soap film.[460] The typical grain size was about 100 lattice spaces. When an external mechanical vibration was employed to the bulk colloidal suspension, however, mitigation and rotation in the grain boundaries were observed under the stress field generated by the vibration. The overall length of the grain boundaries diminished logarithmically with time, with the rate constant being a function of the excitation strength. This phenomenon, known as "mechanical annealing," offers a straightforward route to prepare large 2D single-domain crystals.

Colloidal epitaxy was proposed as a promising route for creating 3D CCs with defined structure and orientation.[461] Epitaxial assembly attracted intense interest in recent years owing to its ease in the self-assembly of block copolymer into 2D periodic structure[194] and fabricating 2D defect-free CCs.[462] Liu and co-workers developed an epitaxial assembly method to guide the crystallization of 2D CCs under an alternating electric field (AEF). In their study, the CCs with a predetermined orientation were prepared at a particular position of an electrode, where a colloidal line was used as an epitaxial template. The control over both the AEF frequency and the template resulted in well-defined linear defects in the CCs. The undesired defects can be *in situ* avoided through a template-guided annealing process.[462] They also fabricated a variety of patterned CCs with adjustable lattice spacing and even with binary lattice spacing by varying the electrode pattern geometry and the AEF.[386] This epitaxial templating approach is fast, amenable, and reversible for the preparation of large-area oriented patterning of CCs. It provides an alternative approach to the fabrication of novel optical/electrical materials and devices, such as electrically tunable photonic waveguides and e-papers, whose properties and functions can be reversibly changed.[463]

In **Section 4.1.5 and Section 4.2.4**, we mentioned that TEOS could be used to fabricate crack-free 2D CCs and inverse opals. In addition, a water-soluble polymer (PVP)[464] was also introduced into the colloidal suspension to minimize the defects density in 2D CCs. The presence of PVP in the aqueous phase facilitates the arrangement of the colloidal particles into more hexagonally close-packed single-crystalline domains during the self-assembly process, leading to a decrease in the defect density. Moreover, the physical stability of the resulting 2D CCs can be enhanced due to the interparticle-bonding and particle-substrate bonding caused by the polymer bridges.

Besides general CCs, photonic structures with special patterns also attracted intense interest. The Yang group reported a method combining soft lithography technique[465] with controlled deformation of a PDMS elastomer stamp, which can transform 2D hcp SiO_2 colloidal sphere arrays into 2D *ncp* crystal.[466] As shown in **Figure 32a**, self-

assembled 2D hcp colloidal sphere arrays were transferred onto the PDMS stamp surface using the lift-up approach. Subsequently, both their lattice structure and lattice spacing could be tuned by mechanical stretching or solvent swelling of as-prepared 2D *ncp* colloidal sphere arrays when they were transferred onto a flat PVA-coated substrate. Afterward, the PVA film was removed via calcination. The resulting *ncp* arrays that fell on the substrate being intact could be deformed, lifted up, and further transferred by another PDMS stamp. Thus, the lattice feature of the patterned CCs could be altered stepwise. Finally, the *hcp* colloidal arrays could be transformed into full-dimensional *ncp* ones in all five 2D Bravais lattices through the combination of anisotropic mechanical stretching and isotropic solvent swelling (**Figure 32b**). This method opens an alternative for preparing unique and complex 1D and 2D *ncp* colloidal crystal structures (**Figure 32c-e**). These as-prepared structures may find broad applications in prototype models or colloidal lithography for optical materials.

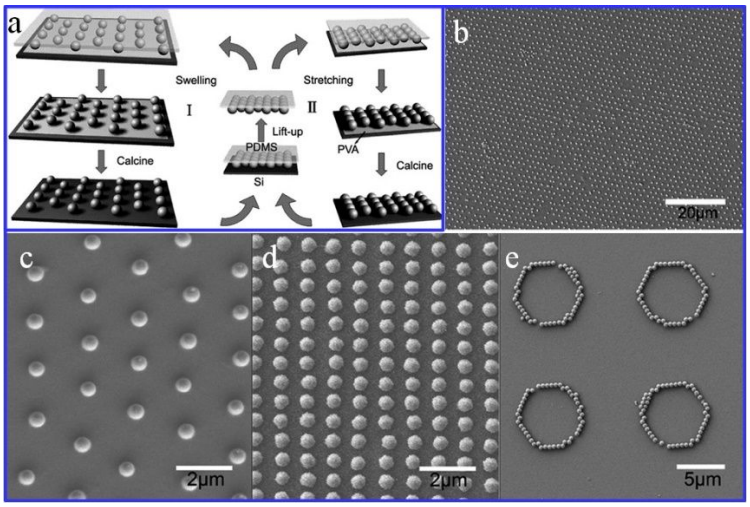

Figure 32. (a) Schematic illustration showing the procedure for the fabrication of 2D *ncp* colloidal sphere arrays with tunable lattice spacing and structures. **(b)** Low-magnification SEM image of the hexagonal *ncp* array of 560-nm SiO_2 colloidal spheres assembled on a silicon wafer via the evaporation of suspension. **(c)** SEM image of the hexagonal *ncp* arrays on a PVA-coated substrate prepared through swelling the PDMS film using pure toluene. **(d)** SEM image of centered rectangular arrays with different parameters prepared by one stretching process. **(e)** A high-resolution image of hexagon array with double-microsphere width. Reprinted from *Langmuir*,[466] copyright 2009 American Chemical Society.

In addition to the above self-assembly methods, which rely on wet self-assembly technique, a 'dry manual' assembly approach was developed,[467] in which dry colloidal spheres were rubbed into the patterned substrate to quickly organize colloidal spheres into perfect 1D and 2D arrays in large scale. Comparing to 'wet self-assembly' method, this is a manual assembly method. Therefore, it is referred to as 'dry manual assembly'. The dry manual assembly approach can organize the dry colloidal spheres into 1D and 2D single crystals on nanolithographically patterned substrates. The obtained 1D and 2D single crystals can be as large as centimeters or larger scales with a well-defined sphere networking pattern. This advanced strategy opens an alternative for the particle organization

beyond the conventional colloidal self-assembly in solution. It should be noted that this method is infeasible for the fabrication of 3D CCs.

5. Emerging applications of advanced self-assembly methods

Self-assembly of CCs has attracted increasing interest due to their wide fundamental and practical applications. A larger number of advanced self-assembly methods have been developed to meet the high requirements of these applications. Meanwhile, in recent years, the rapid development of advanced self-assembly methods further enabled and boosted many emerging applications of CCs, e.g., metasurfaces/metamaterials,[468, 469] microchips,[470] nanolithography,[471] SERS,[472] solar photovoltaics,[473] nanoelectronics,[474] white-lighting LED,[240] microfluidic chips,[475] barcodes,[331] drug delivery,[476] novel PhC sensors,[477-479] biomedical engineering,[480] and others.[481-483] In addition, successful fabrication of cubic diamond and pyrochlore structure of CCs via colloidal self-assembly will open a cPBG at low refractive index contrast. These CCs with a cPBG can be used to improve the performance of a wide range of optical applications, such as optical waveguides,[3] optical cavities,[484] filters and laser resonators,[484] high-efficient lasers,[38] enhancement of nonlinear optics,[485, 486] and optical computing.[487-489]

In this section, we will review the emerging applications of high-quality CCs and unique photonic structures prepared through these advanced self-assembly approaches. Those conventional applications of CCs and emerging applications of PhCs fabricated with top-down methods will not be covered here. It is apparent that high-quality CCs that can be fabricated in large-scale with these advanced methods enable a broad range of emerging applications that CCs made by conventional methods cannot achieve.

5.1 Metasurfaces and Metamaterials

The exploration of novel metamaterials and metasurfaces has attracted tremendous interests in the past two decades for their unprecedented power in manipulating light properties and huge potentials brought forward for novel photonic devices and applications.[490, 491] Metasurfaces and metamaterials with deep sub-wavelength structures in either a thin film or in a bulk material can be formed by either top-down lithography techniques of bottom-up assembly method. The top-down approaches are much more widely adopted for proof of concept and prototype demonstration, but are usually high cost, low throughput and more suitable for a flat surface. The potentially low-cost, free-form, and large-area colloidal self-assembly method would greatly boost the development

of metasurfaces and metamaterials for their applications in e.g., sensing, imaging and quantum devices.[469]

Among various colloidal self-assembly methods, the most straightforward one is to directly self-assemble colloidal particles into metamaterials/metasurfaces. Karg and co-workers demonstrated the fabrication of periodic plasmonic metasurfaces via self-assembly of Ag@Au-PNIPAM nanoparticles **(Figure 33a)**.[492, 493] Monodispersed core@shell colloidal particles were firstly synthesized, and then a monolayer of the noble metal@hydrogel core@shell metamaterials was fabricated via interfacial self-assembly with the assistance of SDS. These studies indicated that colloidal self-assembly is a very powerful tool to fabricate nanophotonic devices.

The most scalable and cost-effective approach to colloidal metasurfaces is the template-assisted self-assembly method. Its pronounced feature, as mentioned in the previous part, is that it can provide precise control over the placement of colloidal particles. For instance, Brugger *et al.* demonstrated the fabrication of metamaterials via template-assisted self-assembly of Au nanorods on topographical templates.[494] In this study, topographical templates with low-wetting traps were used to give rise to highly ordered metamaterials structure, which provide good control over the self-assembly. Through optimizing the overall self-assembly process, Au nanorod arrays with excellent control over the orientations, positions and interparticle spacing were achieved on the centimeter-sized substrates **(Figure 33b)**. Another merit of this method is that it is readily scalable with good reproducibility.

Yang *et al.* reported the self-assembly of Ag polyhedral particles into CCs with the size of millimeter-scale (> 25 mm^2) for metamaterials **(Figure 33c)**.[495] In this study, monodisperse Ag polyhedra were modified with PVP dissolving in DMF and then self-assembled into plasmonic metamaterials via gravitational sedimentation in PDMS reservoirs. The resulting 3D plasmonic metamaterials have great potential in nanophotonics and sensing.

Another strategy to fabricate metamaterials is based on the NSL, a combination of bottom-up self-assembly and top-down lithography techniques. Ravaine *et al.* reported the preparation of double fishnet structured metamaterials using the NSL method.[496] They first assembled 2D PS CCs on a conductive substrate using the interfacial self-assembly method. Then the PS colloidal particles were etched with oxygen plasma to reduce their sizes and to subsequently obtain non-close-packed 2D CCs. The resulting 2D CCs were electrodeposited with Au **(Figure 33d)**. The double fishnet negative-index metamaterials were obtained and exhibited tunable extinction resonances in NIR. Therefore, the combination of electrodeposition with NSL represents an efficient and powerful method for the fabrication of large-area metamaterials at low cost. Most recently, Ravaine and co-workers demonstrated fishnet-like negative-index metamaterials that can respond to light ranging from visible to infrared. They first used a self-assembly method to fabricated large-area CCs followed by a combination of nanoimprint and

electrodeposition.[497] The resulting metamaterials can be prepared on conductive oxides substrate and thus can be implemented for optoelectronic devices. They showed that the metamaterials could be used as an optical sensor for the detection of different liquids. Interestingly, the combination of emerging technologies with PhC-based metamaterials can create flexible and wearable point-of-care with extremely high sensitivity.[498]

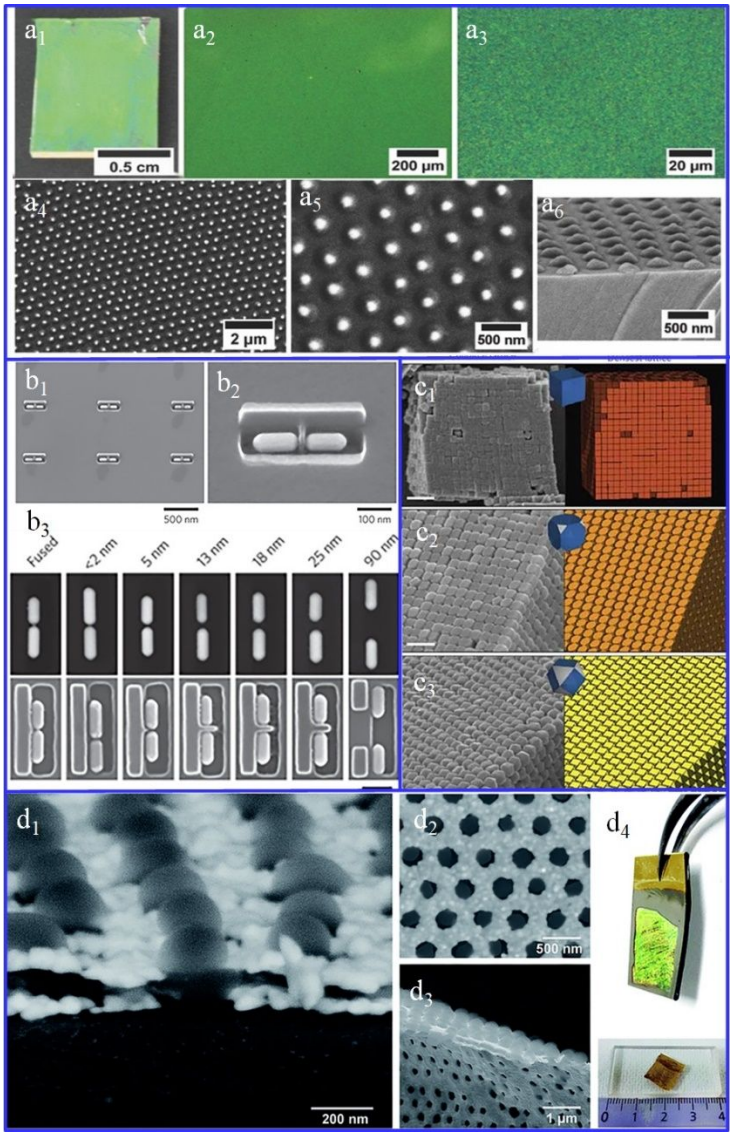

Figure 33. (a) Images of self-assembled Ag@Au colloidal arrays. (**a_1**) A digital photograph of the samples (0.8 cm × 1.2 cm). Bright-field optical microscopy images at (**a_2**) low and (**a_3**) high magnification. Top-view SEM images at (**a_4**) low and at (**a_5**) high magnification. (**a_6**) Side-view SEM images at a tilt angle of 15°. Reprinted from *Advanced Optical Materials*,[493] copyright 2017 WILEY-VCH Verlag GmbH & Co. KGaA, Weinheim**. (b)** Capillary assembly of Au nanorods. (**b_1**) Low-magnification and (**b_2**) high-magnification SEM images at 45° tilt view of Au nanorod dimers assembled within adjacent traps separated by a hydrogen silsesquioxane (HSQ) spacer (low magnification). (**b_3**) The interparticle gap is deterministically controlled by the width of the spacer, as shown in b, where SEM secondary detector images showing Au nanorods (top row) and in-lens images showing Au nanorods, HSQ spacer and trap edges (bottom row). Reprinted from *Nature Nanotechnology*,[494] copyright 2016 Springer Nature. **(c)** SEM images of the colloidal lattices (left) and the corresponding diagrams of their densest lattice packings (right): (**c_1**) cubes; (**c_2**) truncated cubes; (**c_3**) cuboctahedra. Reprinted from *Nature Materials*,[495] copyright 2011 Springer Nature. **(d)** Double fishnet structure metamaterials made by self-assembly and NSL. (**d_1**) Tilted and (**d_2**) top-view SEM images of the hexagonally ordered double fishnet structure acquired after nickel dissolution. (**d_3**) SEM image of a free-standing metamaterial membrane.

Photographs of the samples **(d_4)** on a conductive substrate prior to nickel dissolution and **(d_5)** on a glass substrate after removing nickel. Reprinted from *Nanoscale Advances*,[496] copyright 2019 The Royal Society of Chemistry.

5.2 Displays and LEDs

In the era of information, there is an increasing demand in the development of dynamic displaying technologies for the consideration of both environmental sustainability and advertising. Photonic crystal displays show significant advantages in this field. The structural color of PhCs originates from the reflectance of a PhC due to the existence of a PBG. The periodic structures in the PhCs generate PBG at a specific wavelength and their structural colors can be readily tuned by many structural and material parameters, such as the interparticle separation, crystal orientation, surrounding dielectrics. This property can overcome the drawbacks of the current emission display devices, which can be poorly seen under sunlight or high-light. Also, the structural colors from PhCs do not photo-bleach, leading to higher color durability and structural stability compared with pigments or dyes. Therefore, PhCs show multiple advantages for reflective displays/LEDs applications, such as bright color and wide-viewing angles.[499, 500] In recent years, PhC displays have attracted a great deal of research interest.[49]

Ozin and co-workers pioneered the development of a full-color PhC display using electrically tuned PhCs via self-assembly.[501] In their work, they used a photonic ink (P-Ink) to fabricate a dynamic electric tunable display. The P-Ink consisted of highly ordered silica arrays as an inactive scaffold and a crosslinked polymer network (polyferrocenylsilane, PFS) as an active component. This active component of PFS network can be utilized to adjust the PhC lattice spacing of the SiO_2 colloidal spheres due to the swelling/contraction process in an electric field. The resulting electric responsive materials were electrical bistable with bright light even in a high-light environment. They were able to work at low voltage and can be integrated onto flexible substrates.

Gu and co-workers fabricated displays using the microfluidic-assisted assembly method.[321] In this study, they first prepared magnetochromatic microcapsule arrays, which consisted of a shell layer of transparent photocurable ETPTA and a core of monodispersed magnetic particles. Then these magnetochromatic microcapsules were used as display units, and the light diffraction was determined by the ordered structures that formed due to the external magnetic field. The resulting dynamic tunable displays are very stable and viewing angle-independent.

Chen *et al.* reported a new triphasic microfluidic-directed assembly method to fabricate SCCBs with adjustable controllable structure and shapes.[318] They designed a triphasic microfluidic device that comprises a co-flowing system to generate continuous droplet templates with two immiscible phases. Using this method, monodispersed droplet templates with varying shapes, such as crescent, ellipsoid and spherical, could be obtained through tuning

the interfacial tension of each phase within the microfluidic device. Later, highly ordered SCCBs were achieved via self-assembly of the colloidal particles in the droplet templates. In addition to the shape of the resulting SCCBs can be predicted via adjusting the interfacial tension, this method is versatile for the fabrication of core@shell or Janus SCCBs. They incorporated magnetic nanoparticles into the Janus SCCBs to fabricate a novel multifunctional Janus SCCBs. The Janus SCCBs demonstrated switchable optical properties from "dark" to "bright" when placed in a magnetic field. Therefore, these anisotropic SCCBs are very promising for displays or rewriteable papers.

Onoe *et al.* recently fabricated viewing-angle independent full-color reflective displays with a facile microfluidic-assisted assembly method.[502] They developed a great variety of hemispherical dome-shaped microfluidic channels, which were then injected with different colloidal suspensions by utilizing a channel cut method. Multiple types of SCCBs were obtained within the networks of these single-layered microchannels by centrifuge-based crystallization. The resulting SCCBs are viewing-angle independent and the shape, type of SCCBs and patterning resolution are easy to tune. The shapes of SCCBs can be precisely controlled by changing the shape and thickness, and varying the branches of the microchannels. In addition, the ease in the fabrication of microchannels with many glasses or polymers (e.g., polyethylene terephthalate and parylene) endows the potential of this method to fabricate super thin and flexible displays with fine-resolution.

Song and co-workers reported the fabrication of patterned PhC domes for angle-independent displays using an inkjet printing method.[500] To avoid the coffer-ring effects and cracks formation during inkjet printing, they applied a sliding three-phase contact line in a controlled manner to release the strain generated during colloidal assembly. The patterned PhC domes demonstrated wide viewing angle and a 40-fold enhanced fluorescent intensity upon the introduction of fluorescence molecules. The large-scale fabrication of high-quality angle-independent PhC domes using the inkjet printing method enables potential applications for wide viewing-angle flexible displays.

Recently, Chen and co-workers also developed one kind of SCCBs for white-lighting LED.[240] In this study, a new route named "colloid skin" -regulated assembly is used to mitigate the coffee ring formed during self-assembly. In addition, this approach can be easily combined with other high-throughput techniques, such as bar-coating and inkjet printing, to fabricate different PhC patterns. For example, they combined the "colloid skin"-regulated assembly with bar coating to prepare a high-quality CC film over 90 cm × 70 cm. The resulting CC film was doped with rhodamine 6G, and thus can be used for LED-based white-lighting application.

5.3 Novel PhC Sensors and Microchips

Sensing is one of the most important applications of colloidal PhCs.[57-59] One interesting example is colorimetric sensors based on the structural colors of PhCs.[40, 57-59, 503] When PhCs respond to physical, chemical, or biological stimuli, their diffracted peaks will be altered because of the changes in the lattice spacing, orders and/or surrounding refractive index. This sequence of events produces distinct color changes for detecting target molecules and species. The use of color changes is convenient to estimate the properties and concentrations of the analytes. Measuring the reflection shift also provides additional accuracy to the detection.[504] Compared with electronic sensors or electrochemical sensors, PhC sensors are free of additional power input and easy to perform point-of-care analysis of analytes, which is of particular importance in biological sensing and detections.[503] Therefore, significant advances have been made since the important invention of the PhC sensors by the Asher research group.[214] The rapid development of various advanced self-assembly methods and novel materials further promotes the development of novel PhCs sensors and microchips.[477-479, 505] In recent years, scientists have developed various novel sensors using these advanced self-assembly methods.

Using a tip-flow self-assembly method,[400] the Asher research group fabricated 2D PhCs in a large-area. Based on the 2D PhCs fabricated at the air-liquid interface via self-assembly, they developed a novel 2D PhC sensing technique,[59] which can avoid the disordering of PhC during self-assembly in solutions containing highly concentrated ions or when functionalizing molecular recognition to the hydrogels. Cai *et al.* developed a wide variety of 2D PhC chemical and biosensors through attaching 2D PhC onto protein-based sensor materials.[404, 408, 409] They developed a bovine serum albumin (BSA) hydrogel 2D PhC coulometer for the detection of charged ligands binding to the protein. The 2D PhC BSA hydrogel sensor can be utilized for the detection of surfactants, metal ions, small drugs, and etc., which can bind to BSA protein monomers.[404] This method is very versatile for the synthesis of many protein-based hydrogels. Later, Cai and co-workers developed concanavalin A (Con A) for the detection of *Candida albicans*. The detection of microbial is crucially important for the earlier diagnosis of infectious diseases. However, the detection of *Candida albicans* is very difficult because of the interaction between *Candida albicans* and its specific protein. They fabricated a 2D PhC Con A hydrogel sensor, which enabled multivalent Con A-mannan interaction.[408] Cai and co-workers also reported the use of a glucose/galactose binding protein (GGBP) based 2D protein hydrogel sensor for the detection of glucose in solution.[409] The binding of glucose caused conformational change of GGBP, in which induced the volume phase change of the GGBP hydrogel.

Inkjet printing method is advantageous in the fabrication of patterned PhCs. Therefore, it is very suitable for the development of printable PhC devices. Using the inkjet printing method, scientists developed PhC sensors with

PhC microdots.[506, 507] Song and co-workers fabricated colloidal PhC sensor that consisted of microdots for humidity sensing using the inkjet printing method.[506] They mixed the responsive system of acrylamide and N-isopropyl acrylamide with the poly(St-MMA-AA) colloidal particles to make a colloidal ink, then inkjet printed the ink into PhC microdots followed by UV irradiation. The resulting PhC microdot sensor showed a fast response rate of 1.2 s to water vapor due to the hydrophobic transition of PNIPAm within the gel. Gu and co-workers also developed a patterned colloidal PhC colorimetric sensor using the inkjet printing technology for the fast detection of alcohol vapors.[507] Inspired by the color changes of *Tmesisternus isabellae* in environment with different humidity, they selected mesoporous SiO_2 particles and ethylene glycol as the ink to print into a tree-like pattern on both soft and rigid templates. The resulting patterned PhC sensor demonstrated a response time of 0.5 s to saturated ethanol vapor. This is mainly because the mesoporous structure of SiO_2 particle facilitated the capillary condensation of vapors within the hierarchical pores, leading to the refractive index and color shift of the patterned PhCs. The rapid response rate of both PhC sensors can be attributed to relatively the large specific surface area of the microdots.

The detection of DNA hybridization has attracted intense interest due to its significant role in genetic/pathogenic diseases diagnosis. Scientists have developed multiple PhC sensors for DNA hybridization detection.[327, 508] Song *et al.* reported the development of a fluorescence resonance energy transfer (FRET)-based method for the detection of DNA hybridization.[509] In this study, a self-assembled PhC was utilized to amplify the optical signal, and the detection system achieved greatly enhanced sensitivity with a limit of detection (LoD) of 13.5 fM. This is mainly because the PhCs could enhance the fluorescence emission in the biosensors and thereby improve their sensitivity.[510]

Recently, Kerman *et al.* reported the development of a copolymer-based 2D PhC sensor for the detection of Alzheimer's disease(AD)-related DNA hybridization.[511] The existence of DNA polymorphism Apolipoprotein E4 gene sequence is thought to be the indicator of the development of AD. To detect this AD-related DNA hybridization, they utilized a nanoimprint lithography method to prepare Au-coated 2D PhCs on a flexible copolymer film, followed by decorating with a bi-functionalized polymer. This bi-functionalized polymer can react with the DNA probe that is immobilized on the surface. Upon DNA hybridization, a Fresnel decrease in the reflection spectra of the 2D PhCs or an increase in the LSPR spectra of Au-coated 2D PhCs occurred. Such a sensing platform can be developed into wearable biosensors for disease diagnosis and defense monitoring.

Karr and co-workers explored a label-free PhC sensing method to detect the target p53 gene sequence using a PCCA that was encapsulated with a DNA-responsive hydrogel.[512] In this study, self-assembled 3D colloidal

crystal arrays were embedded within the polymerized responsive hydrogel functionalized with DNA. Upon hybridization of the target p53 sequence, the PhC responsive hydrogel sensor will swell, resulting in an increase in the lattice spacing and correspondingly redshift in the Bragg diffraction. The DNA-responsive PhC hydrogel sensor was shown to detect the target p53 gene sequence with a concentration as low as picomole using a complementary capture probe strand. They also demonstrated that the method developed in this study is highly sensitive to epigenetic changes of the fully methylated target p53 sequence.

5.4 Barcodes

A wide variety of SCCBs have been developed into immunoassays[328] (**Figure 34a**) or barcodes for sensing applications. The SCCB assays or barcodes have been widely used for the detection of DNA(**Figure 34b**),[327, 333] cancer cells,[324] tumor markers,[332, 513] microRNA,[514, 515] metal ions (**Figure 34c**),[516] and many other species.[517]

Gu and co-workers developed hydrogel SCCBs consisting of SiO_2 colloidal particles and poly (ethylene glycol) diacrylate (PEG-DA) using a microfluidic device for the detection of DNA hybridization. [327] Droplet templates containing SiO_2 colloidal particles and PEG-DA monomers solutions generated with the microfluidic device were solidified via UV polymerization, resulting in hydrogel SCCBs, which can be covalently bonded with oligonucleotide probes. The resulting SCCBs bioassays were utilized for the highly sensitive detection of target DNA hybridization with a LoD of 0.66 pM due to their large coding capacity and homogeneous surroundings. Such SCCB bioassays are very promising for gene typing, virus detection, and many other biological applications.

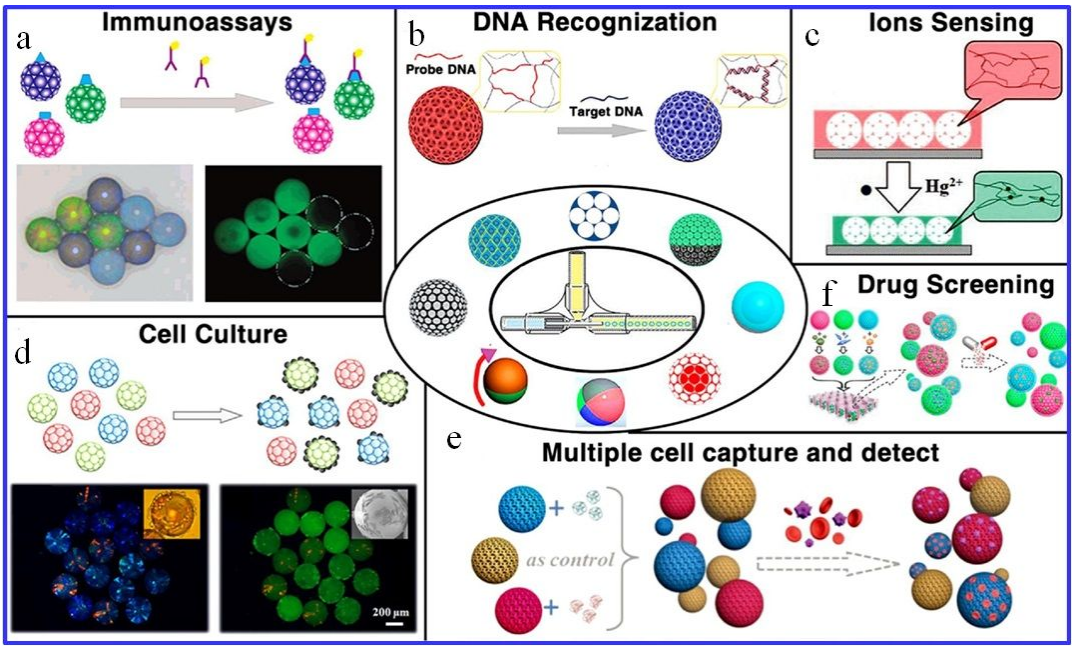

Figure 34. Multiple photonic crystal microspheres fabricated by a microfluidic system for a variety of applications. Microfluidic system for fabricating photonic crystal microspheres through injecting water droplets containing colloidal particles into flowing oil phase (central

scheme). **(a)** Photonic crystal immunoassays prepared by incubation with fluorophore-tagged protein based on a fluorescence analysis method.[328] **(b)** Inverse opal photonic crystal microspheres for DNA recognition.[333] **(c)** Photonic crystal hydrogel consisted of inverse opal photonic crystal microspheres for colorimetric Hg^{2+} detection.[516] **(d)** Opal hydrogel photonic crystal microspheres for cell culture.[518] **(e)** Inverse opal hydrogel microspheres developed for cell capture and detection.[519] **(f)** Core@shell photonic crystal microspheres for drug screening.[520] Reprinted from *Nano Today,*[504] copyright 2018 Elsevier.

Gu *et al.* developed hydrogel SCCBs tagged with QDs for multiplexing DNA detection (**Figure 34b**).[333] During the label-free DNA detection, the specific hybridization between the target DNA and the single-stranded DNA within the bioresponsive hydrogel SCCBs can cause the shrinkage of the hydrogel, leading to the blue shift in the peak position of the Bragg diffraction of the SCCBs. Therefore, the shift in the wavelength can be used as a readout to quantitatively determine the concentration of DNA. The label-free quantum-dot-encoded SCCBs were highly selective and sensitive, and the LoD was determined to be 10^{-9} M. Gu and co-workers explored SCCB barcodes functionalized with aptamer for the capture and detection of circulating tumor cells (CTCs).[324] In this study, a single-emulsion glass capillary microfluidic device was applied to produce droplet templates comprising of SiO_2 colloidal particles, which were used as building blocks to prepare SCCBs after drying. The obtained SCCBs were calcinated at high temperature and subsequently etched with sodium hydroxide to achieve non-closed-parked SCCBs. The resulting SCCB barcodes were then surface-functionalized with poly(amidoamine) (PAMAM) dendrimer. The carboxyl groups on the PAMAM dendrimer can be utilized to immobilize specific DNA aptamers, such as TD05, Sgc8 and Sgd5. Among these three different aptamers, TD05 and Sgc8 showed strong selective and strong binding affinities to Ramos and "CCRF-CEM" cells, respectively. Due to the unique structure of the SCCB barcodes, the larger surface area can facilitate the immobilization of the aptamers, while the patterned nanostructure can promote bioreactions on them. The resulting aptamer-functionalized SCCB barcodes can capture, detect and release different types of CTCs with enhanced sensitivity and reliability, which are very promising for cell diagnosis and prognosis in clinical.

A novel multiplex immunoassays for label-free tumor-marker detection was presented by Gu and colleagues using inverse opal SCCBs.[332] The SCCBs were fabricated using the microfluidic-assisted assembly method by mixing PS and SiO_2 colloidal particles with a certain ratio. After self-assembly, the PS colloidal particles were selectively removed, leaving behind highly ordered SiO_2 inverse opal SCCBs. Then three different antibodies, including anti-human CEA antibody, anti-human CA19-9 antibody, and anti-human CA125 antibody, were covalently bonded to the surface of the SiO_2 inverse opal SCCBs. These three different immunoassays can be used for the selective detection of tumor markers of human CEA, CA19-9, and CA125, respectively, according to the

Bragg diffraction shifts caused by the specific binding of these tumor markers to their specific antibodies. These tumor markers are strongly associated with tumor diseases, such as lung cancer, gastric cancer, and colorectal cancer, respectively. Therefore, the novel multiplex immunoassays based on inverse opal SCCBs are potential for clinical diagnosis, drug screening and discovery.

MiRNAs play significant roles in numerous biological processes, such as metabolism, signal transduction, and cell proliferation. The miRNAs generally play two roles, tumor suppressor genes, or human cancers as oncogenes. The absence of certain types of miRNAs is strongly relevant to the invasion, metastasis and formation of cancer. Therefore, miRNAs are becoming crucial targets for noninvasive blood bioassays. Li *et al.* recently developed mussel-inspired PhC barcodes decorated with graphene oxide (GO) for multiplexed miRNA quantification.[514] In this study, adherable polydopamine mimicking mussels secreted proteins was used to assist the immobilization of GO particles onto the surfaces of the SCCB barcodes. The decoration of GO neither changed the periodic structure of the CCs, nor altered the characteristic reflection peaks of the barcodes. Instead, the encapsulation of GO can improve both the anti-incoherent light-scattering and structural stability of the SCCB barcodes. Later, the SCCB barcodes were functionalized with miRNAs probes using a hybridization chain reaction (HCR), which used to be an effective method for the amplification of genomic and proteomic analysis. The resultant mussel-inspired GO-decorated SCCB barcodes can be used to quickly quantify different miRNA with high sensitivity, high selectivity and good reproducibility, indicating them an ideal platform for multiplexed miRNA quantification and many other clinical applications.

Recently, 2D materials, such as molybdenum disulfide (MoS_2) and GO have been integrated with SCCBs for novel applications. Zhao *et al.* demonstrated the development of MoS_2-integrated SCCBs for multiplex miRNA label-free detection.[513] After the fabrication of SCCBs using the microfluidic-assisted assembly of SiO_2 colloidal particles, the SCCBs were modified with 3-Aminopropyltriethoxysilane (APTES). The resulting APTES-modified SCCBs were positively charged, and thus the MoS_2 nanosheets can be absorbed onto their surface through electrostatic interaction. Then hairpin probes, which were decorated with quantum dots (QDs), were selected to covalently link to MoS_2. Upon coupling, MoS_2 and QDs could form a molecular beacon structure, which led to the quench of the fluorescence. When the resultant MoS_2-integrated SCCBs were exposed to targeting miRNA, the hairpin probes on the SCCBs could bind to the targeting miRNA to form a double strand. This double strand structure separated the QDs from MoS_2 nanosheets, which recovered their fluorescence. The concentration of the miRNAs thus could be determined through the QDs fluorescence measurement since the release of QDs from MoS_2

nanosheets were strongly relying on the hybridized miRNAs concentration. They constructed multiplexed miRNA arrays by using different MoS_2-integrated SCCBs and successfully demonstrated the selective and sensitive detection of several miRNAs that are related to pancreatic cancer. The LoD of 4.2 ± 0.3 nM was optimized and the corresponding linear range of detection from 10 nM to 2 μM for the detection of miRNA associated with pancreatic cancer. Therefore, such MoS_2-integrated SCCBs are promising for tumor markers screening.

Chen *et al.* created porous hydrogel SCCB barcodes with integrated rolling circle amplification (RCA) approach for multiplex circulating miRNA detection.[515] They first fabricated SiO_2 SCCBs with a microfluidic-assisted assembly method. The obtained SiO_2 SCCBs were used as templates for the fabrication of the porous inverse opal hydrogel SCCB barcodes, in which acrylic acid was used as the monomer of the hydrogel, while PEG-DA and poly (ethylene glycol) were used to fabricate scaffold. Then amino-modified DNA sequence probes were immobilized to the porous hydrogel SCCB barcodes. The inverse opal hydrogel SCCB barcodes combined the advantages of both PhCs and RCA, giving rise to excellent performance in the quantification of trace amounts of miRNAs with high sensitivity and good reproducibility. The LoD was reported as low as 20 fM. Therefore, the inverse opal hydrogel SCCB barcodes can work as good platforms for multiplex quantification of miRNAs.

5.5 Drug delivery/screening and cell microcarriers

CCs can also be explored for biomedical applications relying on their unique structural and optical properties. While the 3D or 2D porous frameworks of PhCs provide mechanical supports for cell culture, their optical properties are powerful tools for monitoring cell viability, screening the most effective drugs, and delivering drugs to biological targets. One review has summarized the biomedical applications of inverse opal scaffolds, which will not be covered here.[480]

In recent years, many types of CCs have been developed to act as microcarriers for drug delivery cargos and cells culture (**Figure 34 d, e, f**).[330, 476, 520-522] Gu and co-workers developed novel barcode particles using a colloidal suspension array, which composed of PhC microbubbles.[330] These barcode microbubbles consisted of an inner core of microbubbles, a middle shell of PhCs, and an outer shell of transparent polymers. They can be obtained via a microfluidic devices-assisted assembly. Such a PhC coated shell structure endowed the SCCB microbubbles with both stable codes and a flexible bioassays surface. Moreover, using a microfluidic device, they also fabricated multifunctional SCCB microbubbles through producing multicompartmental microcapsule templates. The resulting SCCB microbubbles can be coded with substantial levels, and their movement can be controlled precisely. Their

sizes can also be tailored, and their overall density in suspension can also be tuned to match the target solution density. These properties endow them with excellent performances for multiplex detection and cell cultures.

Colloidosome capsules are promising for cargos transportation and release. Khashab *et al.* reported the development of nanoscale colloidosome capsules via electrostatic assembly of organosilica colloidal particles for controlled cargo release.[476] Nitrophenylene-doped SiO_2 particles (NBSN-1 and NBSN-2, respectively) with opposite surface charges were used to fabricate colloidosome capsules via electrostatic interactions. The originally negatively charged SiO_2 particles were functionalized with nitrophenylene-ammonium-bridged alkoxysilane, which is positively charged. Among these two different SiO_2 particles, NBSN-2 contained more nitrophenylene-ammonium-bridged alkoxysilane than NBSN-1, and therefore were positively charged. Mixing NBSN-1 and NBSN-2 produced ordered colloidosome capsules due to electrostatic attraction. Upon light irradiation, the photoreaction of nitrophenylene-alkoxysilane moieties on NBSN-2 led the charge of NBSM-2 to reverse to be negatively charged. Consequently, the colloidosome capsules collapsed due to the electrostatic repulsion and the cargos released. The design of such colloidosome capsules can be used for the controlled release of hydrophobic molecules, macromolecules and even nanoparticles, which is more advanced than those porous capsules that are only available for relatively small cargos.

SCCBs made from biocompatible materials are also suitable for drug screening platforms, which are pivotal for biomedical engineering applications. Zhao *et al.* explored core@shell hydrogel SCCBs barcodes based on GelMA for drug screening.[523] Bioactive GelMA hydrogels, which acted as shells, were polymerized to encapsulate the SCCBs to form core@shell SCCBs barcodes. The SCCB barcodes created a 3D extracellular matrix microenvironment, which can facilitate the culture of cells. In the SCCB barcodes, the PhC cores can encode cell spheroids with diffraction peaks during the culture of the cells, whose biological response can be discriminated against during drug screening. They investigated the cytotoxic effect of tegafur (TF) on the SCCB barcode particle-loaded HCT-116 colonic tumor cell spheroids and liver HepG2 cell spheroids using this cell spheroids-on-barcodes platform. The platform was found to be highly efficient for drug screening and enhanced the cytotoxicity of TF against the HCT-116 tumor cell spheroids using simultaneously cultured NIH-3T3 and HepG2 cells.

Zhang and co-workers reported the development of a polyacrylamide (PAAm) hydrogel inverse opal SCCBs for the capture and detection of a wide variety of blood cells.[522] It is challenging to separate and detect blood cells in patients while it is crucially important for hematological disorders diagnosis. The suspended barcode arrays of PAAm hydrogel inverse opal SCCBs were replicated from opal SCCB templates. In these barcodes, the

characteristic reflection peaks arising from stop bands of the inverse opals were used as the code, which was very stable and remained intact during the cell culture and capture. In these barcode SCCBs, the biocompatible hydrogels and the porous structure facilitated the immobilization of probes on their surface, while the highly ordered macropores can promote the bioreactions between the cell surface proteins and the probes. Furthermore, the hydrophilicity property of the PAAm scaffolds of the barcode SCCBs demonstrated excellent performance in capturing multiple blood cells with minimal damage. These exceptional features enabled these PAAm hydrogel inverse opal SCCBs to be an ideal platform for hematological disorders diagnosis and prognosis through capture and detection of multiple blood cells in patients.

5.6 Platforms for Phase Transition Study

In addition to the above emerging practical applications, the self-assembly of colloidal particles is of fundamental interest as well. Equipartition theorem showed that, in thermal equilibrium, any degree of freedom has an average energy of $\frac{1}{2}k_BT$, and the kinetic energy of atoms or molecules is on the order of k_BT. The energy of Brownian motion of colloidal particles is also on the order of k_BT, comparable to their atomic counterparts. However, because colloidal particles are much larger and their dynamics are much slower, it is possible to track these particles under an optical microscope to study the behavior of their atomic counterparts.[524, 525] Thus, the self-assembly of colloidal particles can be used to study the nucleation and growth of crystals,[251, 526-529] the formation of dislocations and defects,[530, 531] the glass transition,[527, 532-535] protein folding,[536] polymerization kinetics,[537] or the abnormal physical properties of water molecules caused by liquid-liquid phase transition.[538-543]

In classic nucleation theory, nucleus is first formed by local fluctuations. The size of the nucleus has to be greater than a certain threshold to favor the growth of crystals, the nucleus with the threshold size is called critical nucleus. In the atomic regime, it is very hard to *in situ* observe the size and shape of the critical nucleus as well as kinetic pathways of nucleation. Gasser *et al.*[528] used colloidal particles to visualize the critical nucleus in the early stage of crystallization, and the kinetic pathways were investigated by Xu and coworkers.[529] The dislocation and crystal defects can be studied using CCs as well.[530, 531]

6. Summary and outlook

Self-assembly of colloidal particles, in general, represents a low-cost and low-energy bottom-up method to fabricate PhCs for various applications as compared to top-down methods. The application of CCs, however, could be impeded by the difficulties in controlling long-range ordering and producing different lattice structures other

than *fcc* lattice. Many advances have been made in the past two decades towards the fabrication of high-quality PhCs in large-area. These novel advanced self-assembly approaches, alternatively, enabled various emerging applications, including metamaterials, sensing, displays, LEDs, drug screening and release, etc. Nevertheless, these technologies to fabricate high-quality PhCs still needs to be further refined before they can be widely used for various practical applications. The unavoidable fact is that CCs in any form are susceptible to cracking after crystallization or thermal/chemical post-treatment. This essentially hinders their adoption as PhC devices for telecommunication applications and makes them less effective in other PhC applications. During the self-assembly process, a suitable dispersion may be one of the key factors in perfecting the crystalline structures. In addition, it is essential to regulate the interparticle potentials, which are dependent on the surface charge of colloidal particles and the properties of the dispersion, such as salt concentration,[544] pH,[545] and ionic strength.[546] Thus, one can optimize the conditions for colloidal assembly and create high-quality functional PhCs by varying the surface chemistry.

To date, among various technologies, the template-directed self-assembly method seems to be a versatile and effective method for fabricating crack-free and controlling the crystalline of the resultant CCs in a large area. However, it is necessary to further refine the method to transfer CCs from a patterned template to a flat substrate to expand their applications. The spin-coating approach is powerful for the mass fabrication of crack-free CCs over a considerably large area, but the crystalline quality is not satisfactory. The other approaches have their own advantages and drawbacks as well. The functionalization of materials with robust and versatile properties and the development of new self-assembly approaches to perfecting the crystalline structure should be emphasized in the future. Tetrahedral colloidal particles coated with DNA have been self-assembled into cubic diamond CCs which can exhibit a cPBG at low refractive index contrast.[38] The fabrication of cubic diamond CCs on a large scale has yet to be achieved. Microgel seems to be a promising material in the fabrication of crack-free CCs but may have limitations from the hydrogel itself and materials that can be used. Some colloidal semiconductor and metal building blocks may possess vast applications, but it remains challenging to control grain boundaries, crystalline orientation, and random defects for functional devices. The combination of the benefits of ease of building functional CCs using self-assembly methods and high-throughput production using a printing technique may be an alternative to fabricate high-quality CCs for a myriad of practical applications. Using self-assembly methods, CCs with diamond symmetry were achieved, which will open cPBG at low refractive index contrast and enable tremendous high-performance optical devices in the future. Moreover, a large number of CCs can be fabricated with different materials and

different functions due to its ease of modification. With the aid of top-down processes (etching, deposition, transfer printing, etc.), a number of useful PhC structures have been created for various applications.[370, 547-549] In the future, the incorporation of self-assembly of CCs into 3D/4D printing could be promising to fabricate on-demand photonic structures for optics, sensing, displays, biomedical, environmental, safety and other applications.[295, 487, 550, 551] It might be possible to use the CCs with cPBG to fabricate all-optical devices and synthetic all-optical computer for optical and quantum computing as well.[293, 495]

Conflicts of Interests

There are no conflicts to declare.

Acknowledgements

This work was primarily supported by from National Natural Science Foundation of China under award No. 22076008, and BUAA Faculty Research Grant under Grant No. ZG216S2094 (Z.C.). Z.C. acknowledges a research scholarship awarded by National University of Singapore and valuable advice from Prof. Sanford Asher at University of Pittsburgh. This work was also partially supported by the joint French-Singaporean MERLION program under Grant No. R-279-000-334-133, and by A*STAR. Yin is grateful for the financial support from the U.S. National Science Foundation (DMR-1810485).

Reference

1. E. Yablonovitch, *Phys. Rev. Lett.*, 1987, **58**, 2059-2062.
2. S. John, *Phys. Rev. Lett.*, 1987, **58**, 2486-2489.
3. J. D. Joannopoulos, S. G. Johnson, J. N. Winn and R. D. Meade, *Photonic Crystals: Molding the Flow of Light*, Princeton University Press, Princeton, NJ USA, 2008.
4. J. B. Jones, E. R. Segnit and N. M. Nickson, *Nature*, 1963, **198**, 1191-1191.
5. J. B. Jones, J. V. Sanders and E. R. Segnit, *Nature*, 1964, **204**, 990-991.
6. S. Yoshioka and S. Kinoshita, *Proc. R. Soc. B-Biol. Sci.*, 2004, **271**, 581-587.
7. S. Yoshioka and S. Kinoshita, *Forma* 2002, **17**, 169-181.
8. E. Gaillou, E. Fritsch, B. Aguilar-Reyes, B. Rondeau, J. Post, A. Barreau and M. Ostroumov, *Am. Miner.*, 2008, **93**, 1865-1873.
9. J. Matejkova-Plskova, D. Jancik, M. Maslan, S. Shiojiri and M. Shiojiri, *Mater. Trans.*, 2010, **51**, 202-208.
10. E. Armstrong and C. O'Dwyer, *J. Mater. Chem. C*, 2015, **3**, 6109-6143.
11. K. M. Ho, C. T. Chan, C. M. Soukoulis, R. Biswas and M. Sigalas, *Solid State Commun.*, 1994, **89**, 413-416.
12. S. Y. Lin, J. G. Fleming, D. L. Hetherington, B. K. Smith, R. Biswas, K. M. Ho, M. M. Sigalas, W. Zubrzycki, S. R. Kurtz and J. Bur, *Nature*, 1998, **394**, 251-253.
13. S. Noda, K. Tomoda, N. Yamamoto and A. Chutinan, *Science*, 2000, **289**, 604-606.
14. G. Subramania and S. Y. Lin, *Appl. Phys. Lett.*, 2004, **85**, 5037-5039.
15. S. P. Ogawa, M. Imada, S. Yoshimoto, M. Okano and S. Noda, *Science*, 2004, **305**, 227-229.
16. M. H. Qi, E. Lidorikis, P. T. Rakich, S. G. Johnson, J. D. Joannopoulos, E. P. Ippen and H. I. Smith, *Nature*, 2004, **429**, 538-542.
17. K. Aoki, H. T. Miyazaki, H. Hirayama, K. Inoshita, T. Baba, K. Sakoda, N. Shinya and Y. Aoyagi, *Nat. Mater.*, 2003, **2**, 117-121.
18. K. Y. Lee, N. LaBianca, S. A. Rishton, S. Zolgharnain, J. D. Gelorme, J. Shaw and T. H. P. Chang, *J. Vac. Sci. Technol., B: Microelectron. Nanometer Struct.--Process., Meas., Phenom.*, 1995, **13**, 3012-3016.
19. M. Campbell, D. N. Sharp, M. T. Harrison, R. G. Denning and A. J. Turberfield, *Nature*, 2000, **404**, 53-56.
20. Y. V. Miklyaev, D. C. Meisel, A. Blanco, G. von Freymann, K. Busch, W. Koch, C. Enkrich, M. Deubel and M. Wegener, *Appl. Phys. Lett.*, 2003, **82**, 1284-1286.
21. J. Scrimgeour, D. N. Sharp, C. F. Blanford, O. M. Roche, R. G. Denning and A. J. Turberfield, *Adv. Mater.*, 2006, **18**, 1557-1560.
22. J. S. King, E. Graugnard, O. M. Roche, D. N. Sharp, J. Scrimgeour, R. G. Denning, A. J. Turberfield and C. J. Summers, *Adv. Mater.*, 2006, **18**, 1561-1565.
23. M. Deubel, M. Wegener, A. Kaso and S. John, *Appl. Phys. Lett.*, 2004, **85**, 1895-1897.
24. V. Mizeikis, K. K. Seet, S. Juodkazis and H. Misawa, *Opt. Lett.*, 2004, **29**, 2061-2063.
25. G. M. Gratson, F. García-Santamaría, V. Lousse, M. Xu, S. Fan, J. A. Lewis and P. V. Braun, *Adv. Mater.*, 2006, **18**, 461-465.
26. K. K. Seet, V. Mizeikis, S. Matsuo, S. Juodkazis and H. Misawa, *Adv. Mater.*, 2005, **17**, 541-545.

27. N. Tétreault, G. von Freymann, M. Deubel, M. Hermatschweiler, F. Pérez-Willard, S. John, M. Wegener and G. A. Ozin, *Adv. Mater.*, 2006, **18**, 457-460.
28. M. Deubel, G. von Freymann, M. Wegener, S. Pereira, K. Busch and C. M. Soukoulis, *Nat. Mater.*, 2004, **3**, 444-447.
29. S. Kawata, H.-B. Sun, T. Tanaka and K. Takada, *Nature*, 2001, **412**, 697-698.
30. G. A. Ozin and S. M. Yang, *Adv. Funct. Mater.*, 2001, **11**, 95-104.
31. C. López, *Adv. Mater.*, 2003, **15**, 1679-1704.
32. Y. N. Xia, B. Gates, Y. D. Yin and Y. Lu, *Adv. Mater.*, 2000, **12**, 693-713.
33. A. Blanco, E. Chomski, S. Grabtchak, M. Ibisate, S. John, S. W. Leonard, C. Lopez, F. Meseguer, H. Miguez, J. P. Mondia, G. A. Ozin, O. Toader and H. M. van Driel, *Nature*, 2000, **405**, 437-440.
34. Y. A. Vlasov, X. Z. Bo, J. C. Sturm and D. J. Norris, *Nature*, 2001, **414**, 289-293.
35. D. J. Norris and Y. A. Vlasov, *Adv. Mater.*, 2001, **13**, 371-376.
36. Y. N. Xia, B. Gates and Z. Y. Li, *Adv. Mater.*, 2001, **13**, 409-413.
37. Y. D. Yin, Y. Lu, B. Gates and Y. N. Xia, *J. Am. Chem. Soc.*, 2001, **123**, 8718-8729.
38. M. He, J. P. Gales, É. Ducrot, Z. Gong, G.-R. Yi, S. Sacanna and D. J. Pine, *Nature*, 2020, **585**, 524-529.
39. Z. Li, F. Yang and Y. Yin, *Adv. Funct. Mater.*, 2020, **30**, 1903467.
40. Z. Li and Y. Yin, *Adv. Mater.*, 2019, **31**, 1807061.
41. A.-P. Hynninen, J. H. J. Thijssen, E. C. M. Vermolen, M. Dijkstra and A. van Blaaderen, *Nat. Mater.*, 2007, **6**, 202-205.
42. D. Morphew, J. Shaw, C. Avins and D. Chakrabarti, *ACS Nano*, 2018, **12**, 2355-2364.
43. A. B. Rao, J. Shaw, A. Neophytou, D. Morphew, F. Sciortino, R. L. Johnston and D. Chakrabarti, *ACS Nano*, 2020, **14**, 5348-5359.
44. Y. Wang, Y. Wang, D. R. Breed, V. N. Manoharan, L. Feng, A. D. Hollingsworth, M. Weck and D. J. Pine, *Nature*, 2012, **491**, 51-55.
45. H. Lin, S. Lee, L. Sun, M. Spellings, M. Engel, S. C. Glotzer and C. A. Mirkin, *Science*, 2017, **355**, 931-935.
46. W. Xu, Z. Li and Y. Yin, *Small*, 2018, **14**, 1801083.
47. F. Meseguer, *Colloids Surf., A*, 2005, **270-271**, 1-7.
48. S.-H. Kim, S. Y. Lee, S.-M. Yang and G.-R. Yi, *NPG Asia Mater.*, 2011, **3**, 25-33.
49. A. C. Arsenault, D. P. Puzzo, I. Manners and G. A. Ozin, *Nat. Photonics*, 2007, **1**, 468-472.
50. H. B. Sunkara, J. M. Jethmalani and W. T. Ford, *Chem. Mater.*, 1994, **6**, 362-364.
51. F. Fleischhaker, A. C. Arsenault, V. Kitaev, F. C. Peiris, G. von Freymann, I. Manners, R. Zentel and G. A. Ozin, *J. Am. Chem. Soc.*, 2005, **127**, 9318-9319.
52. S. H. Foulger, P. Jiang, A. Lattam, D. W. Smith, J. Ballato, D. E. Dausch, S. Grego and B. R. Stoner, *Adv. Mater.*, 2003, **15**, 685-689.
53. Y. J. Liu, Z. Cai, E. S. P. Leong, X. S. Zhao and J. H. Teng, *J. Mater. Chem.*, 2012, **22**, 7609-7613.
54. Y. Zhang, K. Li, F. Y. Su, Z. Y. Cai, J. X. Liu, X. W. Wu, H. L. He, Z. Yin, L. H. Wang, B. Wang, Y. Q. Tian, D. Luo, X. W. Sun and Y. J. Liu, *Opt. Express*, 2019, **27**, 15391-15398.
55. S. Furumi, H. Fudouzi and T. Sawada, *Laser Photonics Rev.*, 2010, **4**, 205-220.
56. A. C. Arsenault, H. Míguez, V. Kitaev, G. A. Ozin and I. Manners, *Adv. Mater.*, 2003, **15**, 503-507.
57. J. Ge and Y. Yin, *Angew. Chem., Int. Ed.*, 2011, **50**, 1492-1522.
58. C. Fenzl, T. Hirsch and O. S. Wolfbeis, *Angew. Chem., Int. Ed.*, 2014, **53**, 3318-3335.
59. Z. Cai, N. L. Smith, J.-T. Zhang and S. A. Asher, *Anal. Chem.*, 2015, **87**, 5013-5025.
60. C. I. Aguirre, E. Reguera and A. Stein, *Adv. Funct. Mater.*, 2010, **20**, 2565-2578.
61. J. F. Galisteo-López, M. Ibisate, R. Sapienza, L. S. Froufe-Pérez, Á. Blanco and C. López, *Adv. Mater.*, 2010, **23**, 30-69.
62. N. Vogel, M. Retsch, C.-A. Fustin, A. del Campo and U. Jonas, *Chem. Rev.*, 2015, **115**, 6265-6311.
63. F. Li, D. P. Josephson and A. Stein, *Angew. Chem., Int. Ed.*, 2011, **50**, 360-388.
64. K. R. Phillips, G. T. England, S. Sunny, E. Shirman, T. Shirman, N. Vogel and J. Aizenberg, *Chem. Soc. Rev.*, 2016, **45**, 281-322.
65. Q. B. Meng, C. H. Fu, Y. Einaga, Z. Z. Gu, A. Fujishima and O. Sato, *Chem. Mater.*, 2002, **14**, 83-88.
66. F. Marlow, Muldarisnur, P. Sharifi, R. Brinkmann and C. Mendive, *Angew. Chem., Int. Ed.*, 2009, **48**, 6212-6233.
67. Y. A. Vlasov, M. A. Kaliteevski and V. V. Nikolaev, *Phys. Rev. B*, 1999, **60**, 1555-1562.
68. D. M. Beggs, M. A. Kaliteevski, S. Brand, R. A. Abram, D. Cassagne and J. P. Albert, *J. Phys.: Condens. Matter*, 2005, **17**, 4049-4055.
69. L. A. Dorado and R. A. Depine, *Phys. Rev. B*, 2009, **79**, 7.
70. R. Rengarajan, D. Mittleman, C. Rich and V. Colvin, *Phys. Rev. E*, 2005, **71**, 11.
71. Y. A. Vlasov, V. Astratov, A. Baryshev, A. Kaplyanskii, O. Karimov and M. Limonov, *Phys. Rev. E*, 2000, **61**, 5784.
72. A. V. Lavrinenko, W. Wohlleben and R. J. Leyrer, *Opt. Express*, 2009, **17**, 747-760.
73. C. Nelson Erik, F. García-Santamaría and V. Braun Paul, *Adv. Funct. Mater.*, 2008, **18**, 1983-1989.
74. P. V. Braun, S. A. Rinne and F. García-Santamaría, *Adv. Mater.*, 2006, **18**, 2665-2678.
75. A. Arsenault, F. Fleischhaker, G. von Freymann, V. Kitaev, H. Miguez, A. Mihi, N. Tétreault, E. Vekris, I. Manners, S. Aitchison, D. Perovic and G. A. Ozin, *Adv. Mater.*, 2006, **18**, 2779-2785.
76. S. F. Liew and H. Cao, *J. Opt.*, 2010, **12**, 8.
77. S. Dosho, N. Ise, K. Ito, S. Iwai, H. Kitano, H. Matsuoka, H. Nakamura, H. Okumura and T. Ono, *Langmuir*, 1993, **9**, 394-411.
78. J. F. Galisteo-Lopez, E. Palacios-Lidon, E. Castillo-Martinez and C. Lopez, *Phys. Rev. B*, 2003, **68**, 8.
79. L. Braginsky and V. Shklover, *Phys. Rev. B*, 2006, **73**, 11.
80. A. V. Baryshev, V. A. Kosobukin, K. B. Samusev, D. E. Usvyat and M. F. Limonov, *Phys. Rev. B*, 2006, **73**, 17.
81. M. V. Rybin, K. B. Samusev and M. F. Limonov, *Phys. Solid State*, 2008, **50**, 436-445.
82. L.-D. Jiang, Q.-F. Dai, T.-H. Feng, J. Liu, L.-J. Wu, S. Lan, A. V. Gopal and V. A. Trofimov, *Chin. Phys. Lett.*, 2009, **26**, 074201.
83. J. Z. Wang, L. Yang, D. F. Lin, Y. H. Luo, D. M. Li and Q. B. Meng, *J. Chem. Phys.*, 2012, **137**, 11.
84. J. F. Galisteo-Lopez and W. L. Vos, *Phys. Rev. E*, 2002, **66**, 5.
85. Z.-Y. Li and Z.-Q. Zhang, *Adv. Mater.*, 2001, **13**, 433-436.

86. Z. Ren, X. Zhang, J. Zhang, X. Li, X. Pan, X. Fei, Z. Cui and B. Yang, *J. Mater. Chem.*, 2008, **18**, 3536-3538.
87. S. A. Rinne, F. García-Santamaría and P. V. Braun, *Nat. Photonics*, 2008, **2**, 52-56.
88. G. von Freymann, S. John, S. Wong, V. Kitaev and G. A. Ozin, *Appl. Phys. Lett.*, 2005, **86**, 053108.
89. R. C. Schroden, M. Al-Daous, C. F. Blanford and A. Stein, *Chem. Mater.*, 2002, **14**, 3305-3315.
90. H. Míguez, N. Tétreault, B. Hatton, S. M. Yang, D. Perovic and G. A. Ozin, *Chem. Commun.*, 2002, 2736-2737.
91. W. Wohlleben, F. W. Bartels, M. Boyle and R. J. Leyrer, *Langmuir*, 2008, **24**, 5627-5635.
92. W. Wohlleben, F. W. Bartels, S. Altmann and R. J. Leyrer, *Langmuir*, 2007, **23**, 2961-2969.
93. G. von Freymann, V. Kitaev, B. V. Lotsch and G. A. Ozin, *Chem. Soc. Rev.*, 2013, **42**, 2528-2554.
94. A. Stein, B. E. Wilson and S. G. Rudisill, *Chem. Soc. Rev.*, 2013, **42**, 2763-2803.
95. H. Cong, B. Yu, J. Tang, Z. Li and X. Liu, *Chem. Soc. Rev.*, 2013, **42**, 7774-7800.
96. Q. Yan, J. Yu, Z. Cai and X. S. Zhao, in *Hierarchically Structured Porous Materials*, Wiley-VCH Verlag GmbH & Co. KGaA, 2011, DOI: 10.1002/9783527639588.ch18, pp. 531-576.
97. H. B. Zheng and S. Ravaine, *Crystals*, 2016, **6**, 25.
98. J. H. Moon and S. Yang, *Chem. Rev.*, 2009, **110**, 547-574.
99. P. V. Braun, *Chem. Mater.*, 2014, **26**, 277-286.
100. P. Xu, A. S. Mujumdar and B. Yu, *Drying Technol.*, 2009, **27**, 636-652.
101. A. L. Liberman-Martin, C. K. Chu and R. H. Grubbs, *Macromol. Rapid Commun.*, 2017, **38**, 1700058.
102. R. Zhang, Z. Qiang and M. Wang, *Adv. Funct. Mater.*, 2021, **31**, 2005819.
103. B. B. Patel, D. J. Walsh, D. H. Kim, J. Kwok, B. Lee, D. Guironnet and Y. Diao, *Sci. Adv.*, 2020, **6**, eaaz7202.
104. Y. Yue and J. P. Gong, *J. Photochem. Photobiol., C*, 2015, **23**, 45-67.
105. Q. Yan, L. Wang and X. S. Zhao, *Adv. Funct. Mater.*, 2007, **17**, 3695-3706.
106. A. Arsenault, F. Fleischhaker, G. v. Freymann, V. Kitaev, H. Miguez, A. Mihi, N. Tétreault, E. Vekris, I. Manners, S. Aitchison, D. Perovic and G. A. Ozin, *Adv. Mater.*, 2006, **18**, 2779-2785.
107. L. V. Woodcock, *Nature*, 1997, **385**, 141-143.
108. G. S. Lozano, L. A. Dorado, R. A. Depine and H. Miguez, *J. Mater. Chem.*, 2009, **19**, 185-190.
109. A. F. Routh and W. B. Russel, *AIChE J.*, 1998, **44**, 2088-2098.
110. W. P. Lee and A. F. Routh, *Langmuir*, 2004, **20**, 9885-9888.
111. E. R. Dufresne, E. I. Corwin, N. A. Greenblatt, J. Ashmore, D. Y. Wang, A. D. Dinsmore, J. X. Cheng, X. S. Xie, J. W. Hutchinson and D. A. Weitz, *Phys. Rev. Lett.*, 2003, **91**, 4.
112. F. Zeng, Z. Sun, C. Wang, B. Ren, X. Liu and Z. Tong, *Langmuir*, 2002, **18**, 9116-9120.
113. S.-L. Kuai, X.-F. Hu, A. Haché and V.-V. Truong, *J. Cryst. Growth*, 2004, **267**, 317-324.
114. E. A. Jagla, *Phys. Rev. E*, 2002, **65**, 046147.
115. M. S. Tirumkudulu and W. B. Russel, *Langmuir*, 2005, **21**, 4938-4948.
116. Z. Zhou, Q. Li and X. S. Zhao, *Langmuir*, 2006, **22**, 3692-3697.
117. N. V. Dziomkina and G. J. Vancso, *Soft Matter*, 2005, **1**, 265-279.
118. A. S. Dimitrov and K. Nagayama, *Langmuir*, 1996, **12**, 1303-1311.
119. P. Jiang, J. F. Bertone, K. S. Hwang and V. L. Colvin, *Chem. Mater.*, 1999, **11**, 2132-2140.
120. P. A. Kralchevsky and N. D. Denkov, *Curr. Opin. Colloid Interface Sci.*, 2001, **6**, 383-401.
121. A. F. Routh and W. B. Russel, *Langmuir*, 1999, **15**, 7762-7773.
122. C. Allain and L. Limat, *Phys. Rev. Lett.*, 1995, **74**, 2981-2984.
123. L. Pauchard, F. Parisse and C. Allain, *Phys. Rev. E*, 1999, **59**, 3737-3740.
124. H. Colina and S. Roux, *Eur. Phys. J. E*, 2000, **1**, 189-194.
125. K. A. Shorlin, J. R. de Bruyn, M. Graham and S. W. Morris, *Phys. Rev. E*, 2000, **61**, 6950-6957.
126. R. C. Chiu, T. J. Garino and M. J. Cima, *J. Am. Ceram. Soc.*, 1993, **76**, 2257-2264.
127. R. C. Chiu and M. J. Cima, *J. Am. Ceram. Soc.*, 1993, **76**, 2769-2777.
128. Z. Cai, E. S. P. Leong, Z. Wang, W. Niu, W. Zhang, S. Ravaine, N. L. Yakovlev, Y. J. Liu, J. Teng and X. Lu, *J. Mater. Chem. C*, 2015, **3**, 11645-11652.
129. P. Meakin, *Thin Solid Films*, 1987, **151**, 165-190.
130. A. T. Skjeltorp and P. Meakin, *Nature*, 1988, **335**, 424-426.
131. E. R. Dufresne, D. J. Stark, N. A. Greenblatt, J. X. Cheng, J. W. Hutchinson, L. Mahadevan and D. A. Weitz, *Langmuir*, 2006, **22**, 7144-7147.
132. D. J. Norris, E. G. Arlinghaus, L. Meng, R. Heiny and L. E. Scriven, *Adv. Mater.*, 2004, **16**, 1393-1399.
133. H.-L. Li and F. Marlow, *Chem. Mater.*, 2006, **18**, 1803-1810.
134. A. Mihi, M. Ocaña and H. Míguez, *Adv. Mater.*, 2006, **18**, 2244-2249.
135. Z. Cai, J. Teng, Q. Yan and X. S. Zhao, *Colloids Surf., A*, 2012, **402**, 37-44.
136. Q. Yan, Z. Zhou and X. S. Zhao, *Langmuir*, 2005, **21**, 3158-3164.
137. K. B. Singh and M. S. Tirumkudulu, *Phys. Rev. Lett.*, 2007, **98**, 4.
138. E. Yablonovitch and T. J. Gmitter, *Phys. Rev. Lett.*, 1989, **63**, 1950-1953.
139. K. Busch and S. John, *Phys. Rev. E*, 1998, **58**, 3896-3908.
140. K. M. Ho, C. T. Chan and C. M. Soukoulis, *Phys. Rev. Lett.*, 1990, **65**, 3152-3155.
141. E. Ducrot, J. Gales, G. R. Yi and D. J. Pine, *Opt. Express*, 2018, **26**, 30052-30060.
142. T. T. Ngo, C. M. Liddell, M. Ghebrebrhan and J. D. Joannopoulos, *Appl. Phys. Lett.*, 2006, **88**, 241920.
143. F. Romano, E. Sanz and F. Sciortino, *J. Chem. Phys.*, 2011, **134**, 174502.
144. D. R. Nelson, *Nano Lett.*, 2002, **2**, 1125-1129.
145. V. N. Manoharan, M. T. Elsesser and D. J. Pine, *Science*, 2003, **301**, 483-487.
146. Z. L. Zhang, A. S. Keys, T. Chen and S. C. Glotzer, *Langmuir*, 2005, **21**, 11547-11551.
147. F. Smallenburg and F. Sciortino, *Nat. Phys.*, 2013, **9**, 554-558.
148. F. Smallenburg, L. Filion and F. Sciortino, *Nat. Phys.*, 2014, **10**, 653-657.

149. Z. Gong, T. Hueckel, G. R. Yi and S. Sacanna, *Nature*, 2017, **550**, 234-238.
150. E. G. Noya, I. Zubieta, D. J. Pine and F. Sciortino, *J. Chem. Phys.*, 2019, **151**, 094502.
151. N. Patra and A. V. Tkachenko, *Phys. Rev. E*, 2017, **96**, 022601.
152. M. Grünwald and P. L. Geissler, *ACS Nano*, 2014, **8**, 5891-5897.
153. F. Romano and F. Sciortino, *Nat. Commun.*, 2012, **3**, 975.
154. A. Neophytou, V. N. Manoharan and D. Chakrabarti, *ACS Nano*, 2021, DOI: 10.1021/acsnano.0c07824.
155. É. Ducrot, M. He, G.-R. Yi and D. J. Pine, *Nat. Mater.*, 2017, **16**, 652-657.
156. G. Avvisati, T. Dasgupta and M. Dijkstra, *ACS Nano*, 2017, **11**, 7702-7709.
157. H. Pattabhiraman, G. Avvisati and M. Dijkstra, *Phys. Rev. Lett.*, 2017, **119**, 157401.
158. T. Dasgupta and M. Dijkstra, *Soft Matter*, 2018, **14**, 2465-2475.
159. P. F. Damasceno, M. Engel and S. C. Glotzer, *ACS Nano*, 2012, **6**, 609-614.
160. W. N. Man, M. Florescu, E. P. Williamson, Y. Q. He, S. R. Hashemizad, B. Y. C. Leung, D. R. Liner, S. Torquato, P. M. Chaikin and P. J. Steinhardt, *Proc. Natl. Acad. Sci. U. S. A.*, 2013, **110**, 15886-15891.
161. S. Imagawa, K. Edagawa, K. Morita, T. Niino, Y. Kagawa and M. Notomi, *Phys. Rev. B*, 2010, **82**, 115116.
162. S. F. Liew, J.-K. Yang, H. Noh, C. F. Schreck, E. R. Dufresne, C. S. O'Hern and H. Cao, *Phys. Rev. A*, 2011, **84**, 063818.
163. S. R. Sellers, W. Man, S. Sahba and M. Florescu, *Nat. Commun.*, 2017, **8**, 14439.
164. J. H. Prosser, T. Brugarolas, S. Lee, A. J. Nolte and D. Lee, *Nano Lett.*, 2012, **12**, 5287-5291.
165. U. U. Ghosh, M. Chakraborty, A. B. Bhandari, S. Chakraborty and S. DasGupta, *Langmuir*, 2015, **31**, 6001-6010.
166. D. Juhue and J. Lang, *Langmuir*, 1993, **9**, 792-796.
167. E. W. S. Hagan, M. N. Charalambides, C. R. T. Young, T. J. S. Learner and S. Hackney, *Prog. Org. Coat.*, 2010, **69**, 73-81.
168. J. A. Lewis, *J. Am. Ceram. Soc.*, 2000, **83**, 2341-2359.
169. E. Santanach Carreras, F. Chabert, D. E. Dunstan and G. V. Franks, *J. Colloid Interface Sci.*, 2007, **313**, 160-168.
170. L. Wang and X. S. Zhao, *J. Phys. Chem. C*, 2007, **111**, 8538-8542.
171. T. Olding, M. Sayer and D. Barrow, *Thin Solid Films*, 2001, **398-399**, 581-586.
172. B. Hatton, L. Mishchenko, S. Davis, K. H. Sandhage and J. Aizenberg, *Proc. Natl. Acad. Sci. U. S. A.*, 2010, **107**, 10354-10359.
173. A. A. Chabanov, Y. Jun and D. J. Norris, *Appl. Phys. Lett.*, 2004, **84**, 3573-3575.
174. M. C. McLeod, C. L. Kitchens and C. B. Roberts, *Langmuir*, 2005, **21**, 2414-2418.
175. A. M. König and D. Johannsmann, *Langmuir*, 2010, **26**, 9437-9441.
176. C. Jin, M. A. McLachlan, D. W. McComb, R. M. De La Rue and N. P. Johnson, *Nano Lett.*, 2005, **5**, 2646-2650.
177. A. Groisman and E. Kaplan, *Europhys. Lett. (EPL)*, 1994, **25**, 415-420.
178. M. I. Smith and J. S. Sharp, *Langmuir*, 2011, **27**, 8009-8017.
179. B. Griesebock, M. Egen and R. Zentel, *Chem. Mater.*, 2002, **14**, 4023-4025.
180. Y. Zhang, J. Wang, Y. Huang, Y. Song and L. Jiang, *J. Mater. Chem.*, 2011, **21**, 14113-14126.
181. X. D. Shi, W. Y. Liu, D. Zhao, X. T. Li, R. M. Dou, K. J. Shea and X. H. Lu, *J. Mater. Chem. C*, 2016, **4**, 7208-7214.
182. S. Nishimura, A. Shishido, N. Abrams and T. E. Mallouk, *Appl. Phys. Lett.*, 2002, **81**, 4532-4534.
183. M. Grzelczak, J. Vermant, E. M. Furst and L. M. Liz-Marzán, *ACS Nano*, 2010, **4**, 3591-3605.
184. T. Ruhl, P. Spahn and G. P. Hellmann, *Polymer*, 2003, **44**, 7625-7634.
185. O. L. J. Pursiainen, J. J. Baumberg, H. Winkler, B. Viel, P. Spahn and T. Ruhl, *Adv. Mater.*, 2008, **20**, 1484-1487.
186. T. Ruhl and G. P. Hellmann, *Macromol. Chem. Phys.*, 2001, **202**, 3502-3505.
187. T. Ruhl, P. Spahn, H. Winkler and G. P. Hellmann, *Macromol. Chem. Phys.*, 2004, **205**, 1385-1393.
188. T. Kanai, T. Sawada, A. Toyotama and K. Kitamura, *Adv. Funct. Mater.*, 2005, **15**, 25-29.
189. Y. Xia and G. M. Whitesides, *Annu. Rev. Mater. Sci.*, 1998, **28**, 153-184.
190. Y. Yin, Z.-Y. Li and Y. Xia, *Langmuir*, 2003, **19**, 622-631.
191. Y. Yin and Y. Xia, *Adv. Mater.*, 2002, **14**, 605-608.
192. A. van Blaaderen, R. Ruel and P. Wiltzius, *Nature*, 1997, **385**, 321-324.
193. Z. Cai, J. Teng, D. Xia and X. S. Zhao, *J. Phys. Chem. C*, 2011, **115**, 9970-9976.
194. I. Bita, J. K. W. Yang, Y. S. Jung, C. A. Ross, E. L. Thomas and K. K. Berggren, *Science*, 2008, **321**, 939-943.
195. C. Jin, Z.-Y. Li, M. A. McLachlan, D. W. McComb, R. M. D. L. Rue and N. P. Johnson, *J. Appl. Phys.*, 2006, **99**, 116109.
196. Y. Yin and Y. Xia, *Adv. Mater.*, 2001, **13**, 267-271.
197. Y. Yin, Y. Lu, B. Gates and Y. Xia, *J. Am. Chem. Soc.*, 2001, **123**, 8718-8729.
198. Y. Xia, Y. Yin, Y. Lu and J. McLellan, *Adv. Funct. Mater.*, 2003, **13**, 907-918.
199. Y. Huang, J. Zhou, B. Su, L. Shi, J. Wang, S. Chen, L. Wang, J. Zi, Y. Song and L. Jiang, *J. Am. Chem. Soc.*, 2012, **134**, 17053-17058.
200. X. Lu, Y. Zhu, T. Cen and L. Jiang, *Langmuir*, 2012, **28**, 9341-9346.
201. M. R. Kim, S. H. Im, Y.-S. Kim and K. Y. Cho, *Adv. Funct. Mater.*, 2013, **23**, 5700-5705.
202. J.-T. Zhang, L. Wang, J. Luo, A. Tikhonov, N. Kornienko and S. A. Asher, *J. Am. Chem. Soc.*, 2011, **133**, 9152-9155.
203. Y. Fang, B. M. Phillips, K. Askar, B. Choi, P. Jiang and B. Jiang, *J. Mater. Chem. C*, 2013, **1**, 6031-6047.
204. P. Jiang and M. J. McFarland, *J. Am. Chem. Soc.*, 2004, **126**, 13778-13786.
205. W. L. Min, P. Jiang and B. Jiang, *Nanotechnology*, 2008, **19**, 7.
206. L. Cui, Y. Zhang, J. Wang, Y. Ren, Y. Song and L. Jiang, *Macromol. Rapid Commun.*, 2009, **30**, 598-603.
207. H. Yang and P. Jiang, *Langmuir*, 2010, **26**, 13173-13182.
208. T. Alfrey, E. B. Bradford, J. W. Vanderhoff and G. Oster, *J. Opt. Soc. Am.*, 1954, **44**, 603-609.
209. S. A. Asher, Crystalline colloidal narrow band radiation filter. *US4632517A*, 1986-12-09, 1986.
210. R. J. Carlson and S. A. Asher, *Appl. Spectrosc.*, 1984, **38**, 297-304.
211. P. A. Rundquist, P. Photinos, S. Jagannathan and S. A. Asher, *J. Chem. Phys.*, 1989, **91**, 4932-4941.
212. S. A. Asher, J. Holtz, L. Liu and Z. Wu, *J. Am. Chem. Soc.*, 1994, **116**, 4997-4998.
213. G. Pan, R. Kesavamoorthy and S. A. Asher, *Phys. Rev. Lett.*, 1997, **78**, 3860-3863.
214. J. H. Holtz and S. A. Asher, *Nature*, 1997, **389**, 829-832.

215. J. H. Holtz, J. S. W. Holtz, C. H. Munro and S. A. Asher, *Anal. Chem.*, 1998, **70**, 780-791.
216. G. Pan, R. Kesavamoorthy and S. A. Asher, *J. Am. Chem. Soc.*, 1998, **120**, 6525-6530.
217. S. A. Asher, V. L. Alexeev, A. V. Goponenko, A. C. Sharma, I. K. Lednev, C. S. Wilcox and D. N. Finegold, *J. Am. Chem. Soc.*, 2003, **125**, 3322-3329.
218. T. Kanai and T. Sawada, *Langmuir*, 2009, **25**, 13315-13317.
219. J. M. Weissman, H. B. Sunkara, A. S. Tse and S. A. Asher, *Science*, 1996, **274**, 959-963.
220. T. Hellweg, C. D. Dewhurst, E. Brückner, K. Kratz and W. Eimer, *Colloid Polym. Sci.*, 2000, **278**, 972-978.
221. J. Zhou, G. Wang, M. Marquez and Z. Hu, *Soft Matter*, 2009, **5**, 820-826.
222. J. Y. Kim, K. Cho, S.-a. Ryu, S. Y. Kim and B. M. Weon, *Sci. Rep.*, 2015, **5**, 13166.
223. A. S. J. Iyer and L. A. Lyon, *Angew. Chem., Int. Ed.*, 2009, **48**, 4562-4566.
224. M. Zhou, F. Xing, M. Ren, Y. Feng, Y. Zhao, H. Qiu, X. Wang, C. Gao, F. Sun, Y. He, Z. Ma, P. Wen and J. Gao, *ChemPhysChem*, 2009, **10**, 523-526.
225. F. R. Alexander, *Rep. Prog. Phys.*, 2013, **76**, 046603.
226. J. Zhou, J. Wang, Y. Huang, G. Liu, L. Wang, S. Chen, X. Li, D. Wang, Y. Song and L. Jiang, *NPG Asia Mater.*, 2012, **4**, e21-e21.
227. L. A. Lyon, Z. Meng, N. Singh, C. D. Sorrell and A. St. John, *Chem. Soc. Rev.*, 2009, **38**, 865-874.
228. S. Wong, V. Kitaev and G. A. Ozin, *J. Am. Chem. Soc.*, 2003, **125**, 15589-15598.
229. Z. Cai, J. Teng, Y. Wan and X. S. Zhao, *J. Colloid Interface Sci.*, 2012, **380**, 42-50.
230. Z. Cai, Y. J. Liu, X. Lu and J. Teng, *ACS Appl. Mater. Interfaces*, 2014, **6**, 10265-10273.
231. Z. Cai, Y. J. Liu, J. Teng and X. Lu, *ACS Appl. Mater. Interfaces*, 2012, **4**, 5562-5569.
232. Z. Cai, Y. J. Liu, E. S. P. Leong, J. Teng and X. Lu, *J. Mater. Chem.*, 2012, **22**, 24668-24675.
233. B.-J. Kim and K.-S. Kang, *Cryst. Growth Des.*, 2012, **12**, 4039-4042.
234. S. Wong, M. Deubel, F. Pérez-Willard, S. John, G. A. Ozin, M. Wegener and G. von Freymann, *Adv. Mater.*, 2006, **18**, 265-269.
235. H.-Y. Ko, J. Park, H. Shin and J. Moon, *Chem. Mater.*, 2004, **16**, 4212-4215.
236. D. Wang, M. Park, J. Park and J. Moon, *Appl. Phys. Lett.*, 2005, **86**, 241114.
237. J. Park, J. Moon, H. Shin, D. Wang and M. Park, *J. Colloid Interface Sci.*, 2006, **298**, 713-719.
238. J. Park and J. Moon, *Langmuir*, 2006, **22**, 3506-3513.
239. L. Cui, Y. Li, J. Wang, E. Tian, X. Zhang, Y. Zhang, Y. Song and L. Jiang, *J. Mater. Chem.*, 2009, **19**, 5499-5502.
240. J. Zhang, Z. Zhu, Z. Yu, L. Ling, C.-F. Wang and S. Chen, *Mater. Horiz.*, 2019, **6**, 90-96.
241. H. Kim, J. Ge, J. Kim, S.-e. Choi, H. Lee, H. Lee, W. Park, Y. Yin and S. Kwon, *Nat. Photonics*, 2009, **3**, 534-540.
242. J. Ge, Y. Hu and Y. Yin, *Angew. Chem., Int. Ed.*, 2007, **46**, 7428-7431.
243. J. Ge and Y. Yin, *Adv. Mater.*, 2008, **20**, 3485-3491.
244. A. P. Alivisatos, K. P. Johnsson, X. Peng, T. E. Wilson, C. J. Loweth, M. P. Bruchez and P. G. Schultz, *Nature*, 1996, **382**, 609-611.
245. C. A. Mirkin, R. L. Letsinger, R. C. Mucic and J. J. Storhoff, *Nature*, 1996, **382**, 607-609.
246. M.-P. Valignat, O. Theodoly, J. C. Crocker, W. B. Russel and P. M. Chaikin, *Proc. Natl. Acad. Sci. U. S. A.*, 2005, **102**, 4225-4229.
247. D. Nykypanchuk, M. M. Maye, D. van der Lelie and O. Gang, *Nature*, 2008, **451**, 549-552.
248. S. Y. Park, A. K. R. Lytton-Jean, B. Lee, S. Weigand, G. C. Schatz and C. A. Mirkin, *Nature*, 2008, **451**, 553-556.
249. W. B. Rogers and V. N. Manoharan, *Science*, 2015, **347**, 639-642.
250. E. Auyeung, T. I. N. G. Li, A. J. Senesi, A. L. Schmucker, B. C. Pals, M. O. de la Cruz and C. A. Mirkin, *Nature*, 2014, **505**, 73-77.
251. Y. Wang, Y. Wang, X. Zheng, É. Ducrot, J. S. Yodh, M. Weck and D. J. Pine, *Nat. Commun.*, 2015, **6**, 7253.
252. J. S. Oh, Y. Wang, D. J. Pine and G.-R. Yi, *Chem. Mater.*, 2015, **27**, 8337-8344.
253. W. B. Rogers, W. M. Shih and V. N. Manoharan, *Nat. Rev. Mater.*, 2016, **1**, 16008.
254. X. Zheng, Y. Wang, Y. Wang, D. J. Pine and M. Weck, *Chem. Mater.*, 2016, **28**, 3984-3989.
255. Y. Wang, I. C. Jenkins, J. T. McGinley, T. Sinno and J. C. Crocker, *Nat. Commun.*, 2017, **8**, 14173.
256. J. S. Oh, S. Lee, S. C. Glotzer, G.-R. Yi and D. J. Pine, *Nat. Commun.*, 2019, **10**, 3936.
257. J. S. Oh, M. He, G.-R. Yi and D. J. Pine, *Langmuir*, 2020, **36**, 3583-3589.
258. W. Liu, M. Tagawa, H. L. Xin, T. Wang, H. Emamy, H. Li, K. G. Yager, F. W. Starr, A. V. Tkachenko and O. Gang, *Science*, 2016, **351**, 582-586.
259. Y. Tian, Y. Zhang, T. Wang, H. L. Xin, H. Li and O. Gang, *Nat. Mater.*, 2016, **15**, 654-661.
260. M. E. Leunissen, C. G. Christova, A.-P. Hynninen, C. P. Royall, A. I. Campbell, A. Imhof, M. Dijkstra, R. van Roij and A. van Blaaderen, *Nature*, 2005, **437**, 235-240.
261. T. Hueckel, G. M. Hocky, J. Palacci and S. Sacanna, *Nature*, 2020, **580**, 487-490.
262. L. Rossi, S. Sacanna, W. T. M. Irvine, P. M. Chaikin, D. J. Pine and A. P. Philipse, *Soft Matter*, 2011, **7**, 4139-4142.
263. Y. Wang, Y. Wang, X. Zheng, G.-R. Yi, S. Sacanna, D. J. Pine and M. Weck, *J. Am. Chem. Soc.*, 2014, **136**, 6866-6869.
264. S. Guo, J. Nozawa, S. Hu, H. Koizumi, J. Okada and S. Uda, *Langmuir*, 2017, **33**, 10543-10549.
265. M. Liu, X. Zheng, V. Grebe, D. J. Pine and M. Weck, *Nat. Mater.*, 2020, **19**, 1354-1361.
266. S. Sacanna, W. T. M. Irvine, P. M. Chaikin and D. J. Pine, *Nature*, 2010, **464**, 575-578.
267. Q. Chen, S. C. Bae and S. Granick, *Nature*, 2011, **469**, 381-384.
268. Q. Chen, J. K. Whitmer, S. Jiang, S. C. Bae, E. Luijten and S. Granick, *Science*, 2011, **331**, 199-202.
269. Q. Chen, J. Yan, J. Zhang, S. C. Bae and S. Granick, *Langmuir*, 2012, **28**, 13555-13561.
270. C. Hertlein, L. Helden, A. Gambassi, S. Dietrich and C. Bechinger, *Nature*, 2008, **451**, 172-175.
271. D. Bonn, J. Otwinowski, S. Sacanna, H. Guo, G. Wegdam and P. Schall, *Phys. Rev. Lett.*, 2009, **103**, 4.
272. V. D. Nguyen, S. Faber, Z. Hu, G. H. Wegdam and P. Schall, *Nat. Commun.*, 2013, **4**, 1584.
273. V. D. Nguyen, M. T. Dang, T. A. Nguyen and P. Schall, *J. Phys.: Condens. Matter*, 2016, **28**, 043001.
274. T. A. Nguyen, A. Newton, S. J. Veen, D. J. Kraft, P. G. Bolhuis and P. Schall, *Adv. Mater.*, 2017, **29**, 1700819.

275. E. Elacqua, X. Zheng and M. Weck, *ACS Macro Lett.*, 2017, **6**, 1060-1065.
276. J. Palacci, S. Sacanna, A. P. Steinberg, D. J. Pine and P. M. Chaikin, *Science*, 2013, **339**, 936-940.
277. J. Palacci, S. Sacanna, S.-H. Kim, G.-R. Yi, D. J. Pine and P. M. Chaikin, *Philos. Trans. R. Soc., A*, 2014, **372**, 20130372.
278. B. Bharti, D. Rutkowski, K. Han, A. U. Kumar, C. K. Hall and O. D. Velev, *J. Am. Chem. Soc.*, 2016, **138**, 14948-14953.
279. X. Zheng, M. Liu, M. He, D. J. Pine and M. Weck, *Angew. Chem., Int. Ed.*, 2017, **56**, 5507-5511.
280. V. Meester and D. J. Kraft, *Soft Matter*, 2018, **14**, 1162-1170.
281. S. Ni, J. Leemann, I. Buttinoni, L. Isa and H. Wolf, *Sci. Adv.*, 2016, **2**, e1501779.
282. E. Elacqua, X. Zheng, C. Shillingford, M. Liu and M. Weck, *Acc. Chem. Res.*, 2017, **50**, 2756-2766.
283. Y. Wang, A. D. Hollingsworth, S. K. Yang, S. Patel, D. J. Pine and M. Weck, *J. Am. Chem. Soc.*, 2013, **135**, 14064-14067.
284. P. Song, Y. Wang, Y. Wang, A. D. Hollingsworth, M. Weck, D. J. Pine and M. D. Ward, *J. Am. Chem. Soc.*, 2015, **137**, 3069-3075.
285. Z. Jia, S. Sacanna and S. S. Lee, *Soft Matter*, 2017, **13**, 5724-5730.
286. N. Yanai, M. Sindoro, J. Yan and S. Granick, *J. Am. Chem. Soc.*, 2013, **135**, 34-37.
287. S. Sacanna, L. Rossi and D. J. Pine, *J. Am. Chem. Soc.*, 2012, **134**, 6112-6115.
288. M. Wang, L. He and Y. Yin, *Mater. Today*, 2013, **16**, 110-116.
289. I. Muševič, M. Škarabot, U. Tkalec, M. Ravnik and S. Žumer, *Science*, 2006, **313**, 954-958.
290. U. Tkalec, M. Ravnik, S. Čopar, S. Žumer and I. Muševič, *Science*, 2011, **333**, 62-65.
291. P. Poulin, H. Stark, T. C. Lubensky and D. A. Weitz, *Science*, 1997, **275**, 1770-1773.
292. H. Mundoor, J.-S. Wu, H. H. Wensink and I. I. Smalyukh, *Nature*, 2021, **590**, 268-274.
293. R. J. Macfarlane, B. Lee, M. R. Jones, N. Harris, G. C. Schatz and C. A. Mirkin, *Science*, 2011, **334**, 204-208.
294. C. Zhang, R. J. Macfarlane, K. L. Young, C. H. J. Choi, L. Hao, E. Auyeung, G. Liu, X. Zhou and C. A. Mirkin, *Nat. Mater.*, 2013, **12**, 741-746.
295. J. C. Crocker, *Nature*, 2020, **585**, 506-507.
296. E. G. Noya, C. Vega, J. P. K. Doye and A. A. Louis, *J. Chem. Phys.*, 2010, **132**, 234511.
297. O. D. Velev, A. M. Lenhoff and E. W. Kaler, *Science*, 2000, **287**, 2240.
298. Y. Masuda, T. Itoh and K. Koumoto, *Adv. Mater.*, 2005, **17**, 841-845.
299. S.-H. Kim, S.-J. Jeon and S.-M. Yang, *J. Am. Chem. Soc.*, 2008, **130**, 6040-6046.
300. Y.-J. Zhao, X.-W. Zhao, J. Hu, J. Li, W.-Y. Xu and Z.-Z. Gu, *Angew. Chem., Int. Ed.*, 2009, **48**, 7350-7352.
301. S.-H. Kim, S. Y. Lee, G.-R. Yi, D. J. Pine and S.-M. Yang, *J. Am. Chem. Soc.* 2006, **128**, 10897-10904.
302. G.-R. Yi, J. H. Moon and S.-M. Yang, *Chem. Mater.*, 2001, **13**, 2613-2618.
303. S.-H. Kim, S.-J. Jeon, G.-R. Yi, C.-J. Heo, J. H. Choi and S.-M. Yang, *Adv. Mater.*, 2008, **20**, 1649-1655.
304. Y. Zhao, L. Shang, Y. Cheng and Z. Gu, *Acc. Chem. Res.*, 2014, **47**, 3632-3642.
305. Y. Zhao, Y. Cheng, L. Shang, J. Wang, Z. Xie and Z. Gu, *Small*, 2015, **11**, 151-174.
306. Y. Xu, X. Zhang, C. Luan, H. Wang, B. Chen and Y. Zhao, *Biosens. Bioelectron.*, 2017, **87**, 264-270.
307. Z. Chen, J. Wu, Y. Wang, C. Shao, J. Chi, Z. Li, X. Wang and Y. Zhao, *Small*, 2019, **15**, 1903104.
308. V. Rastogi, S. Melle, O. G. Calderon, A. A. Garcia, M. Marquez and O. D. Velev, *Adv. Mater.*, 2008, **20**, 4263-4268.
309. K. Xu, J. H. Xu, Y. C. Lu and G. S. Luo, *Cryst. Growth Des.*, 2013, **13**, 926-935.
310. X. Zhao, Y. Cao, F. Ito, H.-H. Chen, K. Nagai, Y.-H. Zhao and Z.-Z. Gu, *Angew. Chem., Int. Ed.*, 2006, **45**, 6835-6838.
311. J. Cui, W. Zhu, N. Gao, J. Li, H. Yang, Y. Jiang, P. Seidel, B. J. Ravoo and G. Li, *Angew. Chem., Int. Ed.*, 2014, **53**, 3844-3848.
312. J. Wang, Y. Hu, R. Deng, R. Liang, W. Li, S. Liu and J. Zhu, *Langmuir*, 2013, **29**, 8825-8834.
313. Y. Kim, C.-Y. Cho, J.-H. Kang, Y.-S. Cho and J. H. Moon, *Langmuir*, 2012, **28**, 10543-10550.
314. J. H. Moon, G. R. Yi, S. M. Yang, D. J. Pine and S. B. Park, *Adv. Mater.*, 2004, **16**, 605-609.
315. J. R. Millman, K. H. Bhatt, B. G. Prevo and O. D. Velev, *Nat. Mater.*, 2005, **4**, 98-102.
316. V. Rastogi, A. A. García, M. Marquez and O. D. Velev, *Macromol. Rapid Commun.*, 2010, **31**, 190-195.
317. L. Shang, F. Shangguan, Y. Cheng, J. Lu, Z. Xie, Y. Zhao and Z. Gu, *Nanoscale*, 2013, **5**, 9553-9557.
318. Z. Yu, C.-F. Wang, L. Ling, L. Chen and S. Chen, *Angew. Chem., Int. Ed.*, 2012, **51**, 2375-2378.
319. S.-H. Kim, J.-G. Park, T. M. Choi, V. N. Manoharan and D. A. Weitz, *Nat. Commun.*, 2014, **5**, 3068.
320. T. Kanai, D. Lee, H. C. Shum, R. K. Shah and D. A. Weitz, *Adv. Mater.*, 2010, **22**, 4998-5002.
321. C. Zhu, W. Xu, L. Chen, W. Zhang, H. Xu and Z.-Z. Gu, *Adv. Funct. Mater.*, 2011, **21**, 2043-2048.
322. Y. Zhao, Z. Xie, H. Gu, L. Jin, X. Zhao, B. Wang and Z. Gu, *NPG Asia Mater.*, 2012, **4**, e25.
323. B. Ye, H. Ding, Y. Cheng, H. Gu, Y. Zhao, Z. Xie and Z. Gu, *Adv. Mater.*, 2014, **26**, 3270-3274.
324. F. Zheng, Y. Cheng, J. Wang, J. Lu, B. Zhang, Y. Zhao and Z. Gu, *Adv. Mater.*, 2014, **26**, 7333-7338.
325. O. D. Velev and S. Gupta, *Adv. Mater.*, 2009, **21**, 1897-1905.
326. T. Kanai, D. Lee, H. C. Shum and D. A. Weitz, *Small*, 2010, **6**, 807-810.
327. J. Hu, X. W. Zhao, Y. J. Zhao, J. Li, W. Y. Xu, Z. Y. Wen, M. Xu and Z. Z. Gu, *J. Mater. Chem.*, 2009, **19**, 5730-5736.
328. Y. Zhao, X. Zhao, C. Sun, J. Li, R. Zhu and Z. Gu, *Anal. Chem.*, 2008, **80**, 1598-1605.
329. Y. Zhao, H. Gu, Z. Xie, H. C. Shum, B. Wang and Z. Gu, *J. Am. Chem. Soc.*, 2013, **135**, 54-57.
330. L. R. Shang, F. F. Fu, Y. Cheng, H. Wang, Y. X. Liu, Y. J. Zhao and Z. Z. Gu, *J. Am. Chem. Soc.*, 2015, **137**, 15533-15539.
331. F. Bian, L. Sun, L. Cai, Y. Wang, Y. Wang and Y. Zhao, *Small*, 2020, **16**, 1903931.
332. Y. Zhao, X. Zhao, J. Hu, M. Xu, W. Zhao, L. Sun, C. Zhu, H. Xu and Z. Gu, *Adv. Mater.*, 2009, **21**, 569-572.
333. Y. Zhao, X. Zhao, B. Tang, W. Xu, J. Li, J. Hu and Z. Gu, *Adv. Funct. Mater.*, 2010, **20**, 976-982.
334. Q. Yang, M. Li, J. Liu, W. Shen, C. Ye, X. Shi, L. Jiang and Y. Song, *J. Mater. Chem. A*, 2013, **1**, 541-547.
335. Y. Hu, J. Wang, H. Wang, Q. Wang, J. Zhu and Y. Yang, *Langmuir*, 2012, **28**, 17186-17192.
336. Z. Zhu, J.-D. Liu, C. Liu, X. Wu, Q. Li, S. Chen, X. Zhao and D. A. Weitz, *Small*, 2020, **16**, 1903939.
337. T. Y. M. Chan, O. Toader and S. John, *Phys. Rev. E*, 2005, **71**.
338. A. Stein, F. Li and N. R. Denny, *Chem. Mater.*, 2008, **20**, 649-666.
339. O. D. Velev, T. A. Jede, R. F. Lobo and A. M. Lenhoff, *Nature*, 1997, **389**, 447-448.
340. B. T. Holland, C. F. Blanford and A. Stein, *Science*, 1998, **281**, 538-540.

341. J. Wang, Q. Li, W. Knoll and U. Jonas, *J. Am. Chem. Soc.*, 2006, **128**, 15606-15607.
342. F. Caruso, R. A. Caruso and H. Möhwald, *Science*, 1998, **282**, 1111-1114.
343. Y. Hotta, Y. Jia, M. Kawamura, N. Omura, K. Tsunekawa, K. Sato and K. Watari, *J. Mater. Sci.*, 2006, **41**, 2779-2786.
344. A. Stein, F. Li and N. R. Denny, *Chem. Mater.*, 2007, **20**, 649-666.
345. A. Stein, B. E. Wilson and S. G. Rudisill, *Chem. Soc. Rev.*, 2013, **42**, 2763-2803.
346. G. I. Waterhouse and M. R. Waterland, *Polyhedron*, 2007, **26**, 356-368.
347. S. W. Choi, J. Xie and Y. Xia, *Adv. Mater.*, 2009, **21**, 2997-3001.
348. Z. Zhang, W. Shen, C. Ye, Y. Luo, S. Li, M. Li, C. Xu and Y. Song, *J. Mater. Chem.*, 2012, **22**, 5300-5303.
349. H. Freimuth, V. Hessel, H. Kölle, M. Lacher, W. Ehrfeld, T. Vaahs and M. Brück, *J. Am. Ceram. Soc.*, 1996, **79**, 1457-1465.
350. X. Chen, L. Wang, Y. Wen, Y. Zhang, J. Wang, Y. Song, L. Jiang and D. Zhu, *J. Mater. Chem.*, 2008, **18**, 2262-2267.
351. R. Bodet, N. Jia and R. E. Tressler, *J. Eur. Ceram. Soc.*, 1996, **16**, 653-664.
352. L. Hu, M. Li, C. Xu, Y. Luo and Y. Zhou, *Surf. Coat. Technol.*, 2009, **203**, 3338-3343.
353. H.-J. Lee, T.-H. Yoon and D.-P. Kim, *J. Phys. Chem. Solids*, 2008, **69**, 2131-2136.
354. G. Qi, C. Zhang and H. Hu, *Ceram. Int.*, 2007, **33**, 891-894.
355. I. K. Sung, Christian, M. Mitchell, D. P. Kim and P. J. A. Kenis, *Adv. Funct. Mater.*, 2005, **15**, 1336-1342.
356. P. Greil, *Adv. Eng. Mater.*, 2000, **2**, 339-348.
357. S. Hore, P. Nitz, C. Vetter, C. Prahl, M. Niggemann and R. Kern, *Chem. Commun.*, 2005, 2011-2013.
358. E. S. Kwak, W. Lee, N.-G. Park, J. Kim and H. Lee, *Adv. Funct. Mater.*, 2009, **19**, 1093-1099.
359. F. García-Santamaría, E. C. Nelson and P. V. Braun, *Phys. Rev. B*, 2007, **76**, 075132.
360. J. W. Galusha, C.-K. Tsung, G. D. Stucky and M. H. Bartl, *Chem. Mater.*, 2008, **20**, 4925-4930.
361. Z. Cai, J. Teng, Z. Xiong, Y. Li, Q. Li, X. Lu and X. S. Zhao, *Langmuir*, 2011, **27**, 5157-5164.
362. L. Wang, Y. Wan, Y. Li, Z. Cai, H.-L. Li, X. S. Zhao and Q. Li, *Langmuir*, 2009, **25**, 6753-6759.
363. V. Ramanan, E. Nelson, A. Brzezinski, P. V. Braun and P. Wiltzius, *Appl. Phys. Lett.*, 2008, **92**, 173304-173303.
364. K. A. Arpin, M. D. Losego, A. N. Cloud, H. Ning, J. Mallek, N. P. Sergeant, L. Zhu, Z. Yu, B. Kalanyan, G. N. Parsons, G. S. Girolami, J. R. Abelson, S. Fan and P. V. Braun, *Nat. Commun.*, 2013, **4**, 2630.
365. N. R. Denny, S. E. Han, D. J. Norris and A. Stein, *Chem. Mater.*, 2007, **19**, 4563-4569.
366. K. A. Arpin, M. D. Losego and P. V. Braun, *Chem. Mater.*, 2011, **23**, 4783-4788.
367. J. S. King, D. Heineman, E. Graugnard and C. J. Summers, *Appl. Surf. Sci.*, 2005, **244**, 511-516.
368. J. S. King, E. Graugnard and C. J. Summers, *Adv. Mater.*, 2005, **17**, 1010-1013.
369. J. S. King, D. P. Gaillot, E. Graugnard and C. J. Summers, *Adv. Mater.*, 2006, **18**, 1063-1067.
370. F. García-Santamaría, M. Xu, V. Lousse, S. Fan, P. V. Braun and J. A. Lewis, *Adv. Mater.*, 2007, **19**, 1567-1570.
371. J. R. Oh, J. H. Moon, H. K. Park, J. H. Park, H. Chung, J. Jeong, W. Kim and Y. R. Do, *J. Mater. Chem.*, 2010, **20**, 5025-5029.
372. K. R. Phillips, T. Shirman, E. Shirman, A. V. Shneidman, T. M. Kay and J. Aizenberg, *Adv. Mater.*, 2018, **30**, 1706329.
373. Q.-B. Meng, Z.-Z. Gu, O. Sato and A. Fujishima, *Appl. Phys. Lett.*, 2000, **77**, 4313-4315.
374. Z. Zheng, K. Gao, Y. Luo, D. Li, Q. Meng, Y. Wang and D. Zhang, *J. Am. Chem. Soc.*, 2008, **130**, 9785-9789.
375. Z. Cai, Y. J. Liu, X. Lu and J. Teng, *J. Phys. Chem. C*, 2013, **117**, 9440-9445.
376. Z. Cai, Z. Xiong, X. Lu and J. Teng, *J. Mater. Chem. A*, 2014, **2**, 545-553.
377. Y. Zhang, Y. Sun, J. Liu, P. Guo, Z. Cai and J.-J. Wang, *Sens. Actuators, B*, 2019, **291**, 67-73.
378. Z. Bao, M. R. Weatherspoon, S. Shian, Y. Cai, P. D. Graham, S. M. Allan, G. Ahmad, M. B. Dickerson, B. C. Church, Z. Kang, H. W. Abernathy Iii, C. J. Summers, M. Liu and K. H. Sandhage, *Nature*, 2007, **446**, 172-175.
379. K. R. Phillips, T. Shirman, E. Shirman, A. V. Shneidman, T. M. Kay and J. Aizenberg, *Adv. Mater.*, 2018, **30**, 1706329.
380. Y. Vasquez, M. Kolle, L. Mishchenko, B. D. Hatton and J. Aizenberg, *ACS Photonics*, 2014, **1**, 53-60.
381. Z. Zhu, J. Zhang, C.-F. Wang and S. Chen, *Macromol. Mater. Eng.*, 2017, **302**, 1700013.
382. S.-Y. Lin, E. Chow, V. Hietala, P. R. Villeneuve and J. D. Joannopoulos, *Science*, 1998, **282**, 274-276.
383. E. Yablonovitch, *J. Opt. Soc. Am. B*, 1993, **10**, 283-295.
384. J. T. Han, D. H. Lee, C. Y. Ryu and K. Cho, *J. Am. Chem. Soc.*, 2004, **126**, 4796-4797.
385. M. H. Kim, S. H. Im and O. O. Park, *Adv. Mater.*, 2005, **17**, 2501-2505.
386. R. Xie and X.-Y. Liu, *Adv. Funct. Mater.*, 2008, **18**, 802-809.
387. C. Li, G. Hong, P. Wang, D. Yu and L. Qi, *Chem. Mater.*, 2009, **21**, 891-897.
388. M. Yamaki, K. Matsubara and K. Nagayama, *Langmuir*, 1993, **9**, 3154-3158.
389. A. S. Dimitrov, C. D. Dushkin, H. Yoshimura and K. Nagayama, *Langmuir*, 1994, **10**, 432-440.
390. M. Kondo, K. Shinozaki, L. Bergstroem and N. Mizutani, *Langmuir*, 1995, **11**, 394-397.
391. F. Pan, J. Zhang, C. Cai and T. Wang, *Langmuir*, 2006, **22**, 7101-7104.
392. C. Li, G. Hong and L. Qi, *Chem. Mater.*, 2010, **22**, 476-481.
393. J. Rybczynski, U. Ebels and M. Giersig, *Colloids Surf., A*, 2003, **219**, 1-6.
394. M. Retsch, Z. Zhou, S. Rivera, M. Kappl, X. S. Zhao, U. Jonas and Q. Li, *Macromol. Chem. Phys.*, 2009, **210**, 230-241.
395. J. Yu, Q. Yan and D. Shen, *ACS Appl. Mater. Interfaces*, 2010, **2**, 1922-1926.
396. H. H. Wickman and J. N. Korley, *Nature*, 1998, **393**, 445-447.
397. S. H. Im and O. O. Park, *Langmuir*, 2002, **18**, 9642-9646.
398. Q. Yan, L. K. Teh, Q. Shao, C. C. Wong and Y.-M. Chiang, *Langmuir*, 2008, **24**, 1796-1800.
399. Z. Dai, Y. Li, G. Duan, L. Jia and W. Cai, *ACS Nano*, 2012, **6**, 6706-6716.
400. J.-T. Zhang, L. Wang, D. N. Lamont, S. S. Velankar and S. A. Asher, *Angew. Chem., Int. Ed.*, 2012, **51**, 6117-6120.
401. F. Xue, S. A. Asher, Z. Meng, F. Wang, W. Lu, M. Xue and F. Qi, *RSC Adv.*, 2015, **5**, 18939-18944.
402. L. E. Scriven and C. V. Sternling, *Nature*, 1960, **187**, 186-188.
403. P. Gao, J. He, S. Zhou, X. Yang, S. Li, J. Sheng, D. Wang, T. Yu, J. Ye and Y. Cui, *Nano Lett.*, 2015, **15**, 4591-4598.
404. Z. Cai, J.-T. Zhang, F. Xue, Z. Hong, D. Punihaole and S. A. Asher, *Anal. Chem.*, 2014, **86**, 4840-4847.
405. J.-T. Zhang, Z. Cai, D. H. Kwak, X. Liu and S. A. Asher, *Anal. Chem.*, 2014, **86**, 9036-9041.
406. J.-T. Zhang, L. Wang, X. Chao and S. A. Asher, *Langmuir*, 2011, **27**, 15230-15235.

407. Z. Cai, D. H. Kwak, D. Punihaole, Z. Hong, S. S. Velankar, X. Liu and S. A. Asher, *Angew. Chem.*, 2015, **127**, 13228-13232.
408. Z. Cai, D. H. Kwak, D. Punihaole, Z. Hong, S. S. Velankar, X. Liu and S. A. Asher, *Angew. Chem., Int. Ed.*, 2015, **54**, 13036-13040.
409. Z. Cai, L. A. Luck, D. Punihaole, J. D. Madura and S. A. Asher, *Chem. Sci.*, 2016, **7**, 4557-4562.
410. Z. Cai, A. Sasmal, X. Liu and S. A. Asher, *ACS Sens.*, 2017, **2**, 1474-1481.
411. F. Xue, Z. Meng, F. Qi, M. Xue and L. Qiu, *Colloid Polym. Sci.*, 2016, **294**, 479-482.
412. N. Vogel, S. Goerres, K. Landfester and C. K. Weiss, *Macromol. Chem. Phys.*, 2011, **212**, 1719-1734.
413. J. R. Oh, J. H. Moon, S. Yoon, C. R. Park and Y. R. Do, *J. Mater. Chem.*, 2011, **21**, 14167-14172.
414. G. Singh, S. Pillai, A. Arpanaei and P. Kingshott, *Adv. Funct. Mater.*, 2011, **21**, 2556-2563.
415. L. He, M. Wang, J. Ge and Y. Yin, *Acc. Chem. Res.*, 2012, **45**, 1431-1440.
416. J. Ge, H. Lee, L. He, J. Kim, Z. Lu, H. Kim, J. Goebl, S. Kwon and Y. Yin, *J. Am. Chem. Soc.*, 2009, **131**, 15687-15694.
417. M. Wang and Y. Yin, *J. Am. Chem. Soc.*, 2016, **138**, 6315-6323.
418. Z. Li, Z. Ye, L. Han, Q. Fan, C. Wu, D. Ding, H. L. Xin, N. V. Myung and Y. Yin, *Adv. Mater.*, 2020, 2006367.
419. Z. Li, J. Jin, F. Yang, N. Song and Y. Yin, *Nat. Commun.*, 2020, **11**, 1-11.
420. X. Chen, Z. Ye, F. Yang, J. Feng, Z. Li, C. Huang, Q. Ke and Y. Yin, *Appl. Mater. Today*, 2020, **20**, 100749.
421. J. Ge, Y. Hu, T. Zhang, T. Huynh and Y. Yin, *Langmuir*, 2008, **24**, 3671-3680.
422. L. He, Y. Hu, M. Wang and Y. Yin, *ACS Nano*, 2012, **6**, 4196-4202.
423. J. Ge, Y. Hu, M. Biasini, W. P. Beyermann and Y. Yin, *Angew. Chem., Int. Ed.*, 2007, **46**, 4342-4345.
424. J. Ge, L. He, J. Goebl and Y. Yin, *J. Am. Chem. Soc.*, 2009, **131**, 3484-3486.
425. J. Ge and Y. Yin, *J. Mater. Chem.*, 2008, **18**, 5041-5045.
426. M. Wang, L. He, Y. Hu and Y. Yin, *J. Mater. Chem. C*, 2013, **1**, 6151-6156.
427. L. He, Y. Hu, H. Kim, J. Ge, S. Kwon and Y. Yin, *Nano Lett.*, 2010, **10**, 4708-4714.
428. X. Zhang, Z. Li, J. Feng, F. Yang, C. Wu, Q. Fan, S. Zhou and Y. Yin, *Adv. Intell. Syst.*, 2019, **1**, 1900099.
429. J. Feng, F. Yang, X. Wang, F. Lyu, Z. Li and Y. Yin, *Adv. Mater.*, 2019, **31**, 1900789.
430. Q. Zhang, M. Janner, L. He, M. Wang, Y. Hu, Y. Lu and Y. Yin, *Nano Lett.*, 2013, **13**, 1770-1775.
431. V. Malik, A. V. Petukhov, L. He, Y. Yin and M. Schmidt, *Langmuir*, 2012, **28**, 14777-14783.
432. L. He, V. Malik, M. Wang, Y. Hu, F. E. Anson and Y. Yin, *Nanoscale*, 2012, **4**, 4438-4442.
433. S. G. Romanov, M. Bardosova, M. Pemble and C. M. S. Torres, *Appl. Phys. Lett.*, 2006, **89**, 043105.
434. M. E. Pemble, M. Bardosova, I. M. Povey, R. H. Tredgold and D. Whitehead, *Phys. B*, 2007, **394**, 233-237.
435. N. Vogel, L. de Viguerie, U. Jonas, C. K. Weiss and K. Landfester, *Adv. Funct. Mater.*, 2011, **21**, 3064-3073.
436. K. Shinotsuka, Y. Kajita, K. Hongo and Y. Hatta, *Langmuir*, 2015, **31**, 11452-11457.
437. P. Massé and S. Ravaine, *Chem. Mater.*, 2005, **17**, 4244-4249.
438. M. Parchine, J. McGrath, M. Bardosova and M. E. Pemble, *Langmuir*, 2016, **32**, 5862-5869.
439. P. Jiang, T. Prasad, M. J. McFarland and V. L. Colvin, *Appl. Phys. Lett.*, 2006, **89**, 011908-011903.
440. P. Jiang and M. J. McFarland, *J. Am. Chem. Soc.*, 2005, **127**, 3710-3711.
441. H. Yang, N. Gozubenli, Y. Fang and P. Jiang, *Langmuir*, 2013, **29**, 7674-7681.
442. S. B. Quint and C. Pacholski, *Soft Matter*, 2011, **7**, 3735-3738.
443. X. Li, J. Weng, Y. Guan and Y. Zhang, *Langmuir*, 2016, **32**, 3977-3982.
444. J. Weng, X. Li, Y. Guan, X. X. Zhu and Y. Zhang, *Langmuir*, 2016, **32**, 12876-12884.
445. S. Liang, Y. Guan and Y. Zhang, *ACS Omega*, 2019, **4**, 5650-5660.
446. B. G. Prevo and O. D. Velev, *Langmuir*, 2004, **20**, 2099-2107.
447. M. H. Kim, S. H. Im and O. O. Park, *Adv. Funct. Mater.*, 2005, **15**, 1329-1335.
448. Z. Chen, P. Zhan, Z. L. Wang, J. H. Zhang, W. Y. Zhang, N. B. Ming, C. T. Chan and P. Sheng, *Adv. Mater.*, 2004, **16**, 417-422.
449. M. Allard, E. H. Sargent, P. C. Lewis and E. Kumacheva, *Adv. Mater.*, 2004, **16**, 1360-1364.
450. J. P. Hoogenboom, C. Rétif, E. de Bres, M. van de Boer, A. K. van Langen-Suurling, J. Romijn and A. van Blaaderen, *Nano Lett.*, 2004, **4**, 205-208.
451. Y. Zeng, M. He and D. J. Harrison, *Angew. Chem., Int. Ed.*, 2008, **47**, 6388-6391.
452. J. Sun, Y. Y. Li, H. Dong, P. Zhan, C. J. Tang, M. W. Zhu and Z. L. Wang, *Adv. Mater.*, 2008, **20**, 123-128.
453. J. Sun, C.-j. Tang, P. Zhan, Z.-l. Han, Z.-S. Cao and Z.-L. Wang, *Langmuir*, 2010, **26**, 7859-7864.
454. X. Ye and L. Qi, *Nano Today*, 2011, **6**, 608-631.
455. X. Ye and L. Qi, *Sci. China: Chem.*, 2014, **57**, 58-69.
456. H. Li, J. Theriault, B. Rousselle, B. Subramanian, J. Robichaud and Y. Djaoued, *Chem. Commun.*, 2014, **50**, 2184-2186.
457. H. Li, G. Vienneau, M. Jones, B. Subramanian, J. Robichaud and Y. Djaoued, *J. Mater. Chem. C*, 2014, **2**, 7804-7810.
458. H. Li, J. F. Wang, J. Robichaud and Y. Djaoued, *Macromol. Res.*, 2019, **27**, 1229-1238.
459. B. Subramanian, G. Theriault, J. Robichaud, N. Tchoukanova and Y. Djaoued, *Mater. Chem. Phys.*, 2020, **244**, 122630.
460. Q. H. Wei and X. L. Wu, *Phys. Rev. E*, 2004, **70**, 020401.
461. W. Lee, A. Chan, M. A. Bevan, J. A. Lewis and P. V. Braun, *Langmuir*, 2004, **20**, 5262-5270.
462. R. Xie and X.-Y. Liu, *Appl. Phys. Lett.*, 2008, **92**, 083106-083103.
463. R. G. Xie and X. Y. Liu, *J. Am. Chem. Soc.*, 2009, **131**, 4976-4982.
464. M. H. Kim, H. K. Choi, O. O. Park and S. H. Im, *Appl. Phys. Lett.*, 2006, **88**, 143127-143123.
465. X. Yan, J. Yao, G. Lu, X. Li, J. Zhang, K. Han and B. Yang, *J. Am. Chem. Soc.*, 2005, **127**, 7688-7689.
466. X. Li, T. Wang, J. Zhang, X. Yan, X. Zhang, D. Zhu, W. Li, X. Zhang and B. Yang, *Langmuir*, 2010, **26**, 2930-2936.
467. N. N. Khanh and K. B. Yoon, *J. Am. Chem. Soc.*, 2009, **131**, 14228-14230.
468. T. Das Gupta, L. Martin-Monier, W. Yan, A. Le Bris, T. Nguyen-Dang, A. G. Page, K.-T. Ho, F. Yesilköy, H. Altug, Y. Qu and F. Sorin, *Nat. Nanotechnol.*, 2019, **14**, 320-327.
469. M. Mayer, M. J. Schnepf, T. A. F. Konig and A. Fery, *Adv. Opt. Mater.*, 2019, **7**, 17.
470. Z. Xie, K. Cao, Y. Zhao, L. Bai, H. Gu, H. Xu and Z.-Z. Gu, *Adv. Mater.*, 2013, **26**, 2413-2418.
471. Z. Zhao, H. Wang, L. Shang, Y. Yu, F. Fu, Y. Zhao and Z. Gu, *Adv. Mater.*, 2017, **29**, 1704569.

472. D. M. Kuncicky, B. G. Prevo and O. D. Velev, *J. Mater. Chem.*, 2006, **16**, 1207-1211.
473. M. T. Hörantner, W. Zhang, M. Saliba, K. Wojciechowski and H. J. Snaith, *Energy Environ. Sci.*, 2015, **8**, 2041-2047.
474. Y. Huang, W. Li, M. Qin, H. Zhou, X. Zhang, F. Li and Y. Song, *Small*, 2017, **13**, 1503339.
475. B. Gao, H. Liu and Z. Gu, *Anal. Chem.*, 2016, **88**, 5424-5429.
476. S. Li, B. A. Moosa, J. G. Croissant and N. M. Khashab, *Angew. Chem., Int. Ed.*, 2015, **54**, 6804-6808.
477. J. Hou, H. Zhang, Q. Yang, M. Li, L. Jiang and Y. Song, *Small*, 2015, **11**, 2738-2742.
478. Y. Huang, F. Li, M. Qin, L. Jiang and Y. Song, *Angew. Chem., Int. Ed.*, 2013, **52**, 7296-7299.
479. M. Qin, Y. Huang, Y. Li, M. Su, B. Chen, H. Sun, P. Yong, C. Ye, F. Li and Y. Song, *Angew. Chem., Int. Ed.*, 2016, **55**, 6911-6914.
480. Y. S. Zhang, C. L. Zhu and Y. N. Xia, *Adv. Mater.*, 2017, **29**, 25.
481. Y. Zhang, Q. Fu and J. Ge, *Small*, 2017, **13**, 1603351.
482. Y. Heo, H. Kang, J.-S. Lee, Y.-K. Oh and S.-H. Kim, *Small*, 2016, **12**, 3819-3826.
483. J. Zhang, Z. Meng, J. Liu, S. Chen and Z. Yu, *ACS Appl. Mater. Interfaces*, 2019, **11**, 42629-42634.
484. E. Yablonovitch, *J. Mod. Opt.*, 1994, **41**, 173-194.
485. M. SoljaČiĆ and J. D. Joannopoulos, *Nat. Mater.*, 2004, **3**, 211-219.
486. P. Bermel, C. Luo, L. Zeng, L. C. Kimerling and J. D. Joannopoulos, *Opt. Express*, 2007, **15**, 16986-17000.
487. A. Arsenault, S. Fournier-Bidoz, B. Hatton, H. Míguez, N. Tétreault, E. Vekris, S. Wong, S. Ming Yang, V. Kitaev and G. A. Ozin, *J. Mater. Chem.*, 2004, **14**, 781-794.
488. Z.-Y. Li and Z.-M. Meng, *J. Mater. Chem. C*, 2014, **2**, 783-800.
489. J. Jot Singh, D. Dhawan and N. Gupta, *Opt. Eng.*, 2020, **59**, 110901.
490. N. I. Zheludev and Y. S. Kivshar, *Nat. Mater.*, 2012, **11**, 917-924.
491. H.-H. Hsiao, C. H. Chu and D. P. Tsai, *Small Methods*, 2017, **1**, 1600064.
492. K. Volk, J. P. S. Fitzgerald, M. Retsch and M. Karg, *Adv. Mater.*, 2015, **27**, 7332-7337.
493. K. Volk, J. P. S. Fitzgerald, P. Ruckdeschel, M. Retsch, T. A. F. König and M. Karg, *Adv. Opt. Mater.*, 2017, **5**, 1600971.
494. V. Flauraud, M. Mastrangeli, G. D. Bernasconi, J. Butet, D. T. L. Alexander, E. Shahrabi, O. J. F. Martin and J. Brugger, *Nat. Nanotechnol.*, 2017, **12**, 73-80.
495. J. Henzie, M. Grünwald, A. Widmer-Cooper, P. L. Geissler and P. Yang, *Nat. Mater.*, 2011, **11**, 131.
496. M. Gómez-Castaño, H. Zheng, J. L. García-Pomar, R. Vallée, A. Mihi and S. Ravaine, *Nanoscale Adv.*, 2019, **1**, 1070-1076.
497. M. Gómez-Castaño, J. L. Garcia-Pomar, L. A. Pérez, S. Shanmugathasan, S. Ravaine and A. Mihi, *Adv. Opt. Mater.*, 2020, **8**, 2000865.
498. K. V. Sreekanth, Y. Alapan, M. ElKabbash, E. Ilker, M. Hinczewski, U. A. Gurkan, A. De Luca and G. Strangi, *Nat. Mater.*, 2016, **15**, 621.
499. H. Gu, Y. Zhao, Y. Cheng, Z. Xie, F. Rong, J. Li, B. Wang, D. Fu and Z. Gu, *Small*, 2013, **9**, 2266-2271.
500. M. Kuang, J. Wang, B. Bao, F. Li, L. Wang, L. Jiang and Y. Song, *Adv. Opt. Mater.*, 2014, **2**, 34-38.
501. A. C. Arsenault, D. P. Puzzo, I. Manners and G. A. Ozin, *Nat. Photonics*, 2007, **1**, 468-472.
502. N. Suzuki, E. Iwase and H. Onoe, *Adv. Opt. Mater.*, 2017, **5**, 7.
503. R. V. Nair and R. Vijaya, *Prog. Quantum Electron.*, 2010, **34**, 89-134.
504. J. Hou, M. Li and Y. Song, *Nano Today*, 2018, **22**, 132-144.
505. Z. Y. Xie, K. D. Cao, Y. J. Zhao, L. Bai, H. C. Gu, H. Xu and Z. Z. Gu, *Adv. Mater.*, 2014, **26**, 2413-2418.
506. L. B. Wang, J. X. Wang, Y. Huang, M. J. Liu, M. X. Kuang, Y. F. Li, L. Jiang and Y. L. Song, *J. Mater. Chem.*, 2012, **22**, 21405-21411.
507. L. Bai, Z. Y. Xie, W. Wang, C. W. Yuan, Y. J. Zhao, Z. D. Mu, Q. F. Zhong and Z. Z. Gu, *ACS Nano*, 2014, **8**, 11094-11100.
508. S. O. Meade, M. Y. Chen, M. J. Sailor and G. M. Miskelly, *Anal. Chem.*, 2009, **81**, 2618-2625.
509. M. Li, F. He, Q. Liao, J. Liu, L. Xu, L. Jiang, Y. Song, S. Wang and D. Zhu, *Angew. Chem., Int. Ed.*, 2008, **47**, 7258-7262.
510. X. H. Wang, R. Z. Wang, B. Y. Gu and G. Z. Yang, *Phys. Rev. Lett.*, 2002, **88**, 4.
511. H. Su, X. R. Cheng, T. Endo and K. Kerman, *Biosens. Bioelectron.*, 2018, **103**, 158-162.
512. K. I. MacConaghy, D. M. Chadly, M. P. Stoykovich and J. L. Kaar, *Analyst*, 2015, **140**, 6354-6362.
513. F. Bian, L. Sun, L. Cai, Y. Wang, Y. Zhao, S. Wang and M. Zhou, *Biosens. Bioelectron.*, 2019, **133**, 199-204.
514. F. Bian, J. Wu, H. Wang, L. Sun, C. Shao, Y. Wang, Z. Li, X. Wang and Y. Zhao, *Small*, 2018, **14**, 1803551.
515. Y. Xu, H. Wang, C. Luan, F. Fu, B. Chen, H. Liu and Y. Zhao, *Adv. Funct. Mater.*, 2018, **28**, 1704458.
516. B. Ye, F. Rong, H. Gu, Z. Xie, Y. Cheng, Y. Zhao and Z. Gu, *Chem. Commun.*, 2013, **49**, 5331-5333.
517. H. Wang, H. Gu, Z. Chen, L. Shang, Z. Zhao, Z. Gu and Y. Zhao, *ACS Appl. Mater. Interfaces*, 2017, **9**, 12914-12918.
518. W. Liu, L. Shang, F. Zheng, J. Lu, J. Qian, Y. Zhao and Z. Gu, *Small*, 2014, **10**, 88-93.
519. B. Zhang, Y. L. Cai, L. R. Shang, H. Wang, Y. Cheng, F. Rong, Z. Z. Gu and Y. J. Zhao, *Nanoscale*, 2016, **8**, 3841-3847.
520. F. Fu, L. Shang, F. Zheng, Z. Chen, H. Wang, J. Wang, Z. Gu and Y. Zhao, *ACS Appl. Mater. Interfaces*, 2016, **8**, 13840-13848.
521. Y. Zhao, X. Zhao, B. Tang, W. Xu and Z. Gu, *Langmuir*, 2010, **26**, 6111-6114.
522. B. Zhang, Y. Cai, L. Shang, H. Wang, Y. Cheng, F. Rong, Z. Gu and Y. Zhao, *Nanoscale*, 2016, **8**, 3841-3847.
523. F. F. Fu, L. R. Shang, F. Y. Zheng, Z. Y. Chen, H. Wang, J. Wang, Z. Z. Gu and Y. J. Zhao, *ACS Appl. Mater. Interfaces*, 2016, **8**, 13840-13848.
524. W. Poon, *Science*, 2004, **304**, 830-831.
525. A. van Blaaderen, *Science*, 2003, **301**, 470-471.
526. P. N. Pusey and W. van Megen, *Nature*, 1986, **320**, 340-342.
527. J. Zhu, M. Li, R. Rogers, W. Meyer, R. H. Ottewill, W. B. Russel, P. M. Chaikin and S. T. S. S. S. Crew, *Nature*, 1997, **387**, 883-885.
528. U. Gasser, E. R. Weeks, A. Schofield, P. N. Pusey and D. A. Weitz, *Science*, 2001, **292**, 258-262.
529. P. Tan, N. Xu and L. Xu, *Nat. Phys.*, 2014, **10**, 73-79.
530. P. Schall, I. Cohen, D. A. Weitz and F. Spaepen, *Science*, 2004, **305**, 1944-1948.
531. P. Schall, I. Cohen, D. A. Weitz and F. Spaepen, *Nature*, 2006, **440**, 319-323.

532. E. R. Weeks, J. C. Crocker, A. C. Levitt, A. Schofield and D. A. Weitz, *Science*, 2000, **287**, 627-631.
533. P. G. Debenedetti and F. H. Stillinger, *Nature*, 2001, **410**, 259-267.
534. E. R. Weeks and D. A. Weitz, *Phys. Rev. Lett.*, 2002, **89**, 4.
535. E. R. Weeks and D. A. Weitz, *Chem. Phys.*, 2002, **284**, 361-367.
536. A. McMullen, M. Holmes-Cerfon, F. Sciortino, A. Y. Grosberg and J. Brujic, *Phys. Rev. Lett.*, 2018, **121**, 6.
537. B. Luo, J. W. Smith, Z. Wu, J. Kim, Z. Ou and Q. Chen, *ACS Nano*, 2017, **11**, 7626-7633.
538. E. Bianchi, J. Largo, P. Tartaglia, E. Zaccarelli and F. Sciortino, *Phys. Rev. Lett.*, 2006, **97**, 4.
539. I. Saika-Voivod, F. Smallenburg and F. Sciortino, *J. Chem. Phys.*, 2013, **139**, 234901.
540. A. Cadien, Q. Y. Hu, Y. Meng, Y. Q. Cheng, M. W. Chen, J. F. Shu, H. K. Mao and H. W. Sheng, *Phys. Rev. Lett.*, 2013, **110**, 5.
541. F. Smallenburg, L. Filion and F. Sciortino, *J. Phys. Chem. B*, 2015, **119**, 9076-9083.
542. F. W. Starr and F. Sciortino, *Soft Matter*, 2014, **10**, 9413-9422.
543. S. Roldán-Vargas, L. Rovigatti and F. Sciortino, *Soft Matter*, 2017, **13**, 514-530.
544. S. C. Rödner, P. Wedin and L. Bergström, *Langmuir*, 2002, **18**, 9327-9333.
545. J. Yamanaka, M. Murai, Y. Iwayama, M. Yonese, K. Ito and T. Sawada, *J. Am. Chem. Soc.*, 2004, **126**, 7156-7157.
546. M. A. Bevan, J. A. Lewis, P. V. Braun and P. Wiltzius, *Langmuir*, 2004, **20**, 7045-7052.
547. J. Zhang, Y. Li, X. Zhang and B. Yang, *Adv. Mater.*, 2010, **22**, 4249-4269.
548. Y. Li, G. Duan, G. Liu and W. Cai, *Chem. Soc. Rev.*, 2013, **42**, 3614-3627.
549. M. Hermatschweiler, A. Ledermann, G. A. Ozin, M. Wegener and G. von Freymann, *Adv. Funct. Mater.* 2007, **17**, 2273-2277.
550. J. R. Raney and J. A. Lewis, *MRS Bull.*, 2015, **40**, 943-950.
551. C. R. Tubio, J. A. Novoa, J. Martin, F. Guitian, J. R. Salgueiro and A. Gil, *RSC Adv.*, 2016, **6**, 2450-2454.